TECHNISCHE UNIVERSITÄT MÜNCHEN

Department Chemie

Fachgebiet Theoretische Chemie

Molecular Dynamics Study of Solvent Reorganization Energies for Electron Transfer Processes in DNA-Related Systems

Egor Vladimirov

Vollständiger Abdruck der von der Fakultät für Chemie der Technischen Universität München zur Erlangung des akademischen Grades eines

Doktors der Naturwissenschaften (Dr. rer. nat.)

genehmigten Dissertation.

Vorsitzender: Univ.-Prof. Dr. Th. Kiefhaber

Prüfer der Dissertation:

1. Univ.-Prof. Dr. N. Rösch
2. Univ.-Prof. Dr. M. Kleber

Die Dissertation wurde am 26.10.2009 bei der Technischen Universität München eingereicht und durch die Fakultät für Chemie am 23.11.2009 angenommen.

Acknowledgements

My special thanks I owe to Prof. Dr. N. Rösch, who was not my formal "Doctorvater", but rather immediate and direct supervisor during all these years of my stay in Germany. Despite, that our intensive interactions were mainly focused on the research activities, he indirectly managed to inspire my interest in german culture and history, which allowed me to see and to understand better the part of the system I was. Several cornerstones, which I attribute so far to a german working culture I learned from him: progress, efficiency, competitiveness and management.

I am thankful to Dr. Anela Ivanova, whose kindness, intelligence, help and support were of a big importance for me. It was always a pleasure to work with her and I feel pity that our collaboration was not so long.

There are two other persons – Prof. Dr. A. Voityuk and Prof. Dr. N. Bazhin, the interactions with whom, were short and had fragmentary character, but nevertheless of a great impact on all my life.

I am thankful to Dr. Alena Kremleva, whose magic ability to make the best out of possible helped me often to take right decisions and to enjoy that pleasant social environment, which was always around her in our group.

The advice of Dr. A. Genest and Dr. S. Bosko, with their ability to feel the pace of computer was helpful many times. I am thankful to Dr. P. Chuichay and Dr. K. Siriwong, who were supportive in many ways and provided first introduction to MD simulations, when I just entered the group.

I thank Dr. Sven Krüger, who despite that huge organizational burden resting on him, could still find the place for me in his long lists of daily tasks and not to forget to help.

...To My Mother

Contents

List of Abbreviations

A	adenine
AFM	atomic force microscopy
B3LYP	hybrid Becke-3-parameter exchange and Lee-Yang-Parr correlation functional
C	cytosine
cc-pVTZ	correlation-consistent polarized valence triple-zeta (basis set)
CR	charge recombination
CS	charge separation
CSh	charge shift
CT	charge transfer
D	donor
DA	donor-acceptor
DCM	dielectric continuum model
DFT	density functional theory
DNA	deoxyribonucleic acid
ESP	electrostatic potential
ET	electron transfer
FFT	fast Fourier transform
FF	force field
fs	femtosecond
FT	Fourier transform
G	guanine
HF	Hartree-Fock (method)
IP	ion-pair
KA	Koji Ando (model)

MD	molecular dynamics
NMR	nuclear magnetic resonance
NP	neutral pair
ns	nanosecond
PB	Poisson-Bolzmann (equation)
PCM	polarizable continuum model
PME	particle-mesh Ewald (method)
POL3	polarizable three-point charge potential (model of water)
ps	picosecond
RESP	restrained electrostatic potential
RMSD	root mean square deviation
R6G	rhodamine 6G
SD	standard deviation
SPC	simple point charge potential (model of water)
STM	scanning tunneling microscopy
T	thymine
TCF	time correlation function
TIP3P	three-point transferable intermolecular potential (model of water)
TIP3P-FQ	variant of TIP3P force field with fluctuating charges (model of water)
UHF	unrestricted Hartree-Fock (method)
Q-model	quadratic coupling model

1 Introduction

1.1 The phenomenon of charge transfer in DNA

The discovery of the structure of DNA by Watson and Crick in 1953[1] was the beginning of a breakthrough, which shaped a new world of biomolecular sciences. The ability of DNA to code the genetic information of the majority of known organisms, to conserve and to transfer it persistently in cell replications over millions of years brought up numerous fundamental questions about the mechanisms acting in living nature. The DNA of highly evolved species comprises milliards of subunits, but is constructed from only a few aromatic molecules. From the point of view of statistical physics, a molecule of this size can not sustain a stable structure and should inevitably undergo irreversible changes with time due to thermal fluctuations or solar radiation, resulting in a continuous series of bond breakages and subsequent aging and degradation of matter. Indeed, such processes take place in DNA but organisms have various means of protection and of repair of its damages.

The amazing mechanism of self-repair and the stable coordinated expression of genes in different locations of DNA point to the idea that these complex processes should be orchestrated by currents flowing through the thread. In other words, *DNA could serve as a molecular wire*. A more detailed inspection of its structure and analogies with solid state physics resulted in a further support of this idea: the double helix is composed of a series of aromatic base-pairs stacked on top of each other and, to a certain extent, can be viewed as a one-dimensional molecular crystal. Not long after the structure of DNA had been unraveled, it was suggested that these π-stacked arrays might be conducting[2] in a fashion similar to organic crystals, which demonstrate hopping or metallic conductivity.[3] Despite numerous fruitful contacts with solid state physics outlined in later studies,[4–6] DNA molecules turned out to possess distinctly different characteristics from conventional crystals, which rendered their description more complicated. It is not only the irregularity of the sequences, but also the very high flexibility of DNA with respect to conformational changes, which modulate the tightness and alignment of π-stacking of adjacent base-pairs. The latter is a crucial factor for expression of conductivity since it determines the degree of overlap between the electronic states of neighboring base-pairs. Other factors contributing to the complexity of electron transport in

DNA are the surrounding medium and the dynamics of counterions that balance negative charges of the sugar-phosphate backbone. Given these briefly outlined complications and the different experimental conditions at which DNA is processed, the scientific community could hardly come to consensus with regard to DNA conductivity during the last decades.

In the current era of nanoelectronics the problem of DNA conductivity received renewed attention due to the expected practical benefits, when in the middle of the 90s the group of Barton[7,8] announced results, which suggested that native DNA could perform as a molecular nanowire. A very promising direction which appeared later is to enhance the intrinsic conductivity of DNA by its inclusion into hybrid composites[9,10] like metal nanoparticle wires in which DNA serves as a template for the embedding of conducting species. There were already several attempts to create a new generation of electronic devices based on self-assembling materials where the inherent properties of DNA were exploited such as conformational transitions: few prototypes of nanodevices based on transitions between different DNA forms,[11] duplexes and triplexes,[12] duplexes and quadruplexes[13] were already produced. DNA with its extraordinary recognition and coding capabilities stemming from the complementarity of strands is a candidate for bio-computing, too.[14] Together with the possible applications in medical diagnostics,[15,16] where DNA could be implemented for fast sensing of various biological materials, this macromolecule represents a prospective source of fascinating discoveries and applications in different fields.

1.2   Experimental approaches to charge transfer in DNA

The most straightforward approach to explore the conductivity of DNA would be to measure directly the current through DNA fragments. Such experiments were already conducted either in the setting of Atomic Force Microscopy (AFM),[17,18] where DNA was spread on mica plates, or in the setting of Scanning Tunneling Microscopy (STM),[19,20] where DNA was commonly deposited on gold. A serious disadvantage of these setups are issues with "electrode contacts" that strongly affect the molecular structure when the tips touch the sample: DNA was found to be too short within these experiments.[21,22] Moreover, the substrate pretreatment, which is necessary to deposit negatively charged DNA onto a mica surface, changes the electric properties of DNA from insulating to conducting.[23,24] For both methods (AFM, STM) there are strong ongoing efforts to avoid non-specific substrate-molecule longitudinal contacts[25,26] by performing measurements for standing molecules covalently bound to electrodes.[27,28] The latter is achieved by forming thiol-gold covalent bonds[29] between complementary strands of DNA, where one strand is attached to the gold surface and the other one to a gold nanoparticle.[30] These experiments[25,26] undoubtedly demonstrated that significant currents exist in DNA, but nevertheless the mechanism of conductivity remains questionable.[31]

The original experiments[7,8] which boosted the interest in electric properties of DNA, were carried out in solution mainly targeting oxidative damage processes of DNA. In these experiments an electron hole (the typical charge carrier in many experiments on DNA) was injected into oligonucleotides through an additional molecular species attached to DNA. Covalent binding of such species to DNA is an important prerequisite for efficient ET.[32] Modified bases or dyes capping (intercalating) the macromolecule served as sources of holes.[8,33,34] The propagation of the hole, after initial oxidation, from a cation G^+ along a DNA π-stack puts an additional requirement on the choice of hole injector which should be suitably charged in order to avoid Coulomb attraction.[35] The guanine cation G^+ can undergo several side reactions like deprotonation or reaction with water/oxygen[34,36,38] forming various products, which are normally described as G^{ox}.[37] A hole injection system introduced by Giese et al.[34,38] employes a chemical reaction that yields a sugar radical cation which exhibits a higher oxidation potential than G and injects a hole into the nearest guanine.[39] The hole injection systems works from the ground state and thus has the advantage that there is no fast back charge transfer process.[39] The incorporation of the latter system allowed first detailed and consistent studies of charge transfer mechanisms in DNA.[35] The advancement of the hole is sequence dependent:[40] a hole is transmitted from its source to the DNA sites with lowest oxidation potentials. The hierarchy of increasing oxidation potentials[41,42] for the four DNA nucleobases is: guanine (G) < adenine (A) < cytosine (C) and thymine (T). Thus, mainly G or a sequence[43] of several adjacent guanines serve as hole acceptors. If guanine G is not present in the sequence context or if there are at least 4 AT base-pairs between nearest guanines, then hole propagation goes through adenines A.[44] The corresponding rates of hole transfer are measured in solution as a function of the distance between hole donor and acceptor by fluorescence quenching methods[7,45] and time-resolved pump-probe spectroscopy.[46,47] The first experiments of Barton and collaborators[7,8] showed that the hole propagates along the DNA stack essentially *distance-independently* and at much higher rates than those typical for proteins. The mechanism with detailed quantitative information on this process was provided later.[35]

Biochemical methods deliver an alternative scheme for detecting electron transfer (ET) processes.[48] The approach relies on gel electrophoresis, which allows the location of oxidatively damaged base-pairs within a DNA strand. These experimentally studied oxidation processes can occur *in vivo* in situations that lead to damages of DNA within cells.[49] The photooxidant is covalently tethered to DNA and intercalated into the double strand; holes are produced, which travel over long distances and preferably damages guanine[50] by performing "chemistry at a distance".[48]

This brief overview of experimental approaches clearly suggests that complementary theoretical studies are required to achieve a consistent picture of ET in DNA.

1.3   Theoretical treatment of charge transfer in DNA

Many experiments on charge transport (CT) in DNA address hole transfer. Therefore theoretical efforts often also describe hole propagation. However, experiments on transfer of electrons were recently reported.[51,52] For the mathematical formalism involved in the present work, such distinction is irrelevant and we will use these terms interchangeably. According to the latest studies,[53,54] the holes in DNA are confined to a single base-pair and quantum effects play a crucial role.[55] The latter are affected by the local environment of a base-pair, its alignment and geometric distortions caused by thermal fluctuations. With respect to propagation along the DNA π-stack, the two competing mechanisms, short-range tunneling (superexchange) and long-range hopping, were finally combined into one superexchange-mediated charge hopping model.[35,56,57] This combined model emphasized the rather complicated character of charge transfer in DNA complexes that contain sequential, interstrand, intrastrand superexchange-mediated and direct interstrand hole transfer.[57] These two mechanisms initially stemmed from interpretations of contradictory data that had been obtained in solution experiments: some results pointed to a rather weak dependence of the CT rates with the donor-acceptor distance[46,58] and other results, from studies of oxidative damage, suggested a strong distance dependence of the rates.[48] It was shown that for short separations (less than four intervening AT base-pairs) hole transfer rates decay exponentially with the distance as is typical for a direct tunneling mechanism.[35] In this case the CT rate decays dramatically with the distance between donor and acceptor sites, where usually guanine moieties are separated by bridges comprised of an increasing number of AT units.[38] When the separation between donor and acceptor sites increases beyond about 3–5 intervening base-pairs, then the mechanism changes to hopping[59] governed by thermal fluctuations.[56,60,61] According to this mechanistic representation of CT, single G or A moieties act as stepping stones for hole transport,[62,63] since they have the lowest oxidation potential among the four native nucleobases.

One of the advantages of hopping theory[56,60,64] is that its description incorporates one main phenomenological parameter, namely the relative rates of elementary hopping steps between G sites that are separated by AT-bridges of different length. Knowledge of the relative rates also enables one to evaluate[65] the distance dependence of charge transfer in experiments on DNA duplexes.[34,38,66,67] Knowledge of relative hopping rates, however, is insufficient for determining how fast a hole generated in DNA can be transferred over a certain distance. To address this issue, absolute rates of different hopping steps should be obtained. This has been done experimentally by performing time-resolved measurements on DNA containing either different charge donor and acceptor moieties[44,68,69] or identical ones, namely, guanine nucleobases in DNA hairpins.[70,71]

1.4   Motivation and overview

In general, elementary CT steps are considered to be affected mainly by two factors: (*i*) the magnitude of the electronic coupling between donor and acceptor; (*ii*) the intensity of molecular motions that ensure an overlap of initial and final quantum states. Electronic coupling and its conformational and distance dependence have received much attention from theoreticians in the recent years.[72,73] Meanwhile, the evaluation of the contribution of molecular motions to transfer rates still seems to be a serious bottleneck when modeling CT reactions.

All theoretical descriptions of electron transfer have two common quantities within the Boltzmann factor which regulates the degree of electronic overlap between donor and acceptor states: the free energy difference $\Delta G°$ between donor and acceptor states, and the so-called "reorganization energy", conventionally denoted as λ. Theoretical estimates of CT rates depend crucially on them, as both enter an exponential term in the mathematical expressions. Marcus originally introduced the reorganization energy[74] to characterize the comparatively slow reorganizational process that occurs as the originally polarized medium, assisted by molecular vibrations, responds to the relocation of the charge. In short, it is via the reorganization energy that the molecular vibrations affect the rate of a CT reaction in an extremely sensitive way.

From experiment one knows that a hole propagates along the DNA π-stack on a scale of tens to hundreds of picoseconds[47] or even of up to nanoseconds,[75] depending on the acceptor moiety and on the number of intervening AT base-pairs. During this time, not only the surrounding water undergoes structural changes (reorientation times of several picoseconds),[76] but also the dynamics of sodium ions (in the range of hundreds of picoseconds)[77] strongly affects the hole energetics.[78,79] As it was recognized both theoretically[80] and experimentally,[81,82] the solvent substantially affects the rate of charge transfer. In addition, experimental studies on oligonucleotides[83,84] indicate that structural distortions of DNA may play a major role in CT. Therefore, modeling of ET rates necessitates a full atomistic description of the system (DNA and solvent) at least on the scale of hundreds of picoseconds. *Based on atomistic considerations of CT, the present work establishes a method that allows one to determine the solvent contribution to the reorganization energy in a direct, accurate way by means of molecular dynamics simulations.*

Molecular dynamics (MD) simulations operating on the timescale of nanoseconds are well established tools for studying the structure and its thermal fluctuations of DNA and its environment.[85,86] Based on empirical force fields, they describe the time evolution of DNA motion[87] and they complement the corresponding information from experimental methods like X-ray crystallography and nuclear magnetic resonance (NMR).

In the present study, MD simulations with an explicit description of DNA and its solvent environment by advanced polarizable force fields are applied in order to estimate the solvent reorganization energy in a quantitative fashion in the framework of the semi-classical Marcus

treatment of CT. A series of studies had been reported[88–91] to evaluate the solvent reorganization energy by MD methods. The current work aims at improving this approach by paying close attention to the electronic polarization.[92] The suggested computational procedure is first established for the classical two-spheres model of Marcus and subsequently transferred to large-scale simulations of biomolecules like DNA and its complexes with the dye Rhodamine 6G (R6G).

Chapter 2 reviews the original concept of the reorganization energy by considering changes in the medium in terms of the reaction coordinate. The physical picture underlying the molecular distortions caused by CT is illustrated. Finally, this chapter provides a brief overview of classical ET theory as developed by Marcus and its most important outcomes. Chapter 3 summarizes modern ET rate theories which show how quantum effects influence the reorganization energy.

Chapters 4 and 5 are devoted to methodological issues related to the computational method for evaluating the solvent reorganization energy. Chapter 4 summarizes existing methods and their shortcomings and justifies the choice of MD for the purposes of the present work. Chapter 5 contains a brief synopsis of key issues related to MD simulations: force fields, electrostatic and van der Waals interactions, electronic polarization, periodic boundary conditions, temperature and pressure control.

Chapter 6 addresses two methodological issues. It introduces MD simulations with a polarizable force field for account of solvent reorganization energy and it compares various ways to analyze the MD data. The evaluation methods and their outcomes are thoroughly tested against the classical two-spheres solute model formulated for CT reactions by Marcus.[93] Special attention is paid to the solvent, the distance dependence of the reorganization energy, the role of the electronic polarization and the application of effective optical dielectric constants for theoretical estimates. Chapters 7 and 8 apply this procedure to the calculation of solvent reorganization energies of DNA duplexes and their complexes with Rhodamine 6G. The results from simulations with and without an explicitly incorporated electronic polarization are compared. The chapters discuss the influence of charge sets, separate contributions of solute and solvent electronic polarizations, and partial contributions of different molecular groups to changes of the solvent reorganization energy. In addition, the distance dependence of the solvent reorganization energies, the influence of DNA conformations and the flexibility of duplexes in ET processes are addressed. Reorganization energies calculated with the polarizable force field are tested against experimental data.

The last chapter provides a summary of the results and an outlook.

2 The Classical Marcus Picture of Electron Transfer. Reorganization Energy

2.1 Solvent response to ET. Reaction coordinate

Before addressing the standard classical approach to electron transfer (ET) due to Marcus,[74,94] a rather simple model[95] of the solvent reorganization enery will be introduced which is restricted to ET between two equivalent electron localization sites A and B in an aqueous solvent. In other words, for simplicity the free energy change $\Delta G°$ between the two CT states is assumed to be zero. This is the so-called *symmetric case*. As an example of typical solvent response to ET between A and B only one physical effect is included, namely, the water dipole moment reorientation.

Also for simplicity, the response due to water reorientation is described for one water molecule only with its oxygen atom fixed at a certain distance above the midpoint of the line connecting sites A and B. Rotation of the water molecule around this point is allowed. The dipole moment μ of the water molecule forms an angle θ with the perpendicular bisector of the line between A and B (Figure 2.1). If the electron is localized on A, the dipole will tend to point towards A; similarly, if the electron is localized on B, then the dipole will be redirected towards B. If the distance between A and B is large enough, there will be two stable orientations of the dipole of the water molecule, characterized by angle θ: $\theta = -\theta_0$ with the electron at A, and $\theta = \theta_0$ with the electron at B. Thus, the angle θ is a measure of the solvent response to ET (or, alternatively, of the polarization change after ET) and could be treated as a reaction coordinate. If the water molecule is situated far from A and B (or the interaction of the water dipole with both centers is weak), then the total potential curve for the rotation of the water molecule around the two ET minima may be approximated as parabolae. With the electron at B one has:

$$U(\theta) = U_0 + \frac{1}{2}U''(0)(\theta - \theta_0)^2 + \dots. \tag{2.1}$$

Terms of higher order than second are neglected. The two ET-relevant parabolae, with minima located at the centers of sites A and B, are shown in Figure 2.1. The constant term U_0 is omitted as long as it is the same for both potential energy curves. The states with the electron residing on site A or B, together with the corresponding potential energy curves, are referred to

in the following text as "reactant", R, and "product" states, P, respectively. Introducing the force constant $f = U''(0)$ as the second derivative of $U(\theta)$ along the reaction coordinate θ, one therefore has:

$$U_R(\theta) = \frac{1}{2}f(\theta + \theta_0)^2 \tag{2.2}$$

$$U_P(\theta) = \frac{1}{2}f(\theta - \theta_0)^2. \tag{2.3}$$

The difference between the two energy expressions, $U_R - U_P = 2f\theta_0\theta$, can be rewritten as:

$$\theta = \frac{1}{2f\theta_0}(U_R - U_P). \tag{2.4}$$

From Eq. (2.4) one notes that the solvent coordinate and the potential energy difference are proportional. Thus either quantity could be used as reaction coordinate. Moreover, the representation of the potential energy as a function of the variable θ reflects only the dependence of the ET energy on one specific geometric parameter, while the representation as a function of $(U_R - U_P)$ implicitly includes all possible factors influencing the charge transfer. Also, the choice of the angle θ used for the present illustration is rather arbitrary; in a similar fashion any other structural parameter, such as bond lengths, bond angles, etc. could be selected. Therefore, in order to be more consistent further on with a general description, we shall present the ET picture only as a function of the potential energy difference $(U_R - U_P)$ and the force constant f will be treated as an average reflecting the overall response of the (aqueous) environment.

Another remark is due regarding a relationship between the free energy and the potential energy. Unlike done so far, one normally considers the whole medium surrounding the donor and the acceptor centers. When the solvent environment in addition is at a certain temperature, then entropic effects may be noticeable and have to be accounted for, i.e. the process of charge
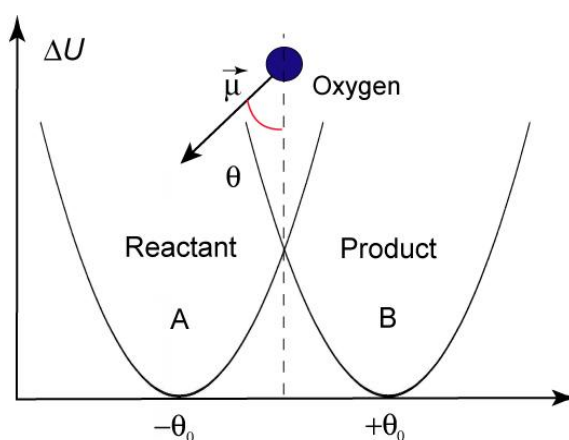
Figure 2.1. Water dipole orientation as a result of electron (negative charge) transfer. The water dipole is oriented towards initial state A.

transfer has to be characterized in terms of free energy. The O−H bond length can be taken as an example. ET from the donor to the acceptor causes bond extension within the water molecules surrounding the donor and bond contraction within those around the acceptor. This process not only causes structural change that affects the orientation of the solvent molecules, but also shifts their vibrational frequencies due to restricted internal atomic motions. The latter results in an additional entropic contribution classically expressed through vibrational statistical sums.[96]

Despite that some vibrational modes could undergo substantial variations, the overall response of the solvent bath coupled to the ET system is usually linear[97] or close to linear,[98] which explains the considerable success of the linear response approximation introduced first by Marcus.[99,100] It preserves the parabolic shape of the solvent potential energy surface and transfers the same parabolic character to the free energy surfaces, i.e. one assumes a constant entropic correction to the potential energy.[92,101] Accepting these two simplifications, the potential energy surface from Figure 2.1 is generalized in terms of the free energy as a function of $(U_R - U_P)$ to give the curves shown on Figure 2.2.

The ordinate of Figure 2.2 is the free energy rather than the potential energy. The abscissa is a reaction coordinate that reflects the differences in the polarization energy and the vibrational energy between reactant and product states to the overall change of the potential energy. This model, which approximates the solvent potentials by parabolae of equal force constants for reactant and product states, Eqs. (2.2) and (2.3), is suitable for describing a limited number of ET processes but, nevertheless, adequately explains ET in aqueous solutions. The *symmetric case* $\Delta G° = 0$ considered here applies to systems where the solute either does not undergo any *net* geometric changes during ET (e.g. in self-exchange reactions like the ferrous-ferric exchange $Fe^{3+}+Fe^{2+}\leftrightarrow Fe^{2+}+Fe^{3+}$), or when the structural transformations can be neglected, as in some approximately symmetric ET reactions in DNA duplexes (e.g. between guanine units *G* (in italics) in the reaction 5'-G*G*$^+$GTTTG*GG*-3'↔5'-G*GG*TTTG*G*$^+$G-3'). The Marcus model will be applied to situations similar to the latter within the present thesis.
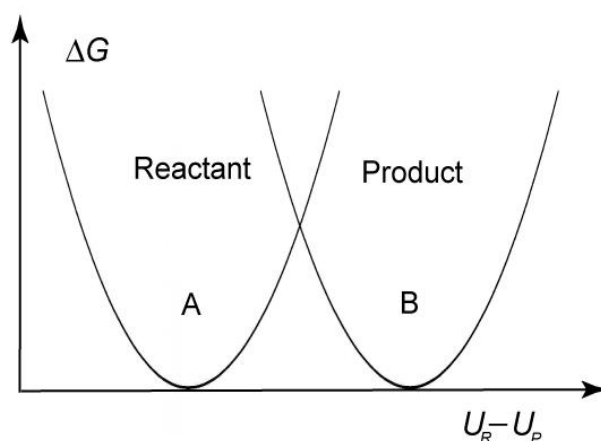
Figure 2.2. Marcus generalization of the solvent response to CT in terms of the free energy ΔG.

2.2   Marcus theory

Now let us consider the more general *asymmetric* case, where the equilibrium free energies at the equilibrium positions of the product and the reactant states differ, $\Delta G° \neq 0$. In other words, unlike above, sites A and B stand either for different chemical species or for substantially different sites within the same solute. It is also assumed that the behavior of all water molecules of the surrounding medium complies with the previously discussed parabolae model approximation (Figure 2.2). Then the free energy barrier $\Delta G^{\neq}$ for the charge transfer reaction is the energy difference between the crossing point of the parabolae and the bottom of the free energy curve of the reactants (Figure 2.3). If one ignores entropy changes, then the free energies are equal to potential energies and the charge transfer occurs at the point U_θ where $U_R(U_\theta) = U_P(U_\theta)$.

Using the definition of the potential energy curves (Eqs. (2.2) and (2.3)), this condition can be expressed as:

$$\frac{1}{2} f \left(U_\theta - U_R \right)^2 = \Delta G° + \frac{1}{2} f \left(U_\theta - U_P \right)^2 \tag{2.5}$$

This equation for the crossing point can be solved:

$$U_\theta = \frac{\Delta G°}{f} \left(\frac{1}{U_P - U_R} \right) + \frac{1}{2} \left(U_R + U_P \right). \tag{2.6}$$

The free energy barrier, or the potential energy barrier when entropy changes are neglected, is:

$$\Delta G^{\neq} = G_R \left(U_\theta \right) - G_R \left(U_R \right) = U_R \left(U_\theta \right) - U_R \left(U_R \right) = \frac{1}{2} f \left(U_\theta - U_R \right)^2. \tag{2.7}$$

If one introduces formally the quantity $\lambda = (1/2)f(U_R - U_P)^2$ and substitutes here the expression for U_θ, Eq. (2.6), one obtains the following simple formula:

$$\Delta G^{\neq} = \frac{1}{4\lambda} \left(\lambda + \Delta G° \right)^2 \tag{2.8}$$

The parameter formally defined as $\lambda = (1/2)f(U_R - U_P)^2$ is a fundamental physical quantity, the so-called *reorganization energy*. The term "reorganization energy" could be understood as the "free energy change that would be required to reorient all atoms and molecules as if they were forming and solvating the product state, but without actual transfer of charge."[95] The physical meaning of this definition will be illustrated and discussed in detail in the next chapters.

From the standard Arrhenius relationship between the free energy of activation and the rate constant of a chemical reaction, the ET rate constant is given as:
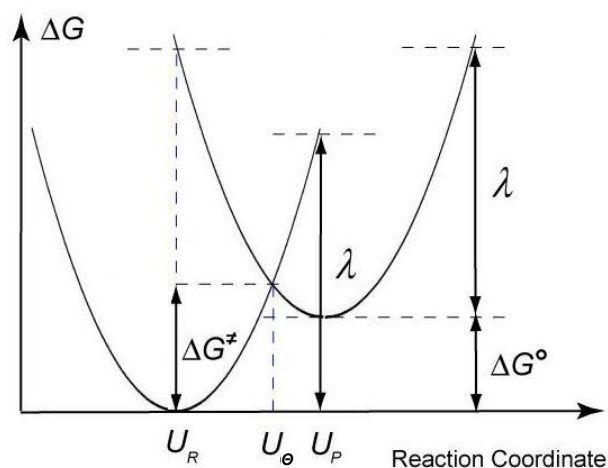
Figure 2.3. Marcus picture of the solvent reorganization energy.

$$k_{ET} = A \exp \left[-\frac{\left(\lambda + \Delta G^{\circ} \right)^2}{4 \lambda k_B T} \right],$$

(2.9)

where the pre-exponential factor *A* has a complex form that reflects its quantum origin. This will be discussed in the following chapter. Equation (2.9) predicts the so-called "bell-shaped" dependence of the ET rate constant k_{ET} as a function of the free energy. An important consequence of Eq. (2.9) is illustrated in Figure 2.4, namely that the rate constant depends on ΔG° in a somewhat counter-intuitive way. Normally, the rate of a chemical reaction depends notably on whether it is exothermic, $\Delta G^{\circ} < 0$, or endothermic, $\Delta G^{\circ} > 0$. However, according to Marcus theory of ET reactions, the reorganization energy ($\lambda > 0$) serves as a reference. In the so-called *normal region*, $-\lambda < \Delta G^{\circ}$ (Figure 2.4), the rate constant increases with higher (corresponds to the so-called *inverted region*, see Figure 2.4) free energy values, but only on the absolute value of the free energy difference between the initial and final states. The quadratic dependence of the ET rate on ΔG° and on the reorganization energy λ was first derived by Marcus and
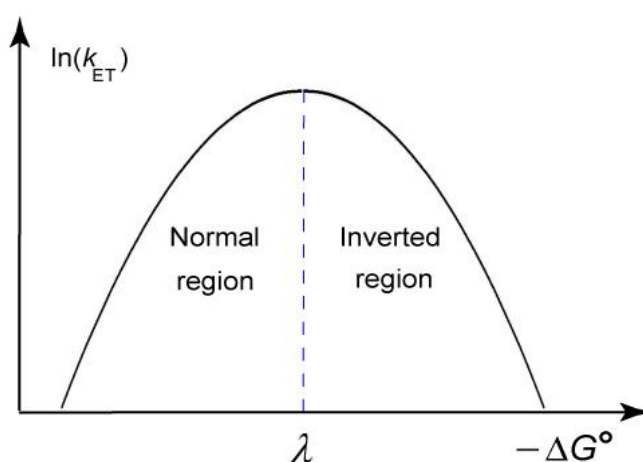
Figure 2.4. Bell-shaped ET rate constant dependence on the free energy.

Hush.[94,102] They represented the total reorganization energy λ as the sum of two contributions: one due to the solvent, λ_s, and another one due to the solute, λ_i (the so-called intramolecular reorganization energy):

$$\lambda = \lambda_s + \lambda_i \tag{2.10}$$

Since their pioneering works, the latter notations became standard in the scientific literature.

2.3   Solvent reorganization energy (λ_s)

The solvent molecules adjacent to the solute, which are polarized due to the presence of the charge on the solute, form its solvation shells. Due to thermal fluctuations, the solvent molecules within these solvation shells (along with the rest of the solvent molecules) are in permanent motion leading to fluctuations of the potential energy of the entire system. Translation and rotation of the solvent molecules bring the system at certain moments to the state along the reaction path, where ET can take place; then the charge relocates to a new site and the additional solvent polarization around the previous site vanishes. Even when a solute with rigid geometry is assumed, the thermal perturbations of the electrostatic field generated by the solvent molecules lead to changes in the solute quantum structure, expressed in terms of elevation or depression of the electronic energy levels. This gives rise to an additional requirement for the charge transfer reaction: only when the energies of the solute electronic quantum levels coincide in the initial and the final state, ET will take place. Despite the fact that in reality the solute geometry is never rigid and that, when it is immersed in the solvent, the two moieties form one common quantum system, the simplification of a rigid geometry is often invoked. It can be accompanied by another approximation, namely, the solvent can be treated as a structureless continuum, in which the discrete character of individual solvent molecules is neglected.

In the following the original idea of Marcus[74] shall be presented how one can determine the solvent polarization $\mathbf{P}(\mathbf{r})$ that arises from the electrostatic field $\mathbf{E}(\mathbf{r})$ of solute and separate it into two contributions, a "slow" one $\mathbf{P}_u(\mathbf{r})$ and a "fast" one $\mathbf{P}_e(\mathbf{r})$,

$$\mathbf{P} = \mathbf{P}_u + \mathbf{P}_e, \tag{2.11}$$

where for convenience the dependence on coordinate $\mathbf{r}$ has been omitted.

In general the polarization $\mathbf{P}$ is comprised of electronic, atomic and orientational parts, which undergo their adjustment with respect to the change of electrostatic field, i.e. in an ET process, on the scale of 10^{-15} sec, 10^{-13} sec, and 10^{-11} sec, respectively.[74] As immediate response to an ET only the fast (electronic) $\mathbf{P}_e$ contribution will adjust itself, while the two other (slow) components, combined in the term $\mathbf{P}_u$, will relax much later. Therefore, the situation right after an ET is a non-equilibrium one with respect to the slow polarization of solvent.

According to the schematic representation in Figure 2.3, the solvent reorganization energy λ_s can be understood as the difference between the equilibrium free energy $G(U_R)$ and the non-equilibrium free energy $G^*(U_P)$:

$$\lambda_s = G^*\left(U_P\right) - G\left(U_R\right), \tag{2.12}$$

where contributions correspond to the same parabola, e.g. the left one in Figure 2.3 which represents the reactants. In the free energy state $G(U_R)$, the minimum energy at U_R on the left parabola (Figure 2.3), both the slow component $\mathbf{P}_u$ and the fast component $\mathbf{P}_e$ of the solvent polarization are in equilibrium with the charge distribution of the reactant. In the non-equilibrium free energy state $G^*(U_P)$, only the fast component $\mathbf{P}_e^*$ is relaxed, while the slow polarization component $\mathbf{P}_u^*$ is not. The latter corresponds to another configuration where the atomic and the orientational characteristics of the solvent are already in equilibrium with the product charge distribution, the minimum energy at point U_P of the right parabola (Figure 2.3).

Following Marcus,[74] one evaluates the initial equilibrium free energy $G(U_R)$ from Eq. (2.12) by exploiting a general property of the polarization $\mathbf{P}$, which in principle may be considered as a dipole moment $\boldsymbol{\mu}$ per unit volume dV,

$$\boldsymbol{\mu} = \mathbf{P}dV. \tag{2.13}$$

The interaction energy of the dipole $\boldsymbol{\mu}$ with the electric field $\mathbf{E}$ is

$$U = -\boldsymbol{\mu}\mathbf{E}. \tag{2.14}$$

If the dipole $\boldsymbol{\mu}$ is an induced dipole, then the work W required to produce it, is

$$W = -\int_{\mathbf{E}=0}^{\mathbf{E}=\mathbf{E}_0} \boldsymbol{\mu}d\mathbf{E} = -\frac{\mu^2}{2\alpha_0}, \tag{2.15}$$

where α_0 is the polarizability of the medium. The value of the induced dipole $\boldsymbol{\mu}$ is proportional to the electric field $\mathbf{E}$,

$$\boldsymbol{\mu} = \alpha_0\,\mathbf{E}. \tag{2.16}$$

When the field $\mathbf{E}$ is suddenly switched off, as is the case in a fast non-adiabatic ET, then the dipole still stores some free energy F,

$$F = W - U = \frac{\mu^2}{2\alpha_0}. \tag{2.17}$$

The total polarizability α_0 also contains two contributions (Eq. 2.11),

$$\alpha_0 = \alpha_u + \alpha_e. \tag{2.18}$$

where α_u and α_e are the contributions to the solvent polarizability that correspond to "slow" and "fast" components, respectively. If one considers the induced dipole moments, that correspond to either polarization process, as independent of each other, then the free energy is given by

$$F_{u,e} = \frac{\mathbf{P}_u^2}{2\alpha_u} + \frac{\mathbf{P}_e^2}{2\alpha_e} . \tag{2.19}$$

However, in addition, it is necessary to take into account that there are other interactions of medium induced dipoles with the total electrostatic field $\mathbf{E}$,

$$\mathbf{E} = \mathbf{E}_c + \mathbf{E}_u + \mathbf{E}_e , \tag{2.20}$$

where $\mathbf{E}_c$, $\mathbf{E}_u$ and $\mathbf{E}_e$ are field contributions that correspond to the charges, the slow and the fast polarization, respectively. The interactions of electrostatic field $\mathbf{E}$ with slow $\mathbf{P}_u$ and fast componenets $\mathbf{P}_e$ give rise to separate free energy contributions:

$$-\mathbf{P}_u \left(\mathbf{E}_c + \mathbf{E}_u + \mathbf{E}_e \right) \tag{2.21}$$

and

$$-\mathbf{P}_e \left(\mathbf{E}_c + \mathbf{E}_u + \mathbf{E}_e \right) . \tag{2.22}$$

One further term contributing to the free energy of the medium arises from the electrostatic field generated by the solute charges themselves,

$$\frac{\mathbf{E}_c^2}{8\pi} . \tag{2.23}$$

Summing all contributions represented in Eq. (2.19)–(2.23) and avoiding double counting, after integration over the entire volume of the solute-solvent system one arrives at the main formula for the total free energy G derived as by Marcus:[74]

$$G = \int \left(\frac{\mathbf{E}_c^2}{8\pi} + \frac{\mathbf{P}_u^2}{2\alpha_u} - \frac{\mathbf{P} \cdot \mathbf{E}_c}{2} - \frac{\mathbf{P}_u \cdot \mathbf{E}}{2} \right) dV + PV \tag{2.24}$$

Here the additional term PV is the work against the external pressure P. Assume that the expression in Eq. (2.24) for the free energy G corresponds to the equilibrium state of the reactant (minimum energy point U_R of the left parabola, Figure 2.3):

$$G \equiv G(U_R). \tag{2.25}$$

One can write a similar expression for the non-equilibrium state $G^*(U_P)$,

$$G^* (U_P) = \int \left(\frac{\mathbf{E}_c^2}{8\pi} + \frac{\mathbf{P}_u^{*2}}{2\alpha_u} - \frac{\mathbf{P}^* \cdot \mathbf{E}_c}{2} - \frac{\mathbf{P}_u^* \cdot \mathbf{E}^*}{2} \right) dV + PV , \tag{2.26}$$

where a star "*" denotes non-equilibrium quantities.

In Eqs. (2.24) and (2.26) it is assumed that in both states the volume of the system stays the same, i.e. is independent of the slow (orientational) polarization $\mathbf{P}_u$. Therefore, the solvent reorganization energy λ_s results as the difference between the free energies of the equilibrium and the non-equilibrium states, given by Eq. (2.24) and (2.26):

$$\lambda_s = -\frac{1}{2} \int \left(\mathbf{P}^* - \mathbf{P} \right) \cdot \mathbf{E}_c \, dV . \tag{2.27}$$

The polarizations **P** of the equilibrium state in Eq. (2.27) is formed by both slow (polarizability α_u) and fast (polarizability α_e) responses of the solvent, because the solvent is fully adjusted to the electrostatic field **E**,

$$\mathbf{P} = \alpha \mathbf{E} = \frac{\alpha}{1 + 4\pi\alpha} \mathbf{E}_c. \tag{2.28}$$

In contrast, the non-equilibrium state with polarization $\mathbf{P}^*$ is characterized only by fast electronic response (polarizability α_e), while the orientational component corresponds to another (final) equilibrium state, i.e. the minimum energy of right parabola U_P on Figure 2.3.

$$\mathbf{P}^* = \alpha_e \mathbf{E}^* = \frac{\alpha_e}{1 + 4\pi\alpha_e} \mathbf{E}_c \tag{2.29}$$

The corresponding polarizabilities, Eqs. (2.28)–(2.29) are related to the optic dielectric constant $\varepsilon^{\mathrm{op}}$,

$$4\pi\alpha = \varepsilon^{\mathrm{op}} - 1, \tag{2.30}$$

and the static dielectric constant $\varepsilon^{\mathrm{st}}$

$$4\pi\alpha_e = \varepsilon^{\mathrm{st}} - 1, \tag{2.31}$$

respectively. Substituting the expressions for polarizations **P** and $\mathbf{P}^*$, Eqs. (2.28)–(2.29), into Eq. (2.27) for λ_s with corresponding polarizabilities from Eqs. (2.30)–(2.31) one arrives at

$$\lambda_s = \frac{1}{8\pi} \int \left(\frac{1}{\varepsilon^{\mathrm{op}}} - \frac{1}{\varepsilon^{\mathrm{st}}} \right) \mathbf{E}_c^2 \, dV. \tag{2.32}$$

Next, one considers the special case of a simplified model where the solute is represented by two rigid spherical units of radii a_D and a_A (for donor and acceptor, respectively) with their centers separated at distance R_{DA}. In the present discussion one considers the model of ionic species, where each of the spheres holds a point charge at its center: in the ion-pair (IP) state the point charges are $q_D = e$, $q_A = -e$; in the neutral-pair (NP) state the charges are $q_D = q_A = 0 \, e$.

By separating the fast electronic polarization from the slow atomic and orientation polarization, Marcus calculated the free energy difference between these two states. Assuming that the static dielectric constant and the high-frequency (optical) dielectric constants in Eq. (2.32) do not vary in space, in other words $\varepsilon^{\mathrm{op}} = \varepsilon_\infty$ and $\varepsilon^{\mathrm{st}} = \varepsilon_0$, one can reduce the calculation of solvent reorganization energy λ_s to the evaluation of the work required to charge this Marcus two-spheres system in vacuum

$$\lambda_s = \left(\frac{1}{\varepsilon_\infty} - \frac{1}{\varepsilon_0} \right) \int \frac{\mathbf{E}_c^2}{8\pi} \, dV = \left(\frac{1}{\varepsilon_\infty} - \frac{1}{\varepsilon_0} \right) \left[\int_0^{-\Delta e} \frac{q_A}{a_A} \, dq_A + \int_0^{\Delta e} \frac{q_D}{a_D} \, dq_A + \int_\infty^{R_{DA}} \frac{\Delta e^2}{r^2} \, dr \right]. \tag{2.33}$$

The first two integrals in the square brackets represent the work required for charging of each sphere and the last term is the electrostatic interaction between the spheres A and D. Finally, this

simplified ET model yields the famous Marcus expression for the solvent reorganization energy λ_s in the form represented below:[94,102,103]

$$\lambda_s = \Delta e^2 \left(\frac{1}{\varepsilon_\infty} - \frac{1}{\varepsilon_0} \right) \left(\frac{1}{2a_D} + \frac{1}{2a_A} - \frac{1}{R_{DA}} \right). \tag{2.34}$$

Here ε_0 is the static dielectric constant, ε_∞ is the high-frequency (optical) dielectric constant of the solvent, and Δe is the charge transferred from the donor to the acceptor unit.

In case of water as solvent[104] with $\varepsilon_\infty = 1.78$ and $\varepsilon_0 = 78.4$ at $T = 298$ K, Eq. (2.34) gives estimates for the solvent reorganization energy in the range 1.0–3.0 eV for $R_{DA} = 5$–10 Å and $a_D = a_A = 3.0$ Å. The latter radii are typical for ET reactions between small organic molecules, like guanine or some organic dye.

It is noteworthy that the dielectric continuum model breaks down if there are specific solute-solvent interactions,[105] dielectric saturation effects[100,106–108] or solute quantum modes coupled to the solvent[109] which will be discussed in detail in Chapter 3.

Reliable simulations of the free energy curves are known only for the two-spheres model[92] because of the extreme computational efforts involved. In DNA, in view of a higher delocalization of the charge, geometric factors and the strong native electrostatic field induced by the negatively charged phosphates), one can expect additional solute-solvent interactions in the presence of a hole to be even weaker than in a two-spheres model. Therefore, for electron hole transfer in DNA the main approximation in the Marcus model associated with the linear response of the solvent should hold, resulting in the parabolic character of the free energy curves with equal curvature. Thus, this approximation was employed in the present thesis for the description of ET in DNA oligomers.

2.4   Solute reorganization energy (λ_i)

Thermal fluctuations do not only set solvent molecules into motion, they also cause distortions of the solute geometry, thereby being the source of a permanent shift of the electronic levels between which ET occurs. This structural change of the solute gives rise to the "internal" reorganization energy λ_i of the solute. Due to the strong chemical bonds that are holding together the atoms of the solute, these geometry distortions affect the positions of electronic levels to a much lesser extent than the "external" causes, namely the polarization due to free rotation and translation of the dipoles of the (small) solvent molecules (see Section 2.3). Mainly the molecular vibrations of the solute contribute to the internal reorganization energy. The energy spacing of the vibronic levels in general is large compared to the thermal energy; therefore, the solute must be treated quantum mechanically. In the latter case, where $\hbar\omega > k_B T$, the vibrations could be modeled as a system of harmonic classical oscillators and the internal reorganization energy λ_i is represented by:[94,95,99,103,110,111]

$$\lambda_i = \sum_k \frac{f_k^R f_k^P}{f_k^R + f_k^P} \Delta x_k^2 \tag{2.35}$$

where the summation runs over all modes k coupled to the ET. f_k^R and f_k^P are the force constants of mode k in the reactant and the product states, respectively. Δx_k is the change in the equilibrium value of the kth normal mode; for modes uncoupled to ET $\Delta x_k = 0$. In case the geometry is rigid enough, then $f_k^R \approx f_k^P = f_k$, and one arrives at a simplified expression for the internal reorganization energy:

$$\lambda_i = \frac{1}{2} \sum_k f_k \Delta x_k^2 \tag{2.36}$$

Unlike the solvent reorganization energy λ_s, the theoretical evaluation of internal reorganization energy λ_i is well established due to the intensive development of quantum mechanical calculations in recent years. Instead of discrete summation over the solute vibrational modes coupled to ET [Eqs. (2.35) and (2.36)], the present work refers to quantum chemical calculations carried out in our group[73,112] at the B3LYP/6-31G(d) level,[113] where the unrestricted Kohn-Sham method was applied for radical-cation states of the base-pair GC and for estimating λ_i in related ET processes.[114,115] The following quantities were computed for the donor and the acceptor: (1) energies of the neutral species at optimized geometries, $E_0(D)$ and $E_0(A)$, (2) energies of the corresponding radical-cations at optimized geometries, $E_+(D^+)$ and $E_+(A^+)$, (3) energies of neutral D and A, calculated at the geometries of the corresponding radical-cations, $E_+(D)$ and $E_+(A)$, and (4) energies $E_0(D^+)$ and $E_0(A^+)$ of the oxidized states D^+ and A^+ at the geometries of the corresponding neutral molecules. Then λ_i for the charge transfer reaction $D^+ + A \rightarrow D + A^+$ is the sum of the reorganization energies of the donor and the acceptor, $\lambda_i = \lambda_i(D) + \lambda_i(A)$, where D and A were taken as a single GC base-pair (in vacuum). The energies $\lambda_i(X)$, X = D, A, are

$$\lambda_i(X) = [E_+(X) - E_+(X^+) + E_0(X^+) - E_0(X)]/2. \tag{2.37}$$

The resulting internal reorganization energy for ET between isolated GC base-pairs was 0.72 eV.[112] A recent DFT study on λ_i in DNA duplexes corroborated this result: λ_i was shown to decrease with the length of the $(GC)_n$ duplexes from 0.72 eV (n = 1) to 0.34 eV (n = 6).[116] Nevertheless, this model study did not account for the solvent stabilization on the geometry relaxation. Therefore, one may consider the estimate of $\lambda_i = 0.34$ eV as an upper limit for hexamer DNA duplexes, which will be invoked also later on in the present study.

3 Reorganization Energy within the Quantum Picture of ET

3.1 Levich-Marcus-Jortner theory

3.1.1 Uncoupled states

Let us inspect once more Eq. (2.9) from Section 2.2, which is used to describe the ET rate. There the constant A has not been defined so far. The exponential term reflects the probability that the thermally fluctuating system reaches the activated complex (formally the crossing point of the two parabolae in Figure 2.3), where the energy conservation law is fulfilled and CT can take place (see Section 2.2). Assuming that this term, which is a function of $\Delta G°$, has a Gaussian shape distribution, it can be normalized to give:

$$k_{ET} = P \cdot \frac{1}{\sqrt{4\pi\lambda k_B T}} \exp\left[-\frac{(\lambda + \Delta G°)^2}{4\lambda k_B T} \right],$$ (3.1)

where P is a constant. The latter representation implies that, while the Gaussian shape function is responsible for the classical probability to reach the cross-section, the constant P is related to the quantum structure of the solute. Consideration of its quantum structure in the two ET states is bound to the probability of the solute being found either in the initial or in the final state.

In the *non-adiabatic limit*, when nuclear motions are fast compared to the ET time scale, the populations of the electronic levels of the solvent and the solute as well as the intramolecular vibrational states remain in thermal equilibrium during ET.[94,110,117,118] Then,

$$P = \frac{2\pi}{\hbar} \langle H_{fi} \rangle^2,$$ (3.2)

where $\langle H_{fi} \rangle$ is the ET matrix element which reflects orbital mixing between initial and final states.

In the *adiabatic limit*, $\langle H_{fi} \rangle$ is considerable, leading to tight coupling between electron and nuclear coordinates. In the classical approximation, the constant A is then given by the weighted

average of the frequencies of the ET-coupled solvent and solute intramolecular vibrational modes ν_k[94,110,119,120]

$$A = \sqrt{\sum_k \lambda_k \nu_k^2 \Big/ \sum_k \lambda_k} \, , \tag{3.3}$$

where $\lambda_k = \frac{1}{2} \sum_k f_k \Delta x_k^2$ is the energy shift of a classical harmonic oscillator due to the change Δx_k of the equilibrium displacement. There are also other expressions for the constant A relating it to the Debye relaxation time.[121,122]

In the adiabatic and non-adiabatic cases summarized above, it was assumed that the probability for the system to reach the parabolae crossing point and the coupling between the quantum states are independent. This means that there are no coupled high (medium) frequency modes or that the temperature is high ($\lambda_k \nu_k^2 << k_B T$). Actually, modes coupled to ET always exist and must be modeled quantum mechanically in order to include transitions from low-lying vibrational levels (nuclear tunneling) in the description of the process.

Moreover, the above treatment of intramolecular reorganization energy leads to problems with the explanation of its temperature dependence at low temperatures. The Marcus expression predicts that the ET rate constant at the zero temperature limit becomes equal to zero but experimental data[123] at low temperatures demonstrate that the rate constant is essentially temperature-independent. Another problem arises for the inverted region. The classical Marcus formula predicts a symmetric fall-off of the ET rate constant in both regions. This is the result of the Gaussian statistics of the solvent thermal bath that is linearly coupled to ET; this setup leads to the picture of intersecting parabolae with equal curvatures. Whether the curvatures of the free energy surfaces are parabolic or not, was intensively investigated.[124] It was found in general that free energy dependence has a distorted bell shape with a steeper slope in the normal
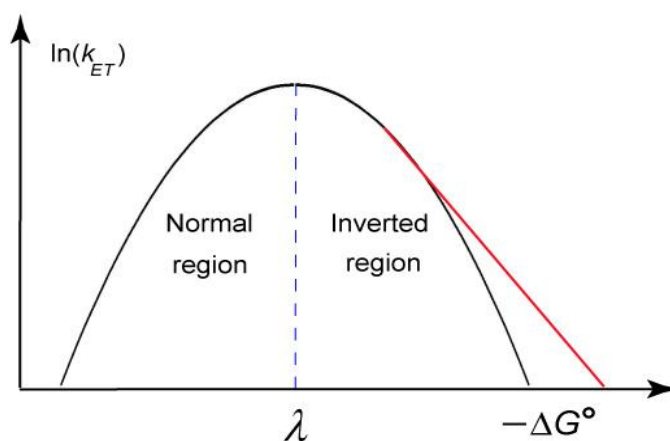
Figure 3.1. ET rate dependence. Schematic comparison of Marcus symmetric bell-shape (black curve) and asymmetric picture with linear dependence on $\Delta G°$ in inverted region (red curve).

region (see Figure 3.1). The bell shape due to the Marcus picture is observed only in the vicinity of the maximum, while away from it in the inverted region the fall-off is linear, in accordance with vibronic models.[125,126] One of the explanations proposed is that in the inverted region preferential transitions to excited vibrational states occur, requiring the inclusion of the quantum structure of the donor-acceptor complex in addition to taking into account solvent fluctuations.

3.1.2 Coupled states

The ET rate can also be addressed from a more general perspective invoking the "Golden Rule" of quantum mechanics, which relates the probability of a change of state per time unit to a transition matrix element:

$$k_{ET} = \frac{2\pi}{\hbar} \left\langle \Psi_i \left| \hat{H}_{fi} \right| \Psi_f \right\rangle^2 \delta\left(E^i - E^f \right) \tag{3.4}$$

Here Ψ_i, Ψ_f are the wave functions of the initial and final states (with eigenvalues E^i, E^f), respectively, and $\hat{H}_{fi}$ is the perturbation that induces the transition. The Dirac delta function ensures that the energy is conserved when the transition takes place. This "Golden Rule" is applicable only in case of weak coupling where the perturbation is small and the transition probability is low.

Application of the Born-Oppenheimer and Condon approximations leads to a partitioning of the total wave functions into an electronic and a nuclear part[102,127,128]

$$k_{ET} = \frac{2\pi}{\hbar} \left\langle \psi_{el}^f \left| \hat{H}_{fi} \right| \psi_{el}^i \right\rangle^2 \left\langle \psi_{vib}^f \left| \psi_{vib}^i \right\rangle^2 \delta\left(E^i - E^f \right), \tag{3.5}$$

where $\psi_{vib}^i, \psi_{vib}^f$ are total vibrational wave functions for the initial and final states and ψ_{el}^i, ψ_{el}^f are their electronic counterparts. The former are products of the wave functions of all normal modes including collective solvent vibrations[129,130]

$$\psi_{vib}^i = \prod_k \chi_{v_k^i}^i \tag{3.6}$$

$$\psi_{vib}^f = \prod_k \chi_{v_k^f}^f \tag{3.7}$$

Here $\chi_{v_k}^i$ and $\chi_{v_k}^f$ are the wave functions of mode k in the initial and final states with the corresponding quantum numbers $v_k^i = E_k^i/\hbar\omega_k$ and $v_k^f = E_k^f/\hbar\omega_k$.

If one assumes that during ET the characteristic frequencies ω_k of the harmonic oscillators are preserved and only the quantum numbers are changed from v_k^i to v_k^f, the vibrational overlap integrals have the form[128,129]

$$\left\langle \chi_{\nu_k^f}^f \middle| \chi_{\nu_k^i}^i \right\rangle = \exp\left(-S_k\right) S_k^{\left(\nu_k^f - \nu_k^i\right)} \frac{\nu_k^i!}{\nu_k^f!} \left[L_{\nu_k^i}^{\left(\nu_k^f - \nu_k^i\right)}\left(S_k\right) \right]^2 , \tag{3.8}$$

with L being a Laguerre polynomial:

$$L_{\nu_k^i}^{\left(\nu_k^f - \nu_k^i\right)}\left(S_k\right) = \sum_{\nu=0}^{\nu_k^i} \frac{\nu_k^f!\left(-S_k\right)^\nu}{\left(\nu_k^i - \nu\right)!\left(\nu_k^f - \nu_k^i + \nu\right)!} . \tag{3.9}$$

S_k is the electron-vibrational coupling constant, also referred to as Huang-Rhys factor: [129,131]

$$S_k = \frac{1}{2}\left(\frac{M_k \omega_k}{\hbar}\right)\left(\Delta x_k\right)^2 \tag{3.10}$$

with the reduced mass M_k of the oscillator k and the corresponding characteristic frequency ω_k. Δx_k is the displacement of that mode. The vibrational overlap integrals account for the extent to which the final and initial states are similar along a normal coordinate.

The vibronic levels of a system in the ground state are populated non-uniformly with probability

$$p\left(\nu_k^i\right) = \frac{\exp\left(-\dfrac{\nu_k^i \hbar \omega_k}{k_B T}\right)}{Z_k} , \tag{3.11}$$

with vibrational partition function

$$Z_k = \sum_{\nu_k^i} \exp\left(-\left(\nu_k^i + \frac{1}{2}\right)\frac{\hbar \omega_k}{k_B T}\right) . \tag{3.12}$$

If $\hbar \omega_k \gg k_B T$, then only the lowest energy level $\nu_k^i = 0$ is populated, allowing a simplified form of the overlap integral

$$\left\langle \chi_{\nu_k^f}^f \middle| \chi_{\nu_k^i=0}^i \right\rangle = \exp\left(-S_k\right) S_k^{\nu_k^f} \frac{1}{\nu_k^f!} \tag{3.13}$$

Modes, which are coupled to ET, have $S_k \neq 0$ or $\hbar \omega_k \neq \hbar \omega_k'$; in all other cases, i.e. if $\hbar \omega_k = \hbar \omega_k'$, these integrals in Eq. (3.13) are equal to 1. As the system moves from the initial to the final state, the sum of all possible changes in Δx_k reflects the geometrical change of the whole solute structure upon ET. These ET-coupled modes are responsible for the electronic absorption and emission band shapes, as well as for overcoming the ET energy barrier. All other modes are not involved in ET. Quantum energy levels of the solvent modes related to charge transfer are normally very closely spaced, i.e. they form a continuum and, hence, the solvent could be treated classically.

Summarizing all these issues concerning the application of the "Golden rule", one ends up with the formula:[94,118,127,132]

$$k_{ET} = \frac{2\pi}{\hbar} \frac{\left\langle \psi_{el}^f \middle| \hat{H}_{fi} \middle| \psi_{el}^i \right\rangle^2}{\sqrt{4\pi\lambda_s k_B T}} \prod_k \sum_{v_k} \sum_{v_{k'}} p(v_k) \left\langle \chi_{v_{k'}} \middle| \chi_{v_k} \right\rangle \exp\left[-\frac{\left(\Delta G^\circ + \sum_k \left(v_{k}^{'} - v_k \right) \hbar\omega_k + \lambda_s \right)^2}{4\lambda_s k_B T} \right] \tag{3.14}$$

which describes ET through a series of vibrational channels from a set of initial levels v_k to a set of final ones v_k'. The solvent is treated classically and included in the exponential distribution function. Frequency changes in the solvent modes due to ET and low-frequency vibrations of the solute are part of ΔG°.[94,132,133]

In the classical limit where $\hbar\omega_k \ll k_B T$ and the partitioning of the reorganization energy $\lambda = \lambda_s + \lambda_i$ is valid,[94,110] the expression for the ET rate constant, Eq. (3.14), simplifies to standard Marcus expression:

$$k_{ET} = \frac{2\pi}{\hbar} \frac{\left\langle \psi_{el}^f \middle| \hat{H}_{fi} \middle| \psi_{el}^i \right\rangle^2}{\sqrt{4\pi\lambda k_B T}} \exp\left[-\frac{\left(\Delta G^\circ + \lambda \right)^2}{4\lambda k_B T} \right]. \tag{3.15}$$

If only one medium- or high-frequency mode is coupled to ET, then only the lowest vibrational level $v_k^i = 0$ is appreciably populated at room temperature, leading to the expression:[94,110]

$$k_{ET} = \frac{2\pi}{\hbar} \frac{\left\langle \psi_{el}^f \middle| \hat{H}_{fi} \middle| \psi_{el}^i \right\rangle^2}{\sqrt{4\pi\lambda_s k_B T}} \sum_{v'} \exp(-S) \frac{S^{v'}}{v'!} \exp\left[-\frac{\left(\Delta G^\circ + v'\hbar\omega_k + \lambda_s \right)^2}{4\lambda_s k_B T} \right]. \tag{3.16}$$

In the latter approximation for the ET rate constant there is no contribution of the vibrational channels to the temperature dependence of the process, since the only involved reaction channels originate from the ground state $v_k^i = 0$, which is always populated. If there are coupled low-frequency vibrations, they can be treated classically and included in Eq. (3.16) by replacing λ_s with $\lambda_{s,L}$ defined by:

$$\lambda_{s,L} = \lambda_s + \sum_l S_l \hbar\omega_l , \tag{3.17}$$

where the summation is performed over the coupled modes.

In the adiabatic limit the frequency factor is controlled by repopulation of a few dominant reaction channels at the crossing point rather than by electronic coupling[134] and the total rate constant cannot exceed the rate feasible through the fastest channel.[134]

If one assumes that only one mode with characteristic frequency $\omega_k = \omega$ and structural factor $S_k = S$ is coupled to ET, then one obtains an approximately linear dependence of $\ln(k_{ET})$ on ΔG° in the inverted region. In this case, the transition is between ground vibrational levels of the initial and the final states ($v' = 0$) and a thermally induced barrier crossing is not necessary. In the limit where $-\Delta G^\circ \gg S\hbar\omega$ and $\hbar\omega \gg k_B T$, one derives an approximate expression for the rate constant of ET:[135,136]

$$k_{ET} = \frac{2\pi}{\hbar} \frac{\left\langle \psi_{el}^f \left| \hat{H}_{fi} \right| \psi_{el}^i \right\rangle^2}{\sqrt{\hbar\omega\left(\left|\Delta G^\circ\right| - \lambda_s\right)}} \exp\left[-S - \frac{\gamma\left(\left|\Delta G^\circ\right| - \lambda_s\right)}{\hbar\omega} + \left(\frac{\gamma+1}{\hbar\omega}\right)^2 \lambda_s k_B T\right], \qquad (3.18)$$

with

$$\gamma = \ln\left[\frac{\left|\Delta G^\circ\right| - \lambda_s}{S\hbar\omega}\right] - 1, \qquad (3.19)$$

This expression indeed yields a linear decrease of $\ln(k_{ET})$ with ΔG°. As discussed in Section 2.2, Eq. (3.15) reveals that the ET rate constant reaches a maximum at $\Delta G^\circ = -\lambda$ and then decreases with increasing $-\Delta G^\circ$ in the inverted region; see the black line in Figure 3.1. The latter phenomenon was predicted by Marcus and also incorporated into the above semi-quantum theory.[137,138]

Nevertheless, theories which combine Gaussian statistics of the solvent nuclear fluctuations with Poisson statistics of the quantum skeletal vibrations predict that in a charge separation (CS) reaction (when a pair of opposite charges appears) and charge recombination (CR) (when a pair of two opposite charges disappears) states the logarithmic dependence of ET rate on the energy gap is still symmetric, which is not observed in experiments performed by Mataga.[124c-g] Simulation of free energy surfaces taking into account effects of non-linear solvation on the CT thermodynamics[4,92,107,139,140] and dynamics[141] demonstrated much smaller distortions of the parabolic shapes of free energy surfaces than those observed experimentally.[124c-g,142] To rationalize the deviations of the theory from experiment, a new model was introduced which is based on the idea that classical ET theories do not consider solute electron density polarization effects, which are significantly larger than non-linear solvation effects.[143,144] In addition, the model accounts for the solvent polarization effects.

3.2   Harmonic bath model

3.2.1   *General approach*

The molecular system sometimes has insufficient kinetic energy to reach the transition state, i.e. the crossing point of the two parabolic potential energy surfaces in the Marcus's picture, Figure 2.3. In that case, tunneling effects become of primary importance for ET to take place. Tunneling processes occur because there is always a non-zero probability for the electronic wave functions to spread beyond the classical turning points. Taking into account nuclear tunneling effects can lead to substantial changes in ET rates either at low temperatures or at high temperatures in the inverted region.[145]

Several approaches have been suggested to include nuclear tunneling effects. One of them has been demonstrated in Section 3.1, where we split all vibrational modes into two parts and treated only a few high-frequency vibrations with the formalism of quantum mechanics. The second part, containing low-frequency modes, could also be described but only as a classical continuum.[126,127]

Another more general approach, which incorporates all frequency modes, is usually known as 'dispersed-polaron'[4,5] or 'spin-boson model'.[5] Warshel first suggested such a scheme[5] where he also demonstrated that the two formulations are identical.[146] The subsequent discussion follows his scheme.[147]

Consider a system of donor (D) and acceptor (A) molecules surrounded by a solvent. The distance between D and A will be kept constant. Assume at the beginning that the molecular vibrations of these two entities are frozen. The time-dependent wave function of the system can be approximated as a product of donor, acceptor and solvent functions:

$$\Psi^i = \psi_{D^+} \cdot \psi_A \cdot \psi_{solvent}^i \tag{3.20}$$

$$\Psi^f = \psi_D \cdot \psi_{A^+} \cdot \psi_{solvent}^f \tag{3.21}$$

where indices *i* and *f* reflect initial and final electronic states of the molecules, respectively.

The effective electronic Hamiltonian for the relevant states, which neglects charge transfer interactions between the solvent and solute molecules, can be written as

$$\hat{H}\left(\vec{R}(t), \vec{r}(t)\right) = \begin{pmatrix} U_{ii} & H_{if} \\ H_{fi} & U_{ff} \end{pmatrix}, \tag{3.22}$$

where $\vec{R}(t)$ and $\vec{r}(t)$ represents the coordinates of the DA system and the solvent molecules, respectively. U_{ii} and U_{ff} are the zero-order diabatic energies of Ψ^i and Ψ^f. These energies could be approximated by semi-empirical potential functions,[148] which describe the energy of the given charged forms of the particular solute state (either DA^+ or D^+A) in a specific solvent. These potential functions include interactions within the D-A system as well as with solvent-induced dipoles. The off-diagonal term $H_{if} = H_{fi}$ is composed of the mixed matrix elements in the absence of the solvent $\left\langle \psi_D \psi_{A^+} \middle| \hat{H} \middle| \psi_{D^+} \psi_A \right\rangle$. As an alternative, $\hat{H}$ can also be an empirical valence bond Hamiltonian from MD simulations.

For convenience, further on the double subscripts *ii* and *ff* of the diagonal elements shall be simplified to

$$U_i = \left\langle \Psi^i \middle| \hat{H} \middle| \Psi^i \right\rangle \tag{3.23}$$

$$U_f = \left\langle \Psi^f \middle| \hat{H} \middle| \Psi^f \right\rangle \tag{3.24}$$

To evaluate the rate constant of ET from state *i* to state *f*, one has to start from the probability of ET during a period of time τ, which is related to the time-dependent wave function. The latter can be represented as

$$\Psi(t) = C_i(t)\Psi_i \exp\left[-\frac{i}{\hbar}\int_0^t U_i(t')dt'\right] + C_f(t)\Psi_f \exp\left[-\frac{i}{\hbar}\int_0^t U_f(t')dt'\right]. \tag{3.25}$$

Invoking the time-dependent Schrödinger equation for $\hat{H}$ and substituting the expression for the time-dependent wave function into it:

$$i\hbar\frac{\partial\Psi(t)}{\partial t} = \hat{H}\Psi(t), \tag{3.26}$$

one obtains two differential equations for the amplitudes C_i and C_f

$$\frac{\partial C_i(t)}{\partial t} = -i\frac{H_{fi}}{\hbar}C_f(t)\exp\left[\frac{i}{\hbar}\int_0^t \Delta U_{fi}(t')dt'\right] \tag{3.27}$$

$$\frac{\partial C_f(t)}{\partial t} = -i\frac{H_{fi}}{\hbar}C_i(t)\exp\left[-\frac{i}{\hbar}\int_0^t \Delta U_{fi}(t')dt'\right] \tag{3.28}$$

where $\Delta U_{fi} = U_f - U_i$. In the non-adiabatic approximation, one neglects the terms $\langle\Psi^i|\partial\Psi^f/\partial t\rangle$, $\langle\Psi^f|\partial\Psi^i/\partial t\rangle$. Assuming the hole initially, at $t = 0$, to be located at D results in the initial conditions $C_i(0) = 1$, $C_f(0) = 0$. For the time range where $C_i \approx 1$, one obtains

$$C_f(\tau) = -i\frac{H_{fi}}{\hbar}\int_0^\tau \exp\left[-\frac{i}{\hbar}\int_0^t \Delta U_{fi}(t')dt'\right]dt. \tag{3.29}$$

If $\tau\cdot H_{fi}/\hbar \ll 1$, then C_i changes fast in time. Then one has to invoke the adiabatic approximation[149] which results in an expression for the amplitude in the final state:

$$C_f(\tau) = -\int_0^\tau \left\langle\Psi^f\left|\frac{\partial\Psi^i}{\partial t}\right\rangle\exp\left[-\frac{i}{\hbar}\int_0^t \Delta U_{fi}(t')dt'\right]dt \tag{3.30}$$

Finally, one can write an approximate expression for the rate constant:

$$k_{ET} = \lim_{\tau\to\infty}\frac{|C_f(\tau)|^2}{\tau}. \tag{3.31}$$

Eq. (3.31) was derived by assuming that at an arbitrarily chosen initial moment $t = 0$, the electron is located at the donor $C_i(t) = 1$. In order to obtain a rate constant independent of the choice of the initial conditions, one has to introduce ensemble averaging over all possible initial conditions $C_i(t)$. According to the ergodic hypothesis, one may replace an ensemble average over the whole phase space, i.e. over all initial coordinates *r* and momenta *p*, by an average along a classical MD trajectory. Therefore, one can write

$$k_{ET} = \lim_{\tau \to \infty} \frac{\left\langle \left| C_f(\tau) \right|^2 \right\rangle_0}{\tau},$$ (3.32)

where $\langle ... \rangle_0$ denotes the ensemble average.

One may invoke the Wiener-Khintchine theorem[150] to represent k_{ET} through the autocorrelation function of the amplitude derivative $\dot{C}_f$ as:

$$k_{ET} = \lim_{\tau \to \infty} \frac{\left\langle \left| \int_0^\tau \dot{C}_f(t) dt \right|^2 \right\rangle_0}{\tau} = \lim_{\tau \to \infty} \int_0^\tau \left\langle \frac{1}{\tau} \int_{-t}^{\tau-t} \dot{C}_f(t) \dot{C}_f(t+\tau) dt \right\rangle_0 dt.$$ (3.33)

Using the fact that for ergodic systems the correlation function is given by the corresponding ensemble average, one arrives at:

$$k_{ET} = \lim_{\tau \to \infty} \int_0^\tau \left\langle \dot{C}_f(t) \dot{C}_f(t+\tau) \right\rangle_0 dt.$$ (3.34)

Substituting the expression for the coefficients C_f one obtains:

$$k_{ET} = \left| \frac{\left\langle H_{fi} \right\rangle}{\hbar} \right|^2 \int_{-\infty}^{\infty} \exp\left(it \frac{\left\langle \Delta U_{fi} \right\rangle_0}{\hbar} \right) \cdot \exp\left[\frac{i}{\hbar} \int_0^t \delta \Delta U_{fi}(t') dt' \right] dt,$$ (3.35)

where

$$\delta \Delta U_{fi}(t) = \Delta U_{fi}(t) - \left\langle \Delta U_{fi} \right\rangle_0.$$ (3.36)

In Appendix A it is shown that the last expression in Eq. (3.35) can be transformed to

$$\gamma(t) = \exp\left[\frac{i}{\hbar} \int_0^t \delta \Delta U_{fi}(t') dt' \right],$$ (3.37)

$$\approx -\frac{1}{\hbar^2} \int_0^t dt'(t-t') \left\langle \delta \Delta U_{fi}(0) \delta \Delta U_{fi}(t') \right\rangle_0$$ (3.38)

Finally, one obtains the rate constant k_{ET} as

$$k_{ET} \approx \left| \frac{\left\langle H_{fi} \right\rangle}{\hbar} \right|^2 \int_{-\infty}^{\infty} \exp\left(it \frac{\left\langle \Delta U_{fi} \right\rangle_0}{\hbar} + \gamma(t) \right) dt.$$ (3.39)

This expression dates back to the works of Lax[151] and Kubo[152] in solid-state physics, addressing non-radiative transitions of an electron trapped in a crystal lattice. That earlier model is based on an exact quantum mechanical formula for the electron transfer in a multidimensional harmonic system.[5]

3.2.2 Harmonic approximation

Let us inspect the parameter $\gamma(t)$ for the case of a molecular system that comprises several harmonic oscillators. The initial and final potentials of the system in semi-classical approximation are given as:

$$U_i(t) = \frac{1}{2}\sum_j \hbar\omega_j q_j^2 \tag{3.40}$$

$$U_f(t) = \frac{1}{2}\sum_j \hbar\omega_j \left(q_j - \Delta x_j\right)^2 + \Delta U_{fi}^0, \tag{3.41}$$

where q_j is the dimensionless displacement coordinate of oscillator j in an arbitrarily chosen moment t of the initial state i. Here, it is assumed that the transfer of an electron to the final state f does not distort the frequencies ω_j of the harmonic oscillators. The quantity ΔU_{fi}^0 represents the potential energy difference between the equilibrium configurations of the oscillators.

To carry out the ensemble average (rhombic brackets) of the potential energy gap between two states, one assumes that an available trajectory is long enough to represent an ensemble average:

$$\left\langle \Delta U_{fi}(t)\right\rangle_0 = -\sum_j \hbar\omega_j q_j \left\langle \lambda_j\right\rangle_0 + \frac{1}{2}\sum_j \hbar\omega_j \left\langle \Delta x_j^2\right\rangle_0 + \left\langle \Delta U_{fi}^0\right\rangle_0 = \frac{1}{2}\sum_j \hbar\omega_j \left\langle \Delta x_j^2\right\rangle_0 + \Delta U_{fi}^0 \tag{3.42}$$

Therefore, according to the earlier definition Eq. (3.36)

$$\delta\Delta U_{fi}(t) = -\sum_j \hbar\omega_j q_j \Delta x_j + \frac{1}{2}\sum_j \hbar\omega_j \Delta x_j^2 - \frac{1}{2}\sum_j \hbar\omega_j \left\langle \Delta x_j^2\right\rangle_0 \tag{3.43}$$

Introducing the coordinates $\tilde{q}_j = \sqrt{2\tilde{n}_j + 1}\cos\left(\omega_j t + \theta_j\right)$, where $\tilde{n}_j + \dfrac{1}{2} = \dfrac{E_j}{\hbar\omega_j}$, one obtains the autocorrelation function in the form

$$\left\langle \delta\Delta U_{fi}(0)\delta\Delta U_{fi}(t)\right\rangle_0 = \hbar^2 \sum_j \Delta x_j^2 \omega_j^2 \left(\tilde{n}_j + \frac{1}{2}\right)\cos\left(\omega_j t\right). \tag{3.44}$$

Then the expression for $\gamma(t)$ becomes

$$\gamma(t) = \sum_j \Delta x_j^2 \left(\tilde{n}_j + \frac{1}{2}\right)\left(\cos\left(\omega_j t\right) - 1\right), \tag{3.45}$$

where $\tilde{n}_j$ is the average occupation number of an oscillator at a given temperature

$$\tilde{n}_j = \frac{1}{\exp\left(\hbar\omega_j / k_B T\right) - 1}. \tag{3.46}$$

Finally, the expression for quantum ET rate is

$$k_{ET} \approx \left| \frac{\langle H_{fi} \rangle}{\hbar} \right|^2 \int_{-\infty}^{\infty} \exp\left(it \frac{\langle \Delta U_{fi} \rangle_0}{\hbar} + \sum_j \Delta x_j^2 \left(\tilde{n}_j + \frac{1}{2} \right) \left(\cos(\omega_j t) - 1 \right) \right) dt \qquad (3.47)$$

The latter formula, derived after a series of approximations, is close to the exact quantum mechanical solution for a harmonic case, obtained by Kubo.[152]

Next, one evaluates k_{ET} for the high-temperature limit, where $\tilde{n}_j \sim k_B T / \hbar \omega_j \gg 1$ and

$$\tilde{n}_j = \frac{1}{\exp(\hbar \omega_j / k_B T) - 1} \approx \frac{k_B T}{\hbar \omega_j} . \qquad (3.48)$$

Expansion of the exponential phase (cosine- and sine-containing terms) up to t^2 yields:

$$k_{ET} \approx \left| \frac{\langle H_{fi} \rangle}{\hbar} \right|^2 \int_{-\infty}^{\infty} \exp\left(it \left(\frac{\langle \Delta U_{fi} \rangle_0 + \frac{1}{2} \sum_j \hbar \omega_j \Delta x_j^2}{\hbar} \right) + t^2 \frac{k_B T}{\hbar^2} \frac{1}{2} \sum_j \hbar \omega_j \Delta x_j^2 \right) dt . \qquad (3.49)$$

Recalling that the integral

$$I = \int_{-\infty}^{\infty} \exp(i \omega t) \exp(-a t^2) dt = \left(\frac{\pi}{a} \right)^{1/2} \exp\left(-\frac{\omega^2}{4a} \right), \qquad (3.50)$$

one arrives at the famous Marcus expression,

$$k_{ET} \approx \left| \frac{\langle H_{fi} \rangle}{\hbar} \right|^2 \left(\frac{\pi}{\frac{k_B T}{\hbar^2} \frac{1}{2} \sum_j \hbar \omega_j \Delta x_j^2} \right)^{\frac{1}{2}} \exp\left(-\frac{\left(\langle \Delta U_{fi} \rangle_0 + \frac{1}{2} \sum_j \hbar \omega_j \Delta x_j^2 \right)^2}{4 k_B T \frac{1}{2} \sum_j \hbar \omega_j \Delta x_j^2} \right) \qquad (3.51)$$

Comparing to Eq. (3.15), one reads off the reorganization energy as:

$$\lambda = \frac{1}{2} \sum_j \hbar \omega_j \Delta x_j^2 . \qquad (3.52)$$

In other words, the reorganization energy is the sum of the energies of the harmonic oscillators at average displacements of those modes which are coupled to the ET reaction. If the electronic coupling strength H_{fi} is known, records of $\Delta U_{fi}(t)$ from MD trajectories provide all the information needed to obtain the rate constant and its temperature dependence. MD simulations can supply the frequencies and the displacements in the so-called Huang-Rhys factors [see Eq. (3.10)] of the vibrational modes that are coupled to the reaction coordinate.

In the present thesis one of the methods for calculating the solvent reorganization energy employs formalism similar to Eq. (3.52). The methodological part, which describes how essentially non-harmonic vibrations of atoms from MD trajectories can be used as a source of a harmonic approximation, is given in Chapter 4. The application of that method for a simplified solute model is described in Chapter 6.

3.3   Q-model

Relatively recently[153] an alternative to the Marcus scheme[102,154] was proposed where the quantum part accounts for internal molecular vibrations of the solute.[126,155,156] According to the former Marcus-Levich-Jortner (MLJ) theory, discussed in Section 3.1, one distinguishes two regions: the normal one with a parabolic rate constant/energy gap dependence and the inverted region with linear-logarithmic variation of k_{ET} with the free energy difference between initial and final states. The MLJ theory combined Gaussian statistics for molecular fluctuations of the solvent and for the vibrational excitations of the solute, but kept the main assumption of Marcus theory which claims that solvent and solute vibrations are coupled linearly.

In the early days of ET theory the linear coupling between solute and solvent was seriously questioned and a quadratic dependence was suggested.[152,157,158] In the following, the latter theory is referred to as Q-model (Q for quadratic coupling), where oscillators are coupled to ET with different force constants. A general solution to this problem was given by Kubo and Toyozawa.[152] Application of that theory was hindered by the fact that the ET rate is not expressed analytically through free energy surfaces $G_{i,f}$ as a function of the potential energy gap between final and initial states of ET, which can be determined in MD simulations.

To interpret kinetic data adequately, alternative approaches to non-linear solvation were suggested where free energy surfaces with parabolic shapes of *different* curvatures were invoked.[124c-g,159] The underlying hypothesis, originally introduced by Kakitani and Mataga,[124c-g] was that dielectric saturation of the first solvation shell in a charge separated (CS) state makes the curvature of the free energy function much larger than in the charged recombined (CR) state. However, Tachiya[106,107] and Warshel[97c,92,160] refuted those approaches as they were able to demonstrate that the free energy surfaces of the final and the initial states are coupled in linear fashion

$$G_f\left(\Delta U_{fi}\right) = G_i\left(\Delta U_{fi}\right) + \Delta U_{fi} \tag{3.53}$$

through the reaction coordinate ΔU_{fi} which is the potential energy gap between the initial and the final states. The result, first obtained by Warshel, is based on the transformation of the statistical probability for the instantaneous potential energy difference between two states ΔU, picked up along the trajectory, to have a particular value of the reaction coordinate ΔU_{fi}.[160]

$$\left\langle \delta\left(\Delta U_{fi} - \Delta U\right)\right\rangle_f = \left\langle \delta\left(\Delta U_{fi} - \Delta U\right)\right\rangle_i \exp\left(\left(\Delta G_0 - \Delta U_{fi}\right)/k_B T\right). \tag{3.54}$$

Consider two electronic states of the D-A complex which are harmonically coupled to a collective solvent coordinate q with the different force constants k_i and k_f for the initial and final states, respectively (see Section 2.1):

$$U_i = I_i - C_i q - \frac{1}{2} k_i q^2 \tag{3.55}$$

$$U_f = I_f - C_f q - \frac{1}{2} k_f q^2 \tag{3.56}$$

where $I_{i,f}$ represent the sum of the electronic energies of the solute in vacuum and the solvation free energies.[153] The parameter C_i defines the strength of linear solute-solvent coupling, similar to Marcus assumptions. The collective coordinate q driving the electronic transition can be projected out from a microscopic liquid-solvent Hamiltonian or represented as a linear combination of harmonic degrees of freedom characterized by spectral density functions.[6b] Thus, the reaction coordinate ΔU_{fi} can be defined as

$$\Delta U_{fi} = \Delta I - \Delta C q - \frac{1}{2} \Delta k q^2, \tag{3.57}$$

where, $\Delta I = I_f - I_i$, $\Delta C = C_f - C_i$ and $\Delta k = k_f - k_i$, respectively. The δ-function in Eq. (3.61) can be represented as a Fourier integral

$$\delta\left(\Delta U_{fi}\right) = \int_{-\infty}^{\infty} \frac{d\xi}{2\pi} \exp\left(i\xi \Delta U_{fi}\right). \tag{3.58}$$

Substituting this expression in Eq. (3.54) and integrating over q (for details see Ref. 153) yields

$$e^{-G_i\left(\Delta U_{fi}\right)+G_{0i}/k_B T} \approx \int_{-\infty}^{\infty} \frac{d\xi}{2\pi} e^{\Phi_i\left(\xi, \Delta U_{fi}\right)}. \tag{3.59}$$

where

$$G_{0i} = I_i - \frac{C_i^2}{2k_i} \tag{3.60}$$

is the equilibrium energy of state i and

$$\Phi_i\left(\xi, \Delta U_{fi}\right) = \frac{i\xi\left(\Delta U_{fi} - \Delta U_{fi}^0\right)}{k_B T} - \frac{\xi \lambda_i \alpha_i^2}{k_B T\left(\xi - \alpha_i\right)}. \tag{3.61}$$

is a generating function. The latter formulation is advantageous in Eq. (3.59) because it can always be expanded as a series in powers of ξ instead of the common practice to employ truncated polynomials for the generation of non-parabolic free energy surfaces.[101,161] The solvent reorganization energy λ_s^i in state i is defined as the second cumulant of the reaction coordinate

$$\lambda_s^i = -\frac{1}{2k_B T} \frac{\partial^2 \Phi_i\left(\xi, 0\right)}{\partial \xi^2}\bigg|_{\xi=0} = \frac{\left\langle \delta \Delta U_{fi}\right\rangle_i^2}{2k_B T}, \tag{3.62}$$

where $\delta \Delta U_{fi}$ is defined as in Eq. (3.36).

The reorganization energy given by Eq. (3.62) is obtained in a straightforward way by averaging over the equilibrium configurations from computer simulations. In order to evaluate the reorganization energy according to Eq. (3.62) one needs to record only the standard deviation of the potential energy gap ΔU_{fi} from its average value along MD trajectories. The reorganization energies λ_s for the initial and final states are not identical as in the standard model of Marcus and are related to each other through the following equations:

$$\alpha_i^3 \lambda_s^i = \alpha_f^3 \lambda_s^f \tag{3.63}$$

$$\alpha_f = \alpha_i + 1, \tag{3.64}$$

where $\alpha_i = k_i/\Delta k$. Eqs. (3.63)–(3.64) reduce the number of independent parameters to three: ΔG_0, α_i and λ_s^i. Compared to the two-parameter model (ΔG_0 and λ) of Marcus-Levich-Jortner, the present Q-model introduces one variable more, which allows more flexibility in terms of a variation of the force constant for the final and initial states, reflecting the difference between fluctuations of the solvent molecules in these states. The standard MLJ theory corresponds to the case when k_i and k_f are equal. The parameter ΔU_{fi}^0 defined through the equilibrium free energy gap $\Delta G_0 = G_{0f} - G_{0i}$ and the reorganization energy λ_s^i can be written as follows:

$$\Delta U_{fi}^0 = \Delta G_0 - \lambda_s^i \frac{\alpha_i^2}{\alpha_f}, \tag{3.65}$$

It defines limitations of the allowed energy fluctuations. This property follows from the asympthotic behavior of the function $\Phi_i(\xi, X)$ and its properties in the complex plane.[153] In contrast, Marcus theory[102,154] leads to an unrestricted band of energy fluctuations where energy gaps of any size can be achieved with non-zero, albeit small, probability.

According to the Q-model, one has to evaluate the complex integral in Eq. (3.59) for ΔU_{fi} values inside the fluctuation band, which includes the essential singularity at $i\alpha_i$. The final analytic expression for ET rates is given[153] by means of the first-order modified Bessel function[162] I_1:

$$k_{ET} = A_i \sqrt{\frac{\lambda_s^i |\alpha_i|^3}{|\Delta U_{fi} - \Delta U_{fi}^0|}} \exp\left[-\left(|\alpha_i| |\Delta U_{fi} - \Delta U_{fi}^0| + \lambda_s^i \alpha_i^2\right)/k_B T\right] \times I_1\left(2\sqrt{|\alpha_i|^3 \lambda_s^i |\Delta U_{fi} - \Delta U_{fi}^0|}/k_B T\right) \tag{3.66}$$

Here, A_i is a normalization factor. The asymptotic expansion[153] of the Bessel function in Eq. (3.66) leads to the free energy potential surfaces which exhibit a linear dependence with respect to the large values of the reaction coordinate ΔU_{fi}. The final free energy surfaces are asymmetric with a steeper branch on the side of the fluctuation boundary ΔU_{fi}^0 and are linearly related to each other as required by the fundamental Eq. (3.60).

All parameters of the Q-model can be evaluated if the solvent reorganization energies $\lambda_s^{i,f}$ are known. One of the computational methods in the next chapters [see method (II) in Section 6.4] is dedicated to an accurate evaluation of the potential energy gaps that define the solvent reorganization energy according to Eq. (3.62).

4 Evaluation of Solvent Reorganization Energy

4.1   Spectral data and methods of simulation

Any ET reaction causes a change in the electronic configuration of the reacting species. According to the Franck-Condon principle, the electronic transition takes place much faster than the motion of the nuclei; therefore, the latter could be regarded as effectively frozen during the transfer. In the electronic state resulting from the fast transition, the surrounding solvent molecules are suddenly subjected to a new electrostatic field and their current configuration becomes unstable. Thus, a subsequent slow nuclear reorientation follows in order to reach the equilibrium that corresponds to the changed solute electron density distribution. In the present chapter a hypothetical solute, which does not undergo any structural changes, as well as only vibronic transitions leading to internal energy conversion, are considered. The change of solvent free energy from the transition ET state to equilibrium is described by the model of Marcus in terms of reorganization energy.[93,99,100] At the point U_θ along the energy surfaces, where the ET takes place (Figure 2.3, Chapter 2), a solvent configuration, which has resulted from a series of particular consecutive thermal fluctuations, serves as the driving force for the reaction. The electronic transition could also occur while the ET complex is in an equilibrium state, but then, in order to facilitate this transition, additional energy must be provided, e.g., through the absorption of light. The latter situation can be used as a rather simple model to illustrate the methods available for describing the charge transfer. If a molecule undergoes an electronic transition through photoexcitation, the subsequent relaxation can be quantified spectroscopically by the Stokes shift,[100,163] which is the difference between the energy of absorption and a selected fluorescence maximum. Comparison with the standard ET picture demonstrates (e.g. see Figure 2.3, Chapter 2) that the energies $\hbar v_1$ of absorption and $\hbar v_2$ of emission (Figure 4.1) can be expressed as follows:

$$\hbar v_1 = \lambda + \Delta G_0 \tag{4.1}$$

$$\hbar v_2 = \lambda - \Delta G_0. \tag{4.2}$$

Therefore, the reorganization energy is half of the Stokes shift:
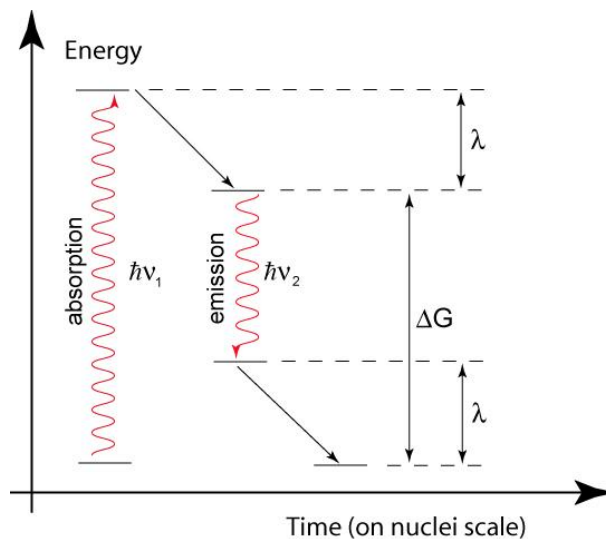
Figure 4.1. Electron transfer reaction through photoexcitation.

$$\lambda = \frac{\hbar\nu_1 - \hbar\nu_2}{2} = \frac{\hbar\Delta\nu_{St}}{2} .$$
(4.3)

This expression for the reorganization energy is based on an assumption introduced by Marcus that the solvent response is linear and, moreover, the changes in the dielectric polarization of the solvent medium[164] for back (emission) and forward (absorption) reactions are the same. In other words, the reorganization energies for transitions either from the reactant to the product or from the product to the reactant are assumed to be equal.

MD simulations allow one to evaluate the emission and absorption energies in terms of differences between the potential energy surfaces which correspond to the product and the reactant states. Assume that absorption and emission occur in the initial (reactant) and the final (product) states described with the total Hamiltonians H_i and H_f, respectively. Then the absorption and emission energies can be expressed as follows

$$\hbar\nu_{abs} = H_f\left(\vec{R}_R\right) - H_i\left(\vec{R}_R\right)$$
(4.4)

$$\hbar\nu_{em} = H_i\left(\vec{R}_P\right) - H_f\left(\vec{R}_P\right),$$
(4.5)

where the vectors $\vec{R}_R$ and $\vec{R}_P$ represent the total solvent coordinates in the reactant and the product states, respectively. In case of vertical transitions the atomic nuclei are 'seen' by the electrons as "frozen" and therefore, the kinetic energy part of the Hamiltonians before and after the transition are equal. Thus, the difference between the full Hamiltonians could be approximated by the difference between the (total) potential energies:

$$\hbar\nu_{abs} = U_f\left(\vec{R}_R\right) - U_i\left(\vec{R}_R\right) = \Delta U\left(\vec{R}_R\right)$$
(4.6)

$$\hbar \nu_{\text{em}} = U_i\left(\vec{R}_P\right) - U_f\left(\vec{R}_P\right) = -\Delta U\left(\vec{R}_P\right). \tag{4.7}$$

For simplicity we dropped the lower index of the total potential energy; formally a positive sign is ascribed to the potential energy gap $\Delta U = \Delta U_{fi} = U_f - U_i$.

The thermal fluctuations of the coordinates $\vec{R}_R$ and $\vec{R}_P$ reflect specific solvent configurations. To deal with experimentally measured values, one has to average over all possible configurations statistically achieved at a certain temperature according to a Boltzmann distribution. These averages $\Delta U\left(\vec{R}_R\right)$ and $-\Delta U\left(\vec{R}_P\right)$ may be generated by MD simulations which yield an ensemble of snapshots along each of the trajectories, which are interpreted to span the configurational space for the reactant and product states, respectively. Then the final expression for the (solvent) reorganization energy becomes

$$\lambda_s = \frac{-\left\langle \Delta U\left(\vec{R}_P\right)\right\rangle_f + \left\langle \Delta U\left(\vec{R}_R\right)\right\rangle_i}{2}, \tag{4.8}$$

where $\left\langle ... \right\rangle_{i,f}$ denotes averaging over the corresponding trajectory. The quantities of Eq. (4.8) are determined in two steps: (*i*) from two trajectories *R* and *P* (which reflect different ET states of the solute, both in thermal equilibrium with their environment) the corresponding sequences of the potential energy values $U_i\left(\vec{R}_R\right)$ and $U_f\left(\vec{R}_P\right)$ result, see Eqs. (4.6)-(4.7); (*ii*) calculation of the potential energy difference between two ET states for each snapshot from *R* and *P* trajectories. Step (*ii*) is carried out by "twisting" the ET state (reflected in charge distribution of solute) to the different one compared to one for which the snapshot was recordered. To span the configuration space in the sense that a meaningful statistical ensemble is generated, the (classical) MD trajectories have to be run for sufficiently long times. Eq. (4.8) represents the main formula for evaluating the reorganization energy according to the classical picture of Marcus; in the following this approach will be denoted as method (I).

The second method, also referred to as method (II) in the following, is based on an evaluation of the standard deviations of the potential energy gaps according to Eq. (3.62). Method (II) for determining solvent reorganization energies can be derived either from the dispersed polaron model of Warshel[5] or seen as a second cumulant of the reaction coordinate in the Q-model, as shown in Eq. (3.62). Yet, it seems preferable to demonstrate its meaning in the spirit of Tachiya,[165] who provided a detailed derivation in a more general fashion.

The physical origin of Eq. (3.62) also lies in the Marcus approximation of solvent linear response. Consider a thermally driven ET reaction, where the transition occurs at some potential energy value $U^{\neq}$, which is achieved rather frequently due to instantaneous thermal fluctuations. Then, the potential energy of the system can be seen as fluctuating around this value. The fluctuations of the potential energy $\Delta U = U^{\neq} - U$ are of a stochastic nature and it is

obvious to assume that they follow a linear response model and therefore exhibit a Gaussian distribution:

$$\varphi\left(\Delta U\right) = \frac{1}{\sqrt{2\pi\sigma^2}} \exp\left[-\frac{\left(U^{\neq}-U\right)^2}{2\sigma^2}\right], \tag{4.9}$$

where σ is the standard deviation of ΔU.

Comparison with the normalized part of the Marcus formula responsible for the Franck-Condon factors, e.g. as represented in Eq. (3.1), reveals that the solvent reorganization energy can be expressed by Eq. (3.62). If one determines the reorganization energy via the standard deviation of the potential energy gap, one does not necessary have to assume that the values of λ_s are equal for the forward and the back reactions.

A third method for estimating λ_s, referred to as method (III), is in general tightly related to method (II) but provide more information as it yields insight into the structure of the fluctuations of the potential energy gap. The method allows one to identify the vibrational modes that drive the ET reaction and even to determine their relative contributions. The method goes back to the dispersed polaron model,[5] which relates the non-harmonic vibrations of the real system to a system of harmonic oscillators.

From the viewpoint of molecular dynamics, the fluctuations of the solute-solvent interaction potential are caused by the (quasi-random) movements of the point charges assigned to each of the solvent atoms. The motion of these point charges could be treated as composed of different vibrational, translational and rotational contributions. To get insight into how the quantity λ_s is formed from contributions of the various modes, it is convenient to invoke the formalism of time correlation functions (TCF) of the solute-solvent potential.

The main idea behind the TCF formalism given below is that the fluctuations of the energy gap ΔU_{fi} along an MD trajectory of a real system in electronic state i (either charge separation, CS, or charge recombination, CR) can be related to the fluctuations of an equivalent harmonic system via the autocorrelation function

$$A_i\left(t\right) = \left\langle \delta U_{fi}\left(t+\tau\right)\delta U_{fi}\left(\tau\right)\right\rangle_i, \tag{4.10}$$

where $\delta U_{fi}\left(t\right) = \Delta U_{fi}\left(t\right) - \left\langle\Delta U_{fi}\left(t\right)\right\rangle_i$ is the deviation of the energy gap fluctuation from its thermal average. The exact expression for the autocorrelation function $A_i(t)$ of a harmonic system is given by Eq. (3.44). According to the Wiener-Khintchine theorem,[150] the magnitude of the Fourier transform of the autocorrelation function is the power spectrum $J\left(\omega\right)/\omega$ of the fluctuations

$$\frac{J\left(\omega\right)}{\omega} = \int\limits_{-\infty}^{\infty} A_i\left(t\right)\exp\left(-i\omega t\right)dt. \tag{4.11}$$

The autocorrelation function of the energy fluctuations of a particle that is coupled linearly to a large number of harmonic oscillators is

$$A_i(t) = \frac{1}{2}\sum_j \coth\left(\frac{\hbar\omega_j}{2k_B T}\right)\left(\hbar\omega_j\Delta x_j\right)^2 \cos\left(\omega_j t\right) \tag{4.12}$$

Here ω_j is the frequency of vibrational mode j of the system and Δx_j is the dimensionless displacement of the normal coordinate. In spite of the fact that some modes could be highly non-harmonic, the overall response of a large molecular system, like DNA or proteins, which have numerous vibrational modes, is expected to be linear. In other words, it is identical to the response of a multidimensional harmonic system.[5,152,166] While the autocorrelation function $A_i(t)$ of Eq. (4.13) differs from the more exact formulation given by Kubo[152] and Lax,[151] both forms of the autocorrelation function transform at high temperatures into [see Eq.(3.48)]:

$$A_i(t) = k_B T\sum_j \hbar\omega_j\Delta x_j^{\,2}\cos\left(\omega_j t\right) \tag{4.13}$$

Fourier transformation (FT) given by Eq. (4.12) of the above equation in the high-temperature limit yields

$$\frac{J(\omega)}{\omega} = \pi k_B T\sum_j \hbar\omega_j\Delta x_j^{\,2}\delta\left(\omega-\omega_j\right). \tag{4.14}$$

The Fourier image of $A_i(t)$ picks out the vibrational modes, which are coupled to the ET reaction because they feature significant nuclear displacements Δx_j between the reactant and product states, which results in a larger contribution to the power spectrum. Integration of the power spectrum produces the solvent reorganization energy in the form referred to as method (III),

$$\lambda_s = \frac{1}{2}\sum_j \hbar\omega_j\Delta x_j^{\,2} = \frac{1}{2\pi k_B T}\int_{-\infty}^{\infty}\frac{J(\omega)}{\omega}d\omega, \tag{4.15}$$

which is an alternative representation of Eq. (3.52) (see Chapter 3).

When one evaluates the solvent reorganization energy according to one of the methods just described, then the main bottleneck is a careful evaluation of the potential energy gaps between the reactants and the products. In order to estimate them, mainly two computational methods were applied, namely atomistic MD simulations or calculations invoking a continuum model.

4.2   Continuum model calculations of λ_s

Marcus first derived a classical electrostatic model for calculating λ_s of an intermolecular electron transfer.[74,93,163] To obtain an analytical expression for λ_s, Eq. (2.34), with this model that is based through the Poisson equation, Marcus approximated the donor and the acceptor molecules as spherical regions separated at a distance R_{DA} (Section 2.3). The spheres are

immersed in a dielectric medium that represents the solvent and is characterized by an optic, ε_∞, and a static, ε_0, dielectric constant. Naturally, this macroscopic scheme lacks atomistic detail. Also, it is necessary limited by the spherical shapes assumed for the donor and the acceptor species. Despite its simplicity, this model was quite popular for interpretation of experimental data in biological systems: it successfully captures the general dependence of λ_s on the D-A separation R_{DA}, the polarizability of the surrounding medium and hence the effect of the solvent not only for rather small molecules like hydrocarbons,[167] but also for estimates of λ_s even in DNA duplexes.[112]

The original Marcus electrostatic model for λ_s also invoked a linear response approximation, specifically for representating the solvent reorganization as a dielectric response.[74,93,163]

Linear response models of the electrostatics, including those based on numerical solutions to the Poisson-Boltzmann (PB) equation, have proven to be highly successful for modeling many equilibrium electrostatic properties of biomolecules having complicated geometry.[112,168-170] A key point of these calculations was the ability to solve the PB equation rapidly and accurately essentially for arbitrary charge and dielectric distributions using numerical methods. This allowed the explicit incorporation of atomically resolved information provided by X-ray crystallography and nuclear magnetic resonance (NMR), including the shape of the biomolecule, the positions of charges and counterions, and the accessibility of solvated ions by the solvent.

For many phenomena the advantages of realistically representing the structural detail of the molecule outweights any approximations entailed by the use of a linear response dielectric model. Another important feature of these models is the inclusion of rational, though implicit, solvent and solvent ion screening effects. These advances in modeling the electrostatic properties of biomolecules have been made possible by improvements[169,170] in the numerical methods and by the rapid increase in computer power.

In the continuum model, the starting point for determining the reorganization energy is the evaluation of differences in the electrostatic free energies between two states, one of which is not at electrostatic equilibrium with the surrounding medium. For further convenience, following the abbreviation introduced in Section 2.3 for Marcus two-spheres model, the state which is in equilibrium with surrounding medium will be denoted as (AD) and its complementary excited analog as (AD)[*]. For both states, the electrostatic potential $\varphi(\mathbf{r})$ as a function of the coordinate $\mathbf{r}$ is given as solution of the following equation,[171]

$$\nabla \cdot \nabla \varphi = -4\pi\rho + 4\pi\nabla \cdot \mathbf{P} \tag{4.17}$$

where $\rho(\mathbf{r})$ is the charge distribution of the fixed charges and $\mathbf{P}(\mathbf{r})$ is the polarization the of medium. This equation is valid irrespective of whether or not the charges and polarization $\mathbf{P}(\mathbf{r})$ of the medium are at equilibrium. It is assumed that the potential gradient arises from some distribution of atomic charges. The latter could represent either a time-averaged equilibrium or

an instantaneous non-equilibrium state of the system. The charge density $\rho(\mathbf{r})$ is usually composed of two contributions: atomic charges $\rho_{at}(\mathbf{r})$ of the main solute, e.g. a biomolecule, and mobile charge, i.e. the counterions $\rho_{ion}(\mathbf{r})$. Following the seminal paper of Marcus,[74] the polarization $\mathbf{P}(\mathbf{r})$ is formed by two contributions: $\mathbf{P}_u(\mathbf{r})$ reflecting the slow component (atomic and orientational) of polarization and $\mathbf{P}_e(\mathbf{r})$ corresponding to the fast electronic component (as discussed in Section 2.3).

The polarization $\mathbf{P}(\mathbf{r})$ at any point in space is proportional to the electrostatic field and to the electric susceptibility $\alpha(\mathbf{r})$:

$$\mathbf{P} = -\alpha\nabla\varphi. \tag{4.18}$$

The susceptibility, defined in terms of the dielectric constant ε as $\alpha(\mathbf{r}) = (\varepsilon(\mathbf{r}) - 1)/4\pi$, can have contributions $\alpha_u(\mathbf{r})$ and $\alpha_e(\mathbf{r})$ from the nuclear and electronic response, respectively, so that

$$\alpha = \alpha_u + \alpha_e. \tag{4.19}$$

In the case of fast ET such as, for example, light absorption (see Figure 4.1) from equilibrium state (AD) to non-equilibrium state (AD)*, only the fast electronic polarization $\mathbf{P}_e(\mathbf{r})$ responds to the sudden change in solute electrostatic field [$\rho_{at}(\mathbf{r})$ "jumps" to $\rho_{at}^*(\mathbf{r})$], while the slow polarization $\mathbf{P}_u(\mathbf{r})$ stays the same for both states.

Therefore, substituting Eqs. (4.18)–(4.19) into Eq. (4.17) yields for equilibrium state (AD)

$$\nabla \cdot \varepsilon^{op}(\mathbf{r})\nabla\varphi = -4\pi\left(\rho_{at} + \rho_{ion}\right), \tag{4.20}$$

and for non-equilibrium state (AD)*

$$\nabla \cdot \varepsilon^{st}(\mathbf{r})\nabla\varphi^* = -4\pi\left(\rho_{at}^* + \rho_{ion}\right) \tag{4.21}$$

where $\varepsilon^{st}(\mathbf{r}) = 4\pi\alpha_e(\mathbf{r}) + 1$ and $\varepsilon^{op}(\mathbf{r}) = 4\pi\alpha(\mathbf{r}) + 1$, respectively.

The charge density of the counterions $\rho_{at}(\mathbf{r})$ depends on the potential φ for (AD) and φ^* for (AD)* state, respectively, with the bulk solvent concentration c_i of each ion of valence z_i:

$$\rho_{ion} = e\sum_i c_i z_i \exp\left(-z_i e\varphi/k_B T\right). \tag{4.22}$$

Evaluation of the electrostatic potentials φ and φ^* from Eqs. (4.21) and (4.22) for any given spatial combination of charges is an important stepping stone towards calculating the solvent reorganization energy λ_s. Invoking Eq. (2.32) from Section 2.3 by adding and subtracting the term that corresponds to the energy of the molecular system in vacuum, it is easy to represent expression for λ_s in a generalized form that is more convenient for the current discussion:

$$\lambda_s = \int\left(\frac{1}{\varepsilon^{op}} - 1\right)\frac{\mathbf{E}_c^2}{8\pi} - \left(\frac{1}{\varepsilon^{st}} - 1\right)\frac{\mathbf{E}_c^2}{8\pi}\, dV = E_{solv}\left(\varepsilon^{op}\right) - E_{solv}\left(\varepsilon^{st}\right). \tag{4.23}$$

Here $\mathbf{E}_c$ is the electrostatic field obtained by solving Eqs. (4.21)–(4.22) and E_{solv} are the free energies of solvation. Thus far, the solvent reorganization energy, as can be seen from Eq. (4.23), is nothing else than the difference of solvation free energies in two solvents effectively

characterized by the static dielectric constant ε^{st} and the high-frequency (optical) dielectric constant ε^{op}. Considering the complicated case of a biomolecular system, where the change of the charges occurs at numerous atomic sites and the dielectric constants vary in space, the solvent reorganization energy λ_s have to be represented in the following form utilized in the previous work of our group:[112]

$$\lambda_s = E_{\text{solv}}\left(\varepsilon_1^{\text{op}};\varepsilon_2^{\text{op}};...\varepsilon_n^{\text{op}};\Delta q_{fi}\right) - E_{\text{solv}}\left(\varepsilon_1^{\text{st}};\varepsilon_2^{\text{st}};...\varepsilon_n^{\text{st}};\Delta q_{fi}\right), \tag{4.24}$$

where $\Delta q_{fi} = q_f - q_i$ is the difference of the charge distribution in the initial and the final states of D and A sites.[167] In the latter equation the dielectric function, $\varepsilon = \varepsilon(\mathbf{r})$, in general a quantity varying in space, is treated in a piecewise fashion as constant within each of n zones: ε_j, ($j = 1 - n$). The latter methodology is employed in the program Delphi II,[169,170] which uses a finite difference solver of the Poisson equation for systems composed of multiple zones. It also affords an estimate of solvent reorganization energies for such complex systems as DNA duplexes.[112] In these calculations, the average geometry of a DNA duplex was initially obtained from MD calculations as a series of snapshots along 1 ns trajectory and then the solvent reorganization energy λ_s for ET between different guanine units was obtained according to Eq. (4.24) by solving the Poisson equation, Eqs. (4.20)–(4.21), where the ions were included explicitly.[112]

Each system (solute and surrounding medium) was divided into five regions ($n = 5$) of different dielectric constants ε_j. For the D (donor) and A (acceptor) zones (confined to a single guanine G units) static and optic dielectric constants were set equal to $\varepsilon_1^{\text{st}} = \varepsilon_1^{\text{op}} = 1$; the next two zones were comprised of the bases and the sugar-phosphate backbones (static dielectric constants $\varepsilon_2^{\text{st}} = 3.4$ and $\varepsilon_3^{\text{st}} = 20.6$, respectively[112,172]) with optic dielectric constants $\varepsilon_2^{\text{op}} = \varepsilon_3^{\text{op}} = 2$. The water medium was considered to be comprised of two regions: "bound water", a layer of 3 Å around the solute (corresponding to the first hydration shell explored by X-ray diffraction[173,174]) and "bulk water" beyond it. The results of Beveridge et al.[174,175] showed that the bound water region has a substantially lower dielectric constant than bulk water. In the vicinity of DNA, the local dielectric constant deviates from the bulk value as a consequence of the much lower mobility of the water molecules which interact with the charged and polar groups of DNA. The picture resulting from X-ray studies shows that the chain of phosphates is surrounded by two solvation shells of regular geometry.[174] The first layer is partially occupied by counterions, and, because of site-specific binding of cations, the structure of this "spine" depends on the DNA sequence.[174] The static dielectric constant of the bound water region is not precisely defined;[112] therefore a series of values, varying from 2 to 80, was employed for the static dielectric constant $\varepsilon_4^{\text{st}}$. For the bulk water zone, $\varepsilon_5^{\text{st}} = 80$ was assumed and both water regions were assigned identical optic dielectric constants $\varepsilon_4^{\text{op}} = \varepsilon_5^{\text{op}} = 1.8$.

The DNA model calculations of the solvent reorganization energy with the parameters just described, carried out in our group,[112] features improvements compared to earlier studies[176,177] in several ways: a larger number of different dielectric zones, more realistic values for the dielectric constants, account for geometry fluctuations of DNA etc. Beratan et al.[177] had assumed only two dielectric zones; the calculations of Tavernier and Fayer[176] may be expected to overestimate somewhat the reorganization energy because a rather large value of the static dielectric constant, $\varepsilon = 12.4$, was assigned to the base stack zone, in contrast to other suggestions which favor the range from 2 to 4.[178] The possible role of structural fluctuations had never been explored before.[176] Such fluctuations were expected to be significant for the interaction of DNA with the surrounding counterions and water molecules.[178] Despite all these issues,[112] the main outcoming of the studies of our group was to point out that the ambiguity in the definition of the dielectric zones and the assignment of their dielectric properties (especially dielectric constants for bound water region) lead to a wide variation of the results for λ_s, but with a noticeable difference, by 0.4–0.9 eV, from the values inferred from experiments, 0.4–1.7 eV, where the lower value corresponds to ET between adjacent guanines and the larger one donor and acceptor separated by three base-pairs.[46,179] Later attempts to bring experimental results and theoretical calculations into agreement by means of dielectric continuum model used a redefinition of the DNA solute cavity as solvent accessible surface area, resulting in $\lambda_s =$ 0.4–1.0 eV for the same range of ET distances, instead of the conventional van der Waals surface which lead to $\lambda_s = 1.4$–2.3 eV. Overall, these latter calculations demonstrated that calculated λ_s results for ET in DNA could be reduced by a factor of 2–3 at a given D-A separations, thereby formally reaching the experimental values.[168]

Thus far, λ_s has been estimated mainly from dielectric continuum models[112,168,176,177,180] dating back to the pioneering work of Marcus[93] and the results cover a wide range of values, depending on the parameterization of the model. A notable drawback of dielectric continuum models is the arguable choice of the spatial partitioning with different dielectric constants assigned, in particular partitions of the solvent in the vicinity of the donor and the acceptor sites of the solute.

4.3   Molecular dynamics calculations of λ_s

Atomistic MD simulations with explicit treatment of the aqueous solvent provide an alternative to the dielectric continuum models. They allow one to record all atomic positions of the molecular system in time (see Chapter 5). For large biological molecules, these calculations usually employ non-polarizable water models where molecules are represented by a system of fixed (atomic) point charges. The most commonly cited of them are the simple point charge (SPC)[181] water model and three-point transferable intermolecular potential (TIP3P).[182] These

are two rigid 3-site water models which reproduce the basic phase structure of water and its thermodynamical properties. There are some further developments of non-polarizable water models like TIP4P[182] (additional fourth site along H-O-H bisector) and TIP5P,[183] which yield better agreement for the density and the radial distribution function at room temperature. One common feature of all of them is that the average contribution of the electronic polarization is implicitly taken into account by an appropriate choice of charges and a suitable parameterization of bonded and non-bonded interactions.[181–183] These kinds of solvent models with omitted electronic polarization have been thoroughly tuned to reproduce well the average thermodynamic properties of molecules in solution and of bulk liquid water. A comparison of non-polarizable models TIP3P,[182] TIP4P[182] with different polarizable analogues like modified fluctuating charge TIP3P-FQ,[90] TIP4P-FQ[247a] concluded[88–90] that explicit representation of electronic polarization does not deliver any noticeable advantage for solvent reorganization energy simulations, yet being significantly more demanding regarding the computational resources.

Few attempts have been made to incorporate explicitly electronic polarization into MD calculations of the solvent reorganization energy.[88,90] They showed either no effect,[89] a negligibly small influence[88,90] or lower[184] compared to the theoretical expectations. Nevertheless, despite these negative computational results, the general understanding[185,186] (that electronic polarization plays an important role in the determination of solvent reorganization energy values) was theoretically well founded and resulted in the common practice to reduce these λ_s values in *a posteriori* fashion by uniform scaling.[91,187] Scaling is frequently used to bring seemingly overestimated values in accordance with experimental data or with results from dielectric continuum models. The choice of a suitalbe scaling factor represents a major challenge; it rests on an average optical dielectric constant, but use of such macroscopic quantitites itself is not well justified at the atomic scale. This is related to the problem of the optical dielectric constant having a spatial variation, which strongly depends on the solute cavity shape and the electrostatic field around it (see the discussion in Section 4.2). The straightforward transfer of a scaling factor from the simplified two-sphere solute model to DNA,[91,187] as well as incorporation[91,187] of the optical dielectric constant from experimental data for pure water[104] was not regarded as a reliable method even by the authors themselves.

In a short note in one of his earlier works, Warshel concluded[92] that the solvent electronic polarization may be important as it may substantially reduce λ_s in computational approaches. Later attempts with polarizable force fields were rather disappointing and gave way to an attitude where these effects were put aside.[88–90] The earlier calculation of Warshel[92] invoked certain approximations to reduce the computational demands and therefore cannot be considered as sufficiently accurate to allow an ultimate judgement on these issues. In fact, a thorough quantitative treatment of solvent reorganization energies remained an open problem till today, for small molecules[88,89] as well as for complex biomolecular systems.[91] On the other

hand, attempts were made to overcome the failure of the straightforward computations with polarizable force fields by invoking more sophisticated theories,[168] which also ultimately required parameterizations that unfortunately were not transparent at a fundamental atomic level.

Therefore, so far, a reliable general procedure for determining solvent reorganization energies for complex systems remained an open question. Given this situation, the present work revisites the application of MD simulations with polarizable force fields (see Chapter 5) for a small model system (Chapter 6) and for large-scale simulations of DNA-related systems (Chapters 7 and 8).

5 Molecular Dynamics Simulations. Methodological Aspects

5.1 Basic theory of molecular dynamics

The tremendous progress of computer science in recent years led to a development of fast and efficient computational methods for the investigation of structure and dynamics of molecular systems.[188,189] Quantum mechanical and force-field based molecular dynamics calculations are probably the two most important tools of computational chemistry.[190] Nowadays, both approaches are proven to reproduce the properties of many materials at least with experimental accuracy. Thus theoretical calculations serve as a main source when experimental data are to be interpreted. Although quantum mechanical calculations have the capacity to describe the electronic structure of molecules, they are still not suitable for studies of macromolecules because of limited computational power. In addition, calculations of thermodynamic properties and conformational analysis do not necessary require a detailed knowledge of the electronic properties. This area is successfully served by (force-field based) molecular dynamics simulations, which follow the classical motion of the nuclei (or ions) and treat mechanical, van der Waals and electrostatic forces of a complex molecular systems as a parameterized function of nuclear positions. The initial atomic coordinates are often provided by X-ray or NMR analysis. The parameters of the interatomic forces are selected to reproduce pertinent properties of the system or derived from results of quantum mechanical calculations. Finally, the Newtonian equations of motions are solved for the nuclei (or ions):

$$\mathbf{F}_i = m_i \mathbf{a}_i = m_i \frac{d^2 \mathbf{r}_i}{dt^2}, \tag{5.1}$$

Here $\mathbf{F}_i$ is the force acting on atom i with mass m_i and acceleration $\mathbf{a}_i$ (the second derivative of the coordinate vector $\mathbf{r}_i$ with respect to time t). The force exerted on atom i is obtained as derivative of the total potential energy of a molecular system with respect to the coordinate vector $\mathbf{r}_i$:

$$\mathbf{F}_i = -\frac{dU(\mathbf{R})}{d\mathbf{r}_i}, \tag{5.2}$$

where **R** is a vector encompassing all atomic coordinates of the molecular system. At the core of molecular dynamics there commonly is a "force field", i.e. a parameterized description of the potential energy surface for a class of systems.

5.2   Force fields

The force field or in other words the total potential energy of a system usually is taken to consist of various energy contributions. Formally they can be divided into two groups: bonded terms (bond stretching, changes of bond angles or torsion angles) and non-bonded terms (mainly to represent van der Waals and Coulomb forces). Each of these terms contains empirical parameters, which are adjusted to reproduce correctly general molecular properties. This fitting is performed in a fragment-by-fragment fashion for families of small molecules or their parts which possess similar physical or chemical properties; one compares force-field results with results of *ab initio* quantum mechanical calculations or with experimental data. The parameters are collected in libraries and usually automatically assigned to the atomic centers of the molecule under study. Given a wide variety of chemical species, especially macromolecules, force fields are normally designed for specific classes of molecules. For example, AMBER,[191] CHARMM[192] and GROMOS[193] force fields are developed to describe proteins and nucleic acids, while the family of MMX[194] force fields is designed for treating mainly small organic compounds.

The total potential energy of the molecular system is given by the general expression:

$$U(\mathbf{R}) = U_{bond} + U_{angle} + U_{torsion} + U_{nonbond} \tag{5.3}$$

The first term in this formula represents the potential energy associated with the stretching of a bond between pairs of chemically bound atoms whose interactions are traditionally approximated with harmonic potentials:

$$U_{bond} = \frac{1}{2} \sum_{bonds} k_b (r - r_0)^2, \tag{5.4}$$

where k_b is a force constant specific for each bond and r_0 is the corresponding equilibrium bond length.

The second term in Eq. (5.3) is related to the deformations of a bond angles θ between three atoms, among which two pairs of atoms are chemically bound. Similar to Eq. (5.4), a harmonic potential is employed as a rule:

$$U_{angle} = \frac{1}{2} \sum_{angles} k_\theta (\theta - \theta_0)^2, \tag{5.5}$$

where k_θ is the force constant of the valence angle and θ_0 is the angle of the equilibrium structure.

The third term is responsible for simulating rotational barriers between atoms separated by three covalent bonds. The motion associated with this term is a rotation around the bond between the two atoms in the middle of a set of four atoms. The torsion potential is assumed to be periodic and can be expressed as a truncated cosine series expansion:

$$U_{torsion} = \frac{1}{2} \sum_{torsions} U_n \left(1 + \cos\left(n\omega - \gamma\right)\right), \tag{5.6}$$

where U_n is the energy barrier for the torsion rotation, n is the multiplicity constant describing the number of minima on the potential energy surface, and ω is the reference torsion angle. The phase shift constant γ defines the value at which the torsion angle has its first minimum.

The last term in Eq. (5.3) represents the non-bonded interactions. The non-bonded term usually contains two parts which describe van der Waals and Coulomb interactions:

$$U_{nonbond} = \sum_i \sum_{j>i} \left(\frac{A_{ij}}{r_{ij}^{12}} - \frac{B_{ij}}{r_{ij}^{6}} \right) + \sum_i \sum_{j>i} \frac{q_i q_j}{\varepsilon r_{ij}} + U_{pol} \tag{5.7}$$

In the case of a polarizable force field, an additional term is introduced that represents the electronic polarization of a molecular system. The latter term will be discussed in detail in one of the following subsections. The van der Waals interaction between two atoms i and j separated at distance r_{ij} arises from a balance between attractive dispersion and repulsive forces. It is often assumed in the form of a Lennard-Jones potential; see the first term in Eq. (5.7). A_{ij} and B_{ij} are parameters specific to atom pairs. The Coulomb potential accounts for the electrostatic interaction in a medium with dielectric constant ε between pairs of atoms i and j with charges q_i and q_j, respectively.

5.3 Integration algorithms

In MD simulations one solves the Newtonian equations of motion through integration algorithms all of which necessary involve a discretization procedure. Also, one assumes that positions, velocities, and accelerations, discretized on a grid, can be approximated by Taylor expansions:

$$\mathbf{r}\left(t + \Delta t\right) = \mathbf{r}\left(t\right) + \mathbf{v}\left(t\right)\Delta t + \frac{1}{2!}\mathbf{a}\left(t\right)\Delta t^2 + \frac{1}{3!}\mathbf{b}\left(t\right)\Delta t^3 + \ldots \tag{5.8}$$

$$\mathbf{v}\left(t + \Delta t\right) = \mathbf{v}\left(t\right) + \mathbf{a}\left(t\right)\Delta t + \frac{1}{2!}\mathbf{b}\left(t\right)\Delta t^2 + \frac{1}{3!}\mathbf{c}\left(t\right)\Delta t^3 + \ldots \tag{5.9}$$

Here $\mathbf{r}$ is the coordinate vector of an atom, $\mathbf{v}$ is the corresponding velocity, $\mathbf{a}$ is the acceleration; $\mathbf{b}$ and $\mathbf{c}$ are derivatives of $\mathbf{r}$ of third and fourth order with respect to time.

If initial coordinates and velocities of all atoms of a system are defined, then the Newtonian principles of dynamics guarantee an evolution of the system with time that can obtained by

integrating the equations of motion. Hence, a representation of the motion as a series of discrete velocity and coordinate values, instead of a continuum, leaves open the question how the discretization procedure has to be implemented in the computations. There are several commonly used algorithms, which perform this step in various ways.

Verlet algorithm. This method[195] defines new positions $\mathbf{r}(t+\Delta t)$ on the basis of the current positions $\mathbf{r}(t)$ and those of the previous time step $\mathbf{r}(t-\Delta t)$ and invokes accelerations $\mathbf{a}(t)$:

$$\mathbf{r}(t+\Delta t) = 2\mathbf{r}(t) - \mathbf{r}(t-\Delta t) + \mathbf{a}(t)\Delta t^2 \tag{5.10}$$

The velocities $\mathbf{v}(t)$ at current time t are calculated from the coordinate values of the previous and the subsequent time steps:

$$\mathbf{v}(t) = \left[\mathbf{r}(t+\Delta t) - \mathbf{r}(t-\Delta t)\right]/2\Delta t , \tag{5.11}$$

where coordinate vector $\mathbf{r}(t)$ is determined with respect to the centre of mass of the unit cell (Section 5.8). The algorithm requires low computer memory although at the expense of precision.

Leap-frog algorithm. This approach[196] first calculates the velocities at a half-step $t+\Delta t/2$ of time from the velocities at time $t-\Delta t/2$ and the accelerations at current time t,

$$\mathbf{v}\left(t+\frac{1}{2}\Delta t\right) = \mathbf{v}\left(t-\frac{1}{2}\Delta t\right) + \mathbf{a}(t)\Delta t \tag{5.12}$$

From these velocities the positions at time $t+\Delta t$ are estimated:

$$\mathbf{r}(t+\Delta t) = \mathbf{r}(t) + \mathbf{v}\left(t+\frac{1}{2}\Delta t\right)\Delta t \tag{5.13}$$

The main advantage of this method is an explicit calculation of velocities. However, the positions and velocities are not synchronized, and, therefore, the calculated kinetic energy does not correspond to the positions defined.

Velocity Verlet algorithm. The handling of the kinetic energy is substantially improved in the currently employed velocity Verlet algorithm,[197] which gives positions, velocities and accelerations at the same time step and in addition, is rather accurate. The dynamic quantities are computed as follows:

$$\mathbf{r}(t+\Delta t) = \mathbf{r}(t) + \mathbf{v}(t)\Delta t + \frac{1}{2}\mathbf{a}(t)\Delta t^2 \tag{5.14}$$

$$\mathbf{v}(t+\Delta t) = \mathbf{v}(t) + \frac{1}{2}\left[\mathbf{a}(t+\Delta t) + \mathbf{a}(t)\right]\Delta t \tag{5.15}$$

5.4   Treatment of electronic polarization

The last term in the non-bonded interactions of the force field, Eq. (5.7), represents the electronic polarization:

$$U_{pol} = -\frac{1}{2}\sum_{i}^{atoms} \mathbf{\mu}_i \mathbf{E}_i^0 , \tag{5.16}$$

where $\mathbf{\mu}_i$ is the dipole moment induced on atom i proportional to the total electric field $\mathbf{E}_i^0$ acting on atom i with polarizability tensor α_i:

$$\mathbf{\mu}_i = \alpha_i \mathbf{E}_i^0 \tag{5.17}$$

The polarization in Eq. (5.16) includes mutual induction of the polarizable sites within a molecule itself (intramolecular polarization) and the polarization induced by an external field. The simplest way to mimic response of electronic polarization is based on isotropic atomic polarizabilities assigned to the atoms to represent bond polarization in the environment of a condensed phase.

The force fields augmented with an expression as Eq. (5.16), where the response due to electronic polarization of a system depends on the field $\mathbf{E}_i^0$, are in essence non-additive ones, because if a single dipole in the system is modified, then it affects the overall electrostatic field, hence all other dipoles, which adjust themselves according to the new electrostic field. Therefore, it is rather difficult to separate electrostatic contributions of different molecular groups from each other and one has to talk about such individual terms with due caution. The integration of the equations of motion for non-additive force fields employs at each time step a number of other techniques in addition to the computational algorithms shown in the previous section. Thus, polarizable force fields are computationally extremely demanding. One of the ways out is a Lagrangian method.

Extended Lagrangian method. The Lagrangian of the molecular system L_0 used to describe the motions of the nuclei in a standard additive (nonpolarizable) force field is augmented by a Lagrangian term, which describes the changes of the dipoles. The total extended Lagrangian L has the form:

$$L = L_0 + \frac{1}{2}\sum_{i=1}^{N} M\dot{\mathbf{\mu}}_i^2 - \left[-\frac{1}{2}\sum_{i=1}^{N} \mathbf{\mu}_i \mathbf{E}_i^0 + \sum_{i=1}^{N} \frac{1}{2\alpha_i}\mathbf{\mu}_i^2 \right], \tag{5.18}$$

where M is a fictitious "mass" associated with the time evolution of the dipoles. The second term on the right-hand side is a kinetic energy of the additional dipolar degrees of freedom. The last two terms correspond to the potential energy of the dipoles and their polarization self-energy. For each single induced dipole the Lagrangian function yields an equation of motion:

$$M\ddot{\mathbf{\mu}}_i \equiv \frac{\partial L}{\partial \mathbf{\mu}_i} = -\frac{\mathbf{\mu}_i}{\alpha_i} + \mathbf{E}_i^0 , \tag{5.19}$$

This equation of motion is formally that of a harmonic oscillator subjected to a field $\mathbf{E}_i^0$. The extended set of equations of motion for both $\ddot{\boldsymbol{\mu}}_i$ and $\ddot{\mathbf{r}}_i$ is integrated by a standard computational method as described above.

Self-consistent method. At each time step the self-consistent method minimizes the total electrostatic energy in an iterative fashion only with respect to electronic polarization degrees of freedom represented by the induced dipoles. Since the induced dipoles $\boldsymbol{\mu}_i$ on all other atoms (i = 1, … N) are also sources of electrostatic field contributions, one arrives at a set of N implicit vector equations for the self-consistent field:

$$\boldsymbol{\mu} = F\left(\boldsymbol{\mu}; \mathbf{r}_1 \ldots \mathbf{r}_N\right),\qquad(5.20)$$

where $\boldsymbol{\mu} = \left(\boldsymbol{\mu}_1 \ldots \boldsymbol{\mu}_N\right)$ denotes the set of induced dipoles and the dependence on the configuration $\left(\mathbf{r}_1 \ldots \mathbf{r}_N\right)$. The last equation is adjusted by introducing a relaxation (mixing) parameter ω:

$$\boldsymbol{\mu} = \omega F\left(\boldsymbol{\mu}\right) + \left(1 - \omega\right)\boldsymbol{\mu}.\qquad(5.21)$$

At each MD time step the configuration of all atomic nuclei in the system is kept fixed, while the polarization energy is minimized to fulfill the condition:

$$\max_{i=1}^N \left|\boldsymbol{\mu}_i^{(j)} - \boldsymbol{\mu}_i^{(j-1)}\right| = \Delta\boldsymbol{\mu}^{(j)} \leq C\qquad(5.22)$$

where C is an arbitrarily chosen constant, which serves as criterion for the convergence of the polarization energy associated with the induced dipoles.

5.5   Representation of the solvent

Conventional non-polarizable models of water such as the simple point charge force field (SPC),[181] or the three-point transferable intermolecular potential (TIP3P)[182] are based on fixed atom-centered charges and have two significant limitations. One of them is that such simplification leads to insufficient flexibility of the description of the molecular charge distribution and results in an electrostatic potential of limited accuracy.[198] Another shortcoming is related to the fact that such models lack the property of an instantaneous electronic response to the molecular environment, in striking disagreement with reality. For example, it is experimentally known that the dipole moment of water changes from 1.85 Debye[199] in the gas phase to 2.1 Debye for the water dimer,[200] to higher values around 2.6 Debye for small water clusters,[200] and finally 2.95 Debye for bulk water.[201] Molecular dynamics simulations of the dielectric properties suggest values of the dipole moment around 2.5 Debye[202,203] for liquid water in order to effectively reproduce bulk thermodynamic properties of water in biomolecular simulations.[182] As non-polarlizable force fields are not sufficiently flexible to reproduce all

pertinent properties of water, the latter choice is at the expense of correct electrostatic potentials.

This conflict can be solved by introducing electronic polarization into the point charge water models.[204] Polarizable water models do a better job with reproducing molecular dipoles in contexts where the hydrogen bonding network of room-temperature bulk water is either partially destroyed or significantly perturbed.[200,205] Polarizability is essential for obtaining accurate energetics in the vicinity of highly polar moieties and small ions.[206,207] A recent MD study demonstrated[208] that the structure of ideal B-DNA in the polarizable water model POL3[209] (three-point charges per molecule) converges to the experimental structure with a much lower RMSD compared to the standard non-polarizable TIP3P.

The POL3 model treats atoms as isotropically polarizable in the spirit of a shell model where the induced dipole is constructed from two point charges connected via an elastic spring located at the nucleus.[210] In addition to reorientations of water molecules with typical experimental times of several picoseconds,[76] this force field captures the fast electronic response and has to be adjusted at each integration time step (typically 0.5–2 fs); the latter is essential for ET.[74] The TIP3P model is able to simulate only reorientational polarization. The present study attempts to account also for the effect of a quasi-instantaneous electronic polarization on the solvent reorganization energy and compares results from the two water models TIP3P (non-polarizable) and POL3 (polarizable).

5.6   Assignment of charges

A key issue of all force fields is the assignment of atomic charges. Non-polarizable force fields are commonly employed when one treats biomolecules in MD studies. The success of non-polarizable force fields based on the effective two-body additive potentials, see Eqs. (5.3)-(5.7), is widespread.[191–194] For instance, the AMBER force field relies on *ab initio* Hartree-Fock 6-31G* calculations to derive RESP atomic charges.[191,211,212] Therefore, it would seem natural to derive charges for polarizable models in a related manner. The charges used in non-polarizable calculations systematically overestimate dipole moments because they implicitly include electronic polarization effects.[213,214] In case of DNA simulations, the scaling of the charges of nuclear bases by a factor of 0.9 yields approximately the charges used in polarizable force fields.[215] However, such empirical scaling cannot be a satisfactory solution since scaling factors need not be transferable. Therefore, a relatively sophisticated procedure is employed to derive atomic charges; see Appendix B for details. At the basis of this procedure lies the suggestion of Warshel[216] to represent the polarization energy with the help of induced dipoles with an isotropic polarization, as introduced by Applequist.[210] In this scheme one first calculates the electrostatic potential (ESP) of a molecule in the gas phase at an accurate quantum mechanical level, employing DFT (B3LYP)[217] calculations with the cc-pVTZ basis

set;[218] then one subtracts the contribution to electrostatic potential due to self-polarization of the molecule before the potential is used for determining the atomic charges.[219] As demonstrated,[219] organic molecules or fragments of biomolecules can be incorporated into the library of the polarizable force field following this procedure.

The present work used two all-atom force fields (FF) that are implemented in the program package AMBER 8:[220]

(i)   *ff99*, which is the 1999 version of the force field by Cornell et al.,[191] with the same atom types, topologies (except for torsional parameters) and charges as the earlier version *ff94*.[191]

(ii)   *ff02*, which is a polarizable variant of *ff99*. The charges are closer to values in the gas phase than those in the non-polarizable force fields. Polarizable dipoles based on isotropic atomic polarizabilities are assigned to the atoms to represent the bond polarization in the environment of a condensed phase. The *ff02* force field uses interactive polarization, which includes the mutual effects of polarizable sites within a molecule (intramolecular polarizability), in addition to the polarization induced by the external field.

5.7   Treatment of electrostatics

The calculation of electrostatic interactions forms the most time-consuming part of a molecular dynamics simulation due to the long-range character of Coulomb interactions, which fall off as the inverse of the distance between a pair of charges. In consequence, more solvent molecules surrounding the solute have to be taken into account to estimate correctly the electrostatic interactions in the system. Numerous approximations have been developed in an attempt to decrease the computational efforts.[190,221,222] They can be classified according to two categories: truncation methods and Ewald summation methods.

Truncation methods neglect electrostatic interactions between two atoms at a separation beyond a threshold also referred to as "cutoff" distance r_{cut}.[223,224] The interactions can be abruptly truncated at the cutoff distance or smoothed by different schemes.[225] The truncation methods scale as $O(N^2)$ with the size of the system and become extremely expensive when the size of the system increases. In addition to a higher demand of computational ressources, they introduce numerous artifacts.[226] For example, trajectories become unstable and biomolecules tend to exhibit unphysical behavior.[87] Therefore, truncation methods are no longer used in MD simulations.

Instead, the *Ewald summation method*[227] is now widely employed to handle the problem of long-range interactions. The method was originally developed to treat the interactions of

particles in a box and with periodic images. Ewald-based methods decompose the electrostatic Coulomb interactions of the form $1/r$ into a sum of two error functions:

$$\frac{1}{r} = \frac{\mathrm{erfc}(r)}{r} + \frac{\mathrm{erf}(r)}{r},$$ (5.23)

where the complementary error function is given by $\mathrm{erfc}(r) = 1 - \mathrm{erf}(r)$.

The benefit of this decomposition is that $\mathrm{erfc}(r)/r$, which gives rise to the "direct space sum", decays very fast, and therefore, a short cutoff can be used to compute this term. The other term $\mathrm{erf}(r)/r$, gives rise to the "reciprocal sum"; its terms do not decay fast but vary very smoothly and therefore can be computed via Fourier transforms. The Particle Mesh Ewald (PME) method, introduced by Darden et al.[222] is a variant where one computes the reciprocal part very efficiently using Fast Fourier Transform routines (FFT). The electrostatic forces computed in the reciprocal space sum are then interpolated back to real space via B-splines. The PME method scales as $O(N\ln N)$, which is considerably faster than the $O(N^2)$ methods with a cutoff. PME provides stable DNA simulations up to microseconds[228] and is mainly used in expensive biomolecular simulations with explicit solvent.

5.8   Periodic boundary conditions

Periodic boundary conditions can be used to simulate bulk properties of large molecular systems surrounded by a solvent as they bypass the problem of simulating systems in "water droplets" with extremely high surface tensions and artificial densities.[220] Instead of considering a single cell containing the dissolved solute, periodic boundary conditions treat an array of replicas, infinite in three dimensions. All these cell images are identical and the molecules inside exhibit synchronous movements with their original-cell counterparts. This approach leads to a sufficiently realistic representation of systems in a condensed phase; it is the most efficient method currently available for such MD simulations.

5.9   Temperature coupling algorithm

The absolute temperature T of a molecular system that contains N atoms is related to the total kinetic energy:

$$\frac{1}{2} N_f k_B T = \sum_{i=1}^{i=N} \frac{m_i v_i^2}{2},$$ (5.24)

where N_f is the number of degrees of freedom of the molecular system. A popular schemes to control the temperature is the Berendsen coupling algorithm,[229] which is based on a coupling of the molecular system to a bath with a reference temperature T_0. One invokes:

$$\frac{dT}{dt} = \frac{T - T_0}{\tau}, \tag{5.25}$$

where τ is a time parameter that controlls the rate of the velocity scaling when the current temperature T deviates from T_0. This method is convenient for creating a correct initial temperature distribution. It was applied in the present work for all calculations of the solvent reorganization energy.

5.10   Pressure coupling algorithm

A real solvated molecular system changes its volume in order to maintain a constant pressure. In such NPT simulations the volume of the unit cell, applied with periodic boundary conditions, changes according to the pressure-controlling algorithm. This scheme is similar in spirit to the temperature coupling algorithm just described.[229] However, here the volume of the unit cell is adjusted in small steps and the positions of all atoms are isotropically scaled.

6 Solvent Reorganization Energy in Marcus Two-spheres Model

6.1 Challenging electronic polarization

In recent years much effort was invested in calculations of the solvent reorganization energy λ_s, a key parameter of electron transfer (ET) theories ever since the pioneering work of Marcus.[93] The solvent contribution λ_s forms the major part of the overall reorganization energy. Systems of increasing complexity have been treated theoretically, from simple ionic solute models[92] to complex systems of biological interest, e.g. proteins[230] or DNA oligomers.[112,168,176,177] The classic Marcus continuum model[93] relates the solvent reorganization energy to the high-frequency dielectric constant, predicting a strong inverse dependence on the dielectric constant in highly polar solvents like water. As the high-frequency dielectric constant is related to the molecular polarizability through the Clausius-Mossotti relation,[231,232] accounting for the electronic polarization in a theoretical approach should notably affect λ_s. Incorporation of the molecular polarizability of the solvent due to the spatial variation of the electrostatic potential in the vicinity of the solute is an essential condition for estimating λ_s.

Several methods have been employed to tackle this problem, like a dielectric continuum model of the solvent[112,168,176,177] (see Section 4.1) or a more sophisticated description of the solvent in terms of a local response function[168,233] Ambigious aspects of implicit solvent (continuum) models are (*i*) the assignment of dielectric constants to regions[112,176] in order to represent the heterogeneity of the solvent in the vicinity of the solute and (*ii*) the controversial definition of the solute cavity in the dielectric medium.[168,176] As a result, in case of complicated systems like DNA, λ_s values may vary by factors of up to 2–3, depending on the choice of parameters.[112,168,176] Atomistic simulations offer an alternative[88–90] that affords an explicit treatment of the aqueous environment without any *ad hoc* parameterization. Incorporation of non-polarizable force fields for water, which is a common practice to reduce computational efforts, leads to the substantial overestimation. of the solvent reorganization energy.[187,233] Thus, the original (unscaled) λ_s value, 1.68 eV, obtained recently[91] from a simulation of ET in a DNA hairpin complex using a non-polarizable force field deviates substantially, almost 0.5 eV, from

the experimental estimate, 1.22 eV.[234] To bring the resulting λ_s values in accordance with experimental data or with results from a dielectric continuum model, a rescaling factor has been introduced to account for electronic polarization in a global post-hoc fashion.[91,187]

Such uniform scaling can be always questioned as an adequate approach for strongly inhomogeneous solutes, which comprise regions of different polarizability, e.g. proteins or DNA oligomers. In the middle of the 1980s, King and Warshel pointed out[92] that accounting for the electronic polarizability of the solvent substantially reduces λ_s, but the outcome of later computational studies contradicted this result.[88,89]

The present study re-investigates the approach to the solvent reorganization energy λ_s via molecular dynamics (MD) simulations, resorting as a first step to a popular simplified model of a solute,[89,235] where the DA complex is chosen to approximate the two-spheres model of Marcus.[93]

In the present chapter charge separation (CS) and charge recombination (CR) processes are explored via MD calculations with an atomistic description of a polarizable aqueous solvent and compared with predictions of the Marcus dielectric continuum model. The results from polarizable and non-polarizable solvent models for various DA distances reveal that they differ by an essentially constant scaling factor,[141b,185,186] which incorporates the optical dielectric constant at a value close to experiment.[104]

6.2   Two-spheres model parameters

To estimate the solvent reorganization energy λ_s of an electron transfer reaction, Marcus introduced a simplified representation of donor and acceptor as spheres of radii a_D and a_A, respectively, with point charges in their centers, at a distance R_{DA} from each other (Figure 6.1). With Δe being the charge transferred from the donor to the acceptor, this model yields[74,93]
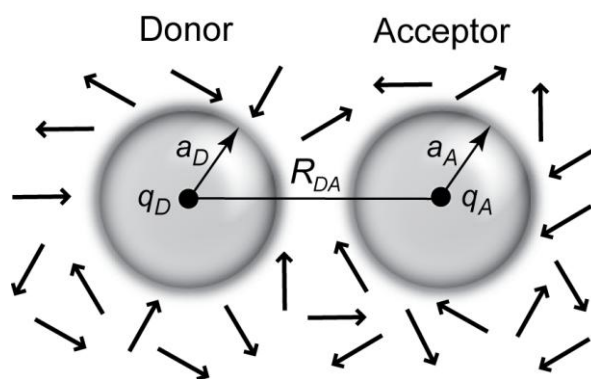
Figure 6.1. Sketch of a two-spheres model solute immersed in an aqueous medium of randomly oriented solvent dipoles. The neutral-pair state (NP) that represents the initial state ($q_A = q_D = 0\ e$) of a charge separation (CS) reaction is depicted.

solvent reorganization energy given by Eq. (2.34), which relates λ_s to the static ε_0 and the high-frequency (optical) dielectric constant ε_∞ of the solvent i.e. the relative permittivities at zero and very high frequencies, respectively.

To describe a simplified solute, which does not undergo any structural changes during MD runs, K. Ando (KA) had suggested a model.[235] In a first step, the present study is aimed at reproducing those MD model parameters as closely as possible with the available software. Therefore, the DA pair, immersed in a solvent box with periodic boundary conditions, was represented by two spherical cavities, defined by Lennard-Jones potentials $U(r) = D_0\{(\sigma/r\}^{12} - (\sigma/r\}^6\}$, as implemented in the program package AMBER 8.[220] The parameters of these two spherical "potential wells" were identical to those chosen by KA:[235] $D_0 = 2$ kcal/mol and $\sigma = 7$ Å. All van der Waals interactions of the solute with atoms of the solvent as well as between donor and acceptor were treated[220] as in that previous MD model.[235] The R_{DA} distance was restrained to the desired values by a harmonic potential with a force constant of 10000 kcal/mol·Å^2. In the ion-pair (IP) state, the point charges $q_D = 1$ e, $q_A = -1$ e were located at the centers of the spheres; in the neutral-pair (NP) state $q_D = q_A = 0$ e. The masses of the D and A spheres were set equal to those of N,N-dimethylaniline ($C_8H_{11}N$) and anthracene ($C_{14}H_{10}$), respectively, as in the original works on photoinduced intermolecular electron transfer.[235,236]

6.3 Molecular dynamics simulations

For the non-polarizable representation of the aqueous environment, the standard additive AMBER force field *ff94*[191] together with the TIP3P model of water[182] were employed. In case of the MD simulations with polarizable description of the medium, the non-additive force field *ff02*, which is the polarizable variant of *ff99*[191,219,237] and the POL3 model of water[209] were used. The polarizabilities of the solute, namely the "spheres" D and A, were always set to zero. The system was created in module *leap* of AMBER 8 and then equilibrated with the module *sander*,[220] following a previously described procedure.[235]

During the heating stage hydrogen-containing bonds of water were always constrained with the SHAKE algorithm[238] and the temperature was increased from 0 K to 300 K within 50 ps, using a NVT ensemble coupled to a heat bath with a Berendsen thermostat.[229] Here and elsewhere the time steps of the MD integration were 0.5 fs, unless explicitly stated otherwise. The next step was an equilibration run of 120 ps in a NPT ensemble with rigid solvent molecules. After the density had converged, atomic velocities were rescaled to 300 K,[89] employing an Andersen temperature-coupling scheme.[239] Subsequently, rescaling to the target temperature of 300 K, with a relaxation time parameter of 0.4 ps, took place 15 times, after each 2000 steps of 0.25 fs. Then a final equilibration run of 20 ps was performed at 300 K in a

NVT ensemble, employing a Berendsen thermostat.[229] Finally, a NVE production run of total length 50 ps was initiated in a NVE ensemble.

Three types of models were explored, varying the type of the solvent, the number of water molecules, and the shape of the unit cell. To study CS and CR processes, for each model two trajectories, for the NP and the IP state, respectively, were produced. The three models were:

(KA')   a cubic box with edges of 25.0 Å containing 500 TIP3P water molecules, following an earlier setup.[235] With this choice of parameters, the density equals that determined for pure TIP3P water, 0.982 g/cm^3.[182]

(TIP3P) a cubic box with edges of 44 Å containing 3000 TIP3P water molecules. The density was set to 1.07 g/cm^3 as obtained from our MD equilibration results on the two-spheres model, see Figure 6.2.

(POL3)   A rectangular box of 42×43×51 Å^3 containing 3000 POL3 water molecules. The density was set to 1.00 g/cm^3, as obtained from our MD equilibration results on the two-spheres model.

Simulations (KA') and (TIP3P) were carried out with the package NAMD (Version 2.6b1)[240] and a smooth cutoff of 12.0 Å, both for electrostatics and the non-bonded interactions, with the switching function activated at a distance of 11.0 Å. Trajectories (POL3) were produced with the package AMBER 8,[220] invoking the particle mesh Ewald method to describe electrostatic interactions,[222,241,242] an iterative scheme for treating the induced dipoles, and an atom-based cutoff of 12.0 Å for the non-bonded interactions and the direct part of the particle mesh Ewald procedure. These initial trajectories were generated for the NP state of the CS reaction and for the IP state of the CR reaction.
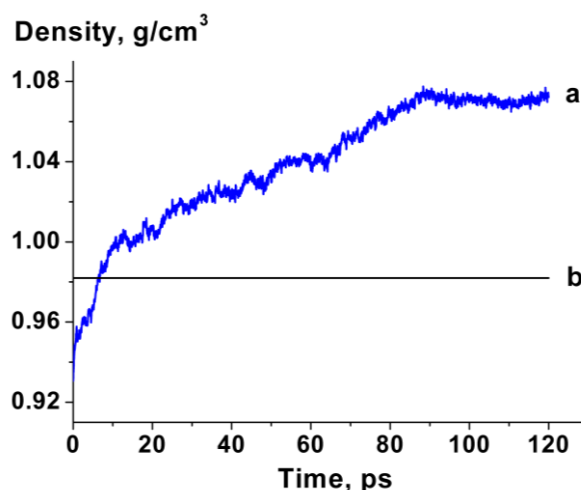

Figure 6.2. Convergence in time of the density of water in the unit cell (a) during the equilibration stage, shown for the typical donor-acceptor distance R_{DA} = 8 Å. Line (b) illustrates the equilibration level obtained by K. Ando with the same setup, see Ref. 235.

Along each production trajectory (KA'), (TIP3P), or (POL3), the snapshots were recorded at intervals of 2 fs. The root-mean-squares (rms) fluctuations of the resulting kinetic temperatures were found in the range of 3–4 K. Conservation of the total energy was monitored via (*i*) the rms deviation of the total energy ΔE(rms), which was always below 0.3 kcal/mol, and (*ii*) the ratio ΔE(rms)/ΔKE(rms), with ΔKE(rms) being the rms deviation of the kinetic energy, which was always below 0.005. These thresholds, typical for MD simulations of similar systems,[222,241] showed that the total energy was well conserved throughout the production runs.

6.4 Trajectory analysis and evaluation of λ_s

Each recorded snapshot was further submitted to a single-point energy calculation, simulated as a single MD step of 0.005 fs, with the charges corresponding to the complementary state of the ET reaction to be studied. All other parameters were preserved identical to the ones from the corresponding production runs of the original MD simulation. The difference ΔU between the total solute-solvent interaction energies of final and initial states of the ET reaction, evaluated at the same nuclear positions of the solvent, is referred to further on as "potential energy gap" (Figure 6.3). For example, in the case of the CS trajectory, the initial and final states of each such calculation would be the corresponding NP and IP states of the DA complex. During such a short single MD step, the nuclei essentially preserve their positions and the kinetic energy remains constant, as can be monitored by a negligibly small change, ~0.001
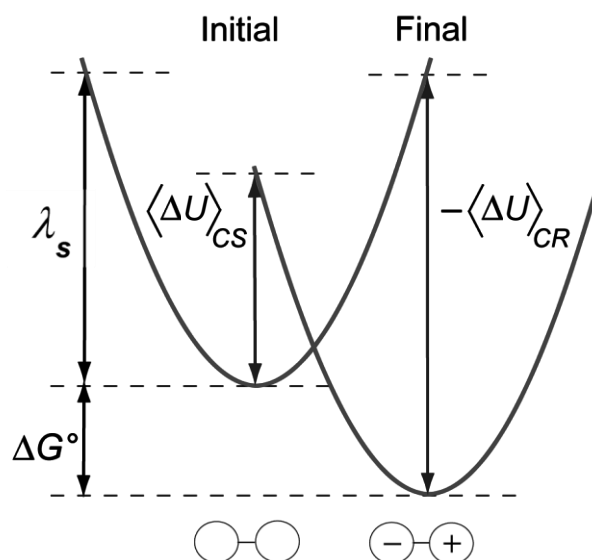
Figure 6.3. Sketch of the parabolic Gibbs free energy curves of the Marcus model, indicating the free energy change $\Delta G°$ upon charge transfer, the reorganization energy λ_s, and the potential energy gaps $\left\langle \Delta U \right\rangle_{CS}$ and $-\left\langle \Delta U \right\rangle_{CR}$ along a reaction path from the initial to the final state of an electron transfer reaction within the two-spheres model.
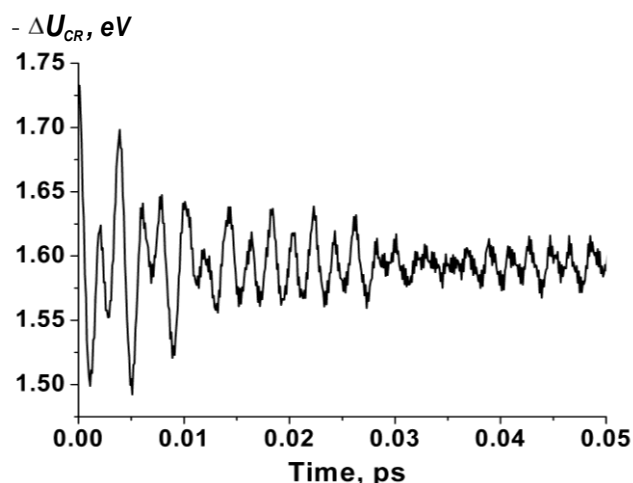
Figure 6.4. Potential energy gap $-\Delta U_{CR}$ calculated for a randomly selected IP snapshot, invoking the extended Lagrangian scheme for the induced dipoles (see text).

kcal/mol, of the total kinetic energy of all particles in the simulation box. Therefore, one can identify this "potential energy gap" as the "vertical" transition between potential energy surfaces of donor and acceptor states (Figure 6.3).

In the (POL3) simulations with a polarizable force field, an iterative method was invoked to determine the induced dipole moments.[242] To ensure good energy conservation during the NVE production runs, the dipole convergence criterion was set to 10^{-7} Debye. The same convergence threshold was employed in the subsequent single-point calculations, which resulted in 7–12 iterations per snapshot along each trajectory.

Recording the potential energy gap (Figure 6.3) is a crucial aspect in the evaluation of the solvent reorganization energy via an atomistic simulation that involves a polarizable force field.[88,89] How accurate the gap can be evaluated is intimately related to the method used to determine the relaxation of induced dipole moments. The most economical approach is a Lagrangian scheme (a modified Car-Parrinello method where fictitious masses are assigned to the charges that represent the induced dipole moments),[242,243] which was employed during the initial phase of this work. (The fictitious mass parameter was set to 0.33 kcal/mol·ps^2/Debye^2 and the time step to 0.1 fs.) However, while recording potential energy gaps, it was noted that the induced dipole moments oscillated in response to the instantaneous rearrangement of the DA charge distribution (Figure 6.4). These oscillations make the evaluation of the solute-solvent potential energy rather inaccurate. Therefore, despite of its rather high computational cost, one had to resort to an iterative scheme,[242] where at each MD time step the induced dipoles were adjusted to minimize the total electrostatic energy of the system.

(I)   The solvent reorganization energy was calculated by averaging the potential energy gap ΔU separately along the equilibrium trajectories for the NP and the IP states (which correspond to CS and CR processes, respecively). The following formula was used:[147]

$$\lambda_s = (-\langle \Delta U \rangle_{CR} + \langle \Delta U \rangle_{CS})/2 \tag{6.1}$$

This equation directly embodies the Marcus picture of two intersecting potential energy curves (Figure 6.3).

(II) Alternatively, the solvent reorganization energy was calculated by averaging the standard deviations σ of the potential energy gaps as obtained by method (I):[147]

$$\lambda_s = (\sigma_{CS}^2 + \sigma_{CR}^2)/4k_BT \tag{6.2}$$

Method II assumes that (*i*) the solute-solvent potential fluctuates in the vicinity of its average value during MD simulations and (*ii*) its thermal fluctuations exhibit a Gaussian distribution.[165] The two values for the forward and the backward reaction are averaged in order to facilitate a direct comparison with the results obtained by approach (I).

(III) Finally, the solvent reorganization energy was evaluated through the integration of the power spectrum:[5,235]

$$\lambda_s = \frac{4}{\pi} \int_0^\infty d\omega J(\omega)/\omega. \tag{6.3}$$

The spectral density $J(\omega)$ is obtained via a cosine transformation of the time correlation function of the potential energy gap ΔU:

$$\langle \delta\Delta U(0)\delta\Delta U(t) \rangle_{cl} = \frac{8k_BT}{\pi} \int_0^\infty d\omega \cos(\omega t) J(\omega)/\omega \tag{6.4}$$

Here, $\delta\Delta U(t) = \Delta U(t) - \langle \Delta U \rangle$ is the fluctuation of the potential energy gap ΔU from its (thermal) average $\langle \Delta U \rangle$. It is noteworthy, that Eq. (6.3) is alternative representation of Eq. (4.15), with the only difference that it utilizes autocorrelation function in a normalized form. This method, along with a separate evaluation of the solvent reorganization energies for CS and CR processes, reveals which modes of the solvent contribute to λ_s. We will present the spectral density in normalized form:[235]

$$\tilde{J}(\omega) = J(\omega)/c \text{ with } c = \int_0^\infty d\omega J(\omega)/\omega. \tag{6.5}$$

6.5 Distance dependence of λ_s in charge separation (CS) reaction

Using a charge separation (CS) / charge recombination (CR) reaction, as a first step before switching to the model (TIP3P) with a non-polarizable force field for water, the results of model (KA') are compared to those of that earlier study.[235] Subsequently, the effective optical

dielectric constant of water that stems from these studies will be discussed; this effective dielectric constand would have to be chosen in a Marcus treatment to reproduce these results. Finally, the effect of a polarizable force field for water will be addressed by comparing the present results from models (TIP3P) and (POL3).

In an attempt to reproduce the results of KA[235] for a similar two-spheres model of a CS/CR reaction, a set of trajectories for model (KA') with a TIP3P water solvent at density of 0.982 g/cm^3, was generated. Inspection of Table 6.1 shows that the present data for model (KA') closely reproduces those results reported earlier,[235] with few minor differences. The present average λ_s values [Table 6.1, model (KA'), method (I)] agree up to 0.1 eV with the earlier results,[235] corroborating that the present model variant and the computational protocol used indeed match the original one. The resulting values of the reorganization energy also follow the expected trend, namely, they increase with the DA separation.

Note, however, that the standard deviations (SD) of the λ_s values of model (KA') are about an order of magnitude larger (Table 6.1) than those reported previously.[235] Nevertheless, one notes that the present notably larger SD values are in full agreement with the physical picture underlying method (II) where the SD value defines the curvature of potential surfaces of states NP and IP in the vicinity of the minima. Unlike the earlier results,[235] the present λ_s values for
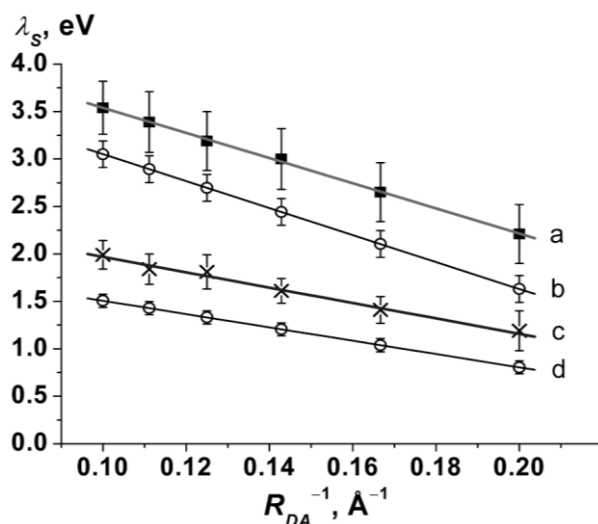
Figure 6.5. Solvent reorganization energy λ_s for a charge separation process represented by a two-spheres model and calculated with method (II). Comparison of various model results and the corresponding linear relationships, fitted to the inverse R_{DA}^{-1} of the donor-acceptor distance (see text): (a) (TIP3P) model, (b) Marcus model, Eq. (2.34), with dielectric constant $\varepsilon_\infty = 1$, (c) (POL3) model, (d) Marcus model with dielectric constant $\varepsilon_\infty = 2$. To the accuracy of the plot, the linear relationship fitted to the (TIP3P) results, scaled with $<\tilde{\varepsilon}_\infty>_{I,II} = 1.80$, coincides with curve (c). Note, that methods (I) (Fig. 6.6) and (II) (Fig. 6.5) deliver almost identical results for λ_s (Table 6.1). The corresponding slopes (see Table 6.4, next section) are hardly distinguishable in corresponding figures.

Table 6.1. Solvent reorganization energy λ_s (eV) of a charge separation/recombination reaction for the range 5–10 Å donor-acceptor distances R_{DA}, calculated with methods (I) and (II) from MD trajectories for three models: (KA'), (TIP3P), and (POL3) (see text).

R_{DA}	KA^a (I)	(KA') (I)	(II)	Δ^b	(TIP3P) (I)	(II)	Δ^b	(POL3) (I)	(II)	Δ^b
5	1.84±0.03	1.86±0.23	2.15	0.48	1.98±0.24	2.21	0.31	1.10±0.18	1.19	0.16
6	2.27±0.03	2.31±0.25	2.43	0.29	2.47±0.26	2.65	0.31	1.38±0.19	1.41	0.14
7	2.62±0.04	2.73±0.27	2.84	0.15	2.85±0.28	3.00	0.32	1.59±0.20	1.61	0.13
8	3.00±0.04	3.05±0.29	3.23	0.32	3.19±0.29	3.19	0.31	1.72±0.22	1.81	0.18
9	3.21±0.04	3.30±0.30	3.48	0.26	3.41±0.30	3.39	0.32	1.83±0.22	1.84	0.16
10	3.42±0.04	3.41±0.31	3.69	0.39	3.49±0.30	3.54	0.28	1.98±0.23	1.99	0.15

[a] Ref. 235.

[b] The range $\Delta = |\lambda_s^{CS} - \lambda_s^{CR}|/2$ characterizes the difference of the λ_s values of charge separation and recombination processes that are averaged for obtaining the result of method (II).

model (KA') calculated with method (II) based on standard deviations of the energy gap, are consistent within 0.2–0.3 eV with the solvent reorganization energies obtained by method (I). In contrast, if one applied method (II) to SD results of the original KA set, the resulting λ_s values would be two orders of magnitude smaller than the corresponding values determined by method (I); this casts some doubt on the standard deviations reported previously.[235]

It is noteworthy, that standard deviations obtained by method (I) [Table 6.1, models (KA') to (POL3)] were calculated as average SD values for the CS and CR gaps, $\sigma = (\sigma_{CS}^2 + \sigma_{CR}^2)^{1/2}/2$. The results obtained from thermodynamic integration show[92] that despite the different amplitudes of the potential energy gap fluctuations for the CS and CR processes, the free energy surfaces of the corresponding processes exhibit similar curvatures. Therefore method (I) yields reliable average values of the solvent reorganization energy.

In Table 6.1 we chose to characterize the uncertainty of the average λ_s values of method (II) not by the standard error, but rather by the range $\Delta = |\lambda_s^{CS} - \lambda_s^{CR}|/2$, that results from the fact that forward and backward ET processes are not symmetric, $\lambda_s^{CS} \neq \lambda_s^{CR}$. Individual values of potential energy gaps, as well as the solvent reorganization energies λ_s^{CS} and λ_s^{CR} are provided in Table 6.2. Both methods (I) and (II) may further be corrected to account for the non-linear response of the solvent to an instantaneous charge transfer.[101] Such corrections, which are beyond the assumptions of Marcus theory considered in this work, would not alter the values presented in Table 6.1, because they change λ_s^{CS} and λ_s^{CR} in opposite directions, by about 0.1 eV each.[101]

Table 6.2. Potential energy gaps of ion-pair (IP) and neutral-pair (NP) trajectories forming solvent reorganization energy values for models (TIP3P) and (POL3). Solvent reorganization energies λ_s^{CR} and λ_s^{CS} were calculated as $\sigma^2/2k_BT$ where σ is the standard deviation of the corresponding potential energy gap. All values are in eV.

| | (TIP3P) | | | | (POL3) | | | |
| | IP | | NP | | IP | | NP | |
R_{DA}	$-\langle\Delta U\rangle_{CR}$	λ_s^{CR}	$\langle\Delta U\rangle_{CS}$	λ_s^{CS}	$-\langle\Delta U\rangle_{CR}$	λ_s^{CR}	$\langle\Delta U\rangle_{CS}$	λ_s^{CS}
5	3.99±0.36	2.53	-0.02±0.31	1.90	2.48±0.27	1.39	-0.27±0.23	0.98
6	4.92±0.40	2.96	0.01±0.34	2.21	3.06±0.28	1.55	-0.29±0.26	1.27
7	5.74±0.41	3.32	-0.03±0.37	2.68	3.55±0.30	1.77	-0.38±0.27	1.41
8	6.39±0.42	3.47	0.00±0.40	2.89	3.98±0.32	1.98	-0.52±0.29	1.63
9	6.84±0.44	3.72	-0.03±0.40	3.07	4.29±0.32	2.01	-0.59±0.29	1.68
10	6.93±0.43	3.82	0.02±0.41	3.26	4.59±0.33	2.14	-0.63±0.31	1.84

With regard to model (KA') it has to be noted that at DA separation of $R_{DA} = 10$ Å, the periodic box affords only one solvation shell along the direction from donor to acceptor, because with a box length $L = 25$ Å, $R_{DA} = 10$ Å, and radius $a = 3.5$ Å of donor and acceptor spheres (see subsequent section of the text), one has $(L - R_{DA} - 2a) / 2 \approx 4$ Å left to opposite sides of the box. Therefore, model (TIP3P), which features a significantly larger unit cell (44 Å,

Table 6.3. Solvent reorganization energy λ_s (eV) of a charge separation/recombination reaction for the range 5–10 Å donor-acceptor distances R_{DA}, calculated with method (III) from MD trajectories for three models: (KA'), (TIP3P), and (POL3) (see text).

| | (KA') | | (TIP3P) | | (POL3) | |
R_{DA}	III	Δ^a	III	Δ^a	III	Δ^a
5	2.13	0.46	2.21	0.30	1.20	0.13
6	2.44	0.30	2.65	0.32	1.42	0.14
7	2.82	0.16	3.00	0.33	1.62	0.14
8	3.25	0.31	3.19	0.32	1.80	0.15
9	3.49	0.25	3.39	0.33	1.84	0.16
10	3.70	0.39	3.54	0.31	2.02	0.16

[a] The range $\Delta = |\lambda_s^{CS} - \lambda_s^{CR}|/2$ characterizes the difference of the λ_s values of charge separation and recombination processes that are averaged for obtaining the result of method (III).
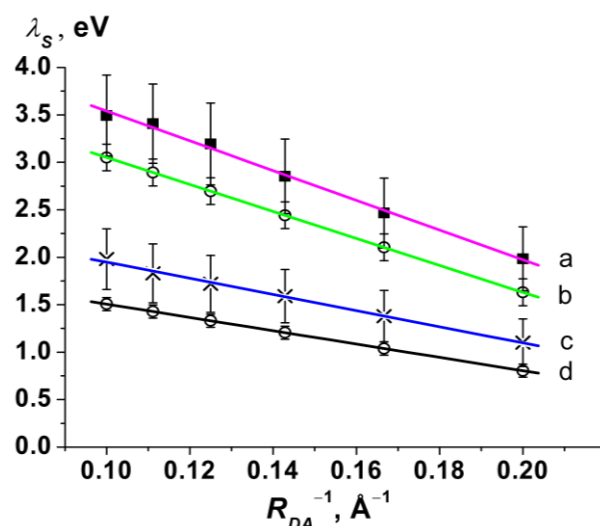
Figure 6.6. Solvent reorganization energy λ_s (eV) for a charge separation process represented by a two-spheres model and calculated with method (I). Comparison of various model results and the corresponding linear relationships, fitted to the inverse R_{DA}^{-1} (Å^{-1}) of the donor-acceptor distance (see text): (a) model (TIP3P), (b) Marcus model, Eq. (2.34), with optical dielectric constant $\varepsilon_\infty = 1$, (c) model (POL3), (d) Marcus model with optical dielectric constant $\varepsilon_\infty = 2$. To the accuracy of the plot, the linear relationship fitted to the (TIP3P) results, scaled with $<\tilde{\varepsilon}_\infty>_{I,II} = 1.80$, coincides with curve (c).

see above) was employed; for that two-spheres model system, the density converged to 1.07 g/cm^3 during equilibration (Figure 6.2). Comparison of the results (KA') and (TIP3P) from method (I) shows on average the latter λ_s values to be larger at all distances studied, by about 0.1–0.15 eV (Table 6.1). Not unexpectedly, the improved solvation in model (TIP3P) increased the potential energy gaps calculated both for NP and IP states. The λ_s values of model (TIP3P) from method (II) showed a slightly flatter distance dependence, with values higher at separations R_{DA} up to 7 Å and lower beyond (Table 6.1). The latter observation may be rationalized as follows: for states which are not adequately solvated, as for model (KA') at larger DA separation, the fluctuations of the solute-solvent potential energy due to thermal motion will be larger, resulting in an artificially increased potential energy gap. This seems to be especially noticeable for the λ_s values of method (II) from model (KA') at DA separations of 8 Å and beyond, where the local potential gradients from the two charges are higher.

The calculations with model (POL3) using the polarizable force field *ff02* followed the same protocol as for model (TIP3P). Further on, only the results of the two models (TIP3P) and (POL3) will be discussed. When the effect of electronic polarization is represented with a polarizable force field for water, the resulting values of the solvent reorganization energy from model (POL3) are substantially reduced, to almost half of those from the model (TIP3P), for the whole range of DA separations R_{DA} considered (Table 6.1, Figure 6.5 and Figure 6.6). It is
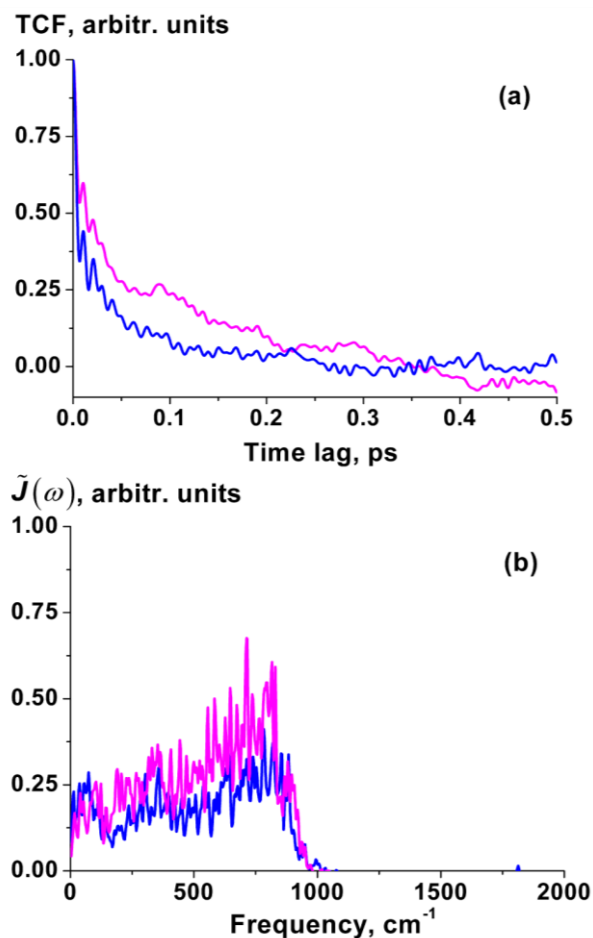
Figure 6.7. (a) Time correlation functions of the deviation $\delta\Delta U(t)$ of the potential energy gap from its average for charge separation and recombination processes: comparison of neutral-pair (NP) state (blue line) and ion-pair (IP) state (purple line) obtained with model (POL3) at the donor-acceptor separation R_{DA} = 5Å; (b) the corresponding normalized spectral density functions $\tilde{J}(\omega)$. The scale was chosen to facilitate comparison with the results of Ref. 235 (see text).

gratifying to note that the λ_s results of model (POL3) from methods (I) and (II) agree within 0.1 eV.

Method (III) yields the values of the solvent reorganization energy (Table 6.3) via integration of the spectral density function (see above), which agree within a few percents with the corresponding results of method (II) (Table 6.1). The rather negligible differences likely are related to details of the numerical procedure, where the cosine transform of the TCF was calculated from the first 5000 points (20 % of the full data set, representing 10 ps). After a symmetrization of the data set, a discrete Fourier transform was employed in combination with a Blackman window to reduce the bias of the truncation. The resolution of the resulting spectral density was 1.67 cm^{-1}.
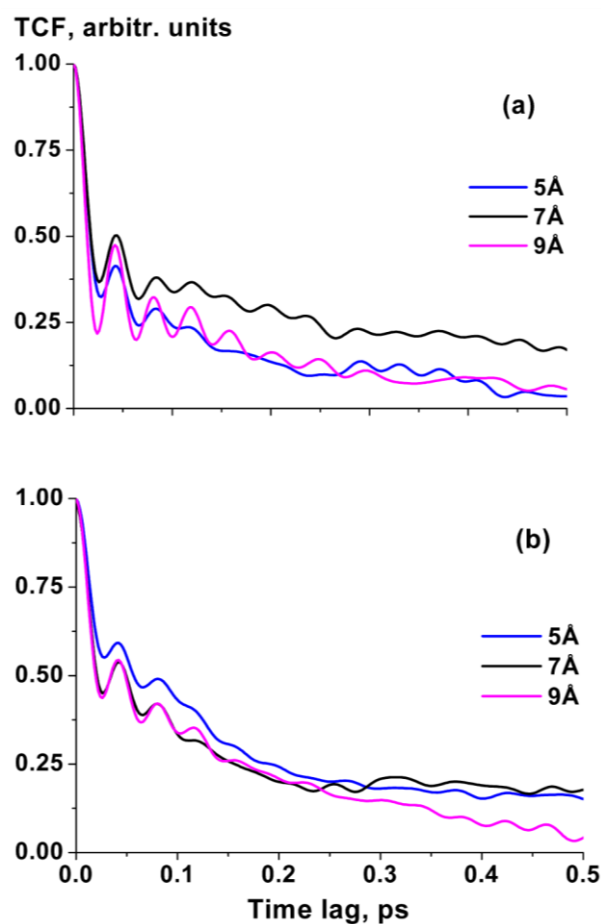
Figure 6.8. Time correlation functions of the deviation $\delta\Delta U(t)$ of the potential energy gap from its average for charge separation and recombination processes. Comparison of (a) neutral-pair (NP) and (b) ion-pair (IP) states for different donor-acceptor separations R_{DA} (Å) obtained with model (POL3).

Whereas the solvent reorganization energies calculated with the present polarizable water model POL3 differ from those reported earlier with the TIP3P-FQ force field,[89] the time correlation functions from both computational approaches in general are quite similar, for both the NP and the IP states. The time correlation function for $R_{DA} = 5$Å shows a slightly slower relaxation in the IP than in the NP state (Figure 6.7), as found earlier.[89] This trend is preserved for larger donor-acceptor distances R_{DA} (Figure 6.8).[89]

The spectral density functions $\tilde{J}(\omega)$ of the NP and IP states clearly illustrate the qualitative differences between the CS and CR processes (Figure 6.7), which do not seem to have been reported earlier. The curvatures of the potential energy surfaces are very similar, as is reflected by the fact that differences Δ between the solvent reorganization energies λ_s^{CS} and λ_s^{CR} are almost constant, ~0.15 eV, in the range of R_{DA} distances studied [Table 6.1, method (II), model (POL3)]. At larger R_{DA} separations, entropic differences, reflected in the differences between the spectra of the NP and IP states, become more important, hence imply larger deviations from the situation of uniform curvatures of the corresponding "parabolae" that are assumed in the

Marcus model.[93] The fact that entropic differences between NP and IP states increase with distance R_{DA} was not discussed in the context of earlier work,[92] where the equality of curvatures of free energy parabolae was tested for relatively small separation distance of 5 Å within the two-spheres model. Indeed, the electrostatic field of two closely located charges of A and D spheres in the IP state is negligibly small above mid-range distances. The latter results in relatively small differences between the electrostatic fields of the NP and IP states and a similar mobility of the surrounding water molecules; note the similarity of the spectra of Figure 6.7. At large donor-acceptor separations R_{DA} in the IP state stronger gradients of the electrostatic field in the vicinity of the solute reduce the mobility of the surrounding water molecules, which leads to increasing deviations from the Marcus picture of parabolae of equal curvature; see Ref. 244 and references therein.

6.6   Electronic polarization and effective optical dielectric constant in a CS reaction

The distance dependence of the solvent reorganization energy is one of the crucial aspects of ET.[245,246] Figures 6.5 and 6.6 compare results of methods (I) and (II) for various computational strategies. The λ_s values from both the (TIP3P) and the (POL3) models vary linearly with R_{DA}^{-1} as predicted by the dielectric continuum model of Marcus.[74,93] The results for both methods (I) and (II) are very similar; cf. Figures 6.5 and 6.6. Details of the various least-squares fits are provided in Table 6.4. In Figures 6.5 and 6.6, for comparison, are shown the results of the Marcus model, Eq. (2.34), for the same two-spheres solute, calculated for the high-frequency dielectric constants $\varepsilon_\infty = 1$ and $\varepsilon_\infty = 2$, respectively; see Table 6.5. Here, the error bars are due to the uncertainty with which the radii $a_D = a_A = 3.18 \pm 0.10$ Å could be determined from the radial distribution functions, calculated as the distance between the center of each sphere, A or D, and the oxygen atoms of the surrounding water molecules. These results of the Marcus model show

Table 6.4. Coefficients A and B of linear fits y = A + Bx of the solvent reorganization energy λ_s (eV) as function of the inverse x = $R_{DA}^{-1}(Å^{-1})$ of the donor-acceptor distance.

Method	Model	A, eV	B, eV·Å	R[a]	SD[b]
(I)	(TIP3P)	5.11±0.48	-15.68±3.17	0.998	0.148
	(POL3)	2.80±0.36	-8.51±2.38	0.999	0.096
(II)	(TIP3P)	4.87±0.52	-13.26±3.63	0.999	0.055
	(POL3)	2.77±0.27	-7.99±1.87	0.995	0.222

[a] Correlation coefficient of the linear fit of the solvent reorganization energy as function of the inverse R_{DA}^{-1} (Å^{-1}) of the donor-acceptor distance.

[b] Standard deviation of the linear fit of the solvent reorganization energy as function of the inverse R_{DA}^{-1} (Å^{-1}) of the donor-acceptor distance.

Table 6.5. Solvent reorganization energy λ_s (eV) calculated for the Marcus two-spheres model (sphere radii $a_D = a_A = 3.18\pm0.10$ Å) in a dielectric continuum medium with optical dielectric constants $\varepsilon_\infty = 1$ and $\varepsilon_\infty = 2$.

	λ_s	
R_{DA}	$\varepsilon_\infty = 1$	$\varepsilon_\infty = 2$
5	1.63±0.14	0.81±0.07
6	2.10±0.14	1.04±0.07
7	2.44±0.14	1.21±0.07
8	2.70±0.14	1.33±0.07
9	2.89±0.14	1.43±0.07
10	3.05±0.14	1.51±0.07

essentially a linear variation with R_{DA}^{-1}. The least-squares fit to the (KA) data[235] on the basis of Eq. (2.34) results in an effective optical dielectric constant $\bar{\varepsilon}_\infty = 0.90\pm0.02$ (Table 6.6). This value, obtained by means of method (I), underestimates the optical dielectric constant $\varepsilon_\infty = 1$ that one expects for a non-polarizable force field.[221] As the standard deviation of the λ_s values of model set (KA)[235] is too small, method (II) does not lead to meaningful results. Setup (KA') respresents our attempt to reproduce the original model.[235] It resulted in the values $\bar{\varepsilon}_\infty = 0.89\pm0.17$ for methods (I) and $\bar{\varepsilon}_\infty = 0.83\pm0.22$ for method (II); see Table 6.6. These results are still below the expected value, $\varepsilon_\infty = 1$, but the results of method (I) for models (KA) and (KA') are in accordance with each other. Also, taking into account the determined standard deviations, both results (KA'), for methods (I) and (II), agree very well with each other and, within the reported standard deviations, reproduce the value of the optical dielectric constant for a non-polarizable force field.

Similar to previous findings,[235] the (TIP3P) results for λ_s are uniformly ~0.5 eV larger than those of the Marcus model for $\varepsilon_\infty = 1$; see Figures 6.5 and 6.6. The corresponding effective optical dielectric constants, $\bar{\varepsilon}_\infty = 0.91\pm0.18$ for method (I) and 1.07±0.29 for method (II) (Table 6.6) show similar trends as the values from model (KA'), but now almost symmetrically bracket the target $\varepsilon_\infty = 1$.

To examine the influence of electronic polarization of the solvent on λ_s, Ando carried out MD simulations with the TIP3P-FQ force field of water[247] where the atomic charges are allowed to vary in response to the local electrostatic field. In these simulations, the TIP3P-FQ library was slightly modified for technical reasons.[89] When fitted to the Marcus model, Eq. (2.34), the distance dependence of solvent reorganization energies obtained from this

Table 6.6. Effective high-frequency dielectric constants $\bar{\varepsilon}_\infty$ and $\tilde{\varepsilon}_\infty$ derived for charge separation and recombination from calculated results for the solvent reorganization energy λ_s of various solvent models, applying methods (I) and (II).

	Model	(I)	(II)
$\bar{\varepsilon}_\infty^{\,a}$	KA^b	0.90±0.02	–
	(KA')	0.89±0.17	0.83±0.22
	(TIP3P)	0.91±0.18	1.07±0.29
	TIP3P-FQ^c	1.11±0.07	–
	(POL3)	1.66±0.45	1.76±0.40
$\tilde{\varepsilon}_\infty^{\,d}$		1.79±0.29	1.81±0.25

^{a} From fits of the distance dependence of λ_s to the Marcus model, Eq. (2.34).

^{b} TIP3P (non-polarizable force field). Standard deviation calculated from the original data of Ref. 235.

^{c} TIP3P-FQ (polarizable force field). Standard deviation calculated from the original data of Ref. 235.

^{d} From scaling the result for λ_s from model (TIP3P) (non-polarizable force field) to the result obtained with model (POL3) (polarizable force field).

polarizable solvent treatment translates into the effective optical dielectric constant $\bar{\varepsilon}_\infty$ = 1.11±0.07 (Table 6.6).

The computational strategy elaborated for model (TIP3P) was further employed but accounted for electronic polarization with the polarizable water model POL3, which features fixed charges and induced dipoles on each atom. The latter model yielded $\bar{\varepsilon}_\infty$ = 1.66±0.45 for methods (I) and $\bar{\varepsilon}_\infty$ = 1.76±0.40 for method (II) (Table 6.6) from the distance dependence of the solvent reorganization energy. Both values of the present study are substantially closer to the conventional experimental estimate of the high-frequency dielectric constant for water, 1.79,[104] than the value $\bar{\varepsilon}_\infty$ = 1.11±0.07 previously derived from the TIP3P-FQ calculations. In this context, it is noteworthy to emphasize once again that the present improved results for the effective optical dielectric constant are likely a consequence of the computational procedure that was chosen for estimating the potential energy gap, rather than an argument for the superiority of one solvent model over the other.

When the solvent reorganization energy was determined from MD simulations with a (standard) non-polarizable force field,[89,187] then in various cases the effect of the electronic polarization of the solvent has been introduced in an *a posteriori* fashion[141b,185,186] by applying a scaling factor, derived from the Marcus model:

$$\kappa = \left(\tilde{\varepsilon}_\infty^{-1} - \varepsilon_0^{-1} \right) \Big/ \left(1 - \varepsilon_0^{-1} \right) \tag{6.6}$$

Here, $\tilde{\varepsilon}_\infty$ denotes yet another effective high-frequency (optical) dielectric constant, that differs from $\bar{\varepsilon}_\infty$ which was derived from fitting the distance dependence of the solvent reorganization energy (see above). The scaling factor κ can be derived from quantum mechanical considerations with model Hamiltonians, where one separates slow orientational and fast electronic polarizations of the solvent.[141b,185,186] In a more straightforward fashion, one can also obtain κ from Eq. (2.34) when one relates λ_s values obtained with polarizable and non-polarizable solvent models. Various scaling factors have been suggested to bring theoretical results closer to experiment, $\tilde{\varepsilon}_\infty = \varepsilon_\infty (\text{exp.}) = 1.79$[91,187] or $\tilde{\varepsilon}_\infty = \bar{\varepsilon}_\infty = 1.11$[91] (see above). In these cases, as in the present work, the experimental value $\varepsilon_0 = 78.4$ (water at 298 K) was used.[91,187]

However, rather than introducing such scaling *ad hoc*, it seems more consistent to derive a scaling factor κ by relating two λ_s values from corresponding simulations with polarizable and non-polarizable force fields, e.g. as in models (POL3) and (TIP3P) of the present work (Table 6.1). The scaling factors κ obtained in this fashion translate to effective optical dielectric constants $\tilde{\varepsilon}_\infty = 1.79\pm0.29$ for method (I) and 1.81 ± 0.25 for method (II), Table 6.5. These latter results are in excellent agreement with the standard experimental value $\varepsilon_\infty = 1.79$ for water.[104] Figures 6.5 and 6.6 also show the results of model (TIP3P) [method (II)], rescaled with the average effective high-frequency dielectric constant $< \tilde{\varepsilon}_\infty >_{I,II} = 1.80\pm0.27$ as obtained with methods (I) and (II). In both cases, the rescaled (TIP3P) data sets essentially coincide (to the accuracy of the plot) with the corresponding results obtained for model (POL3) [linear fit (c) of either figure]; for details see Table 6.7.

Ultimately, one would like to derive an average effective high-frequency dielectric constant by relating results of classical MD calculations with a non-polarizable force field to those of *ab initio* MD calculations instead of classical MD with a polarizable force field. For some time, this likely may not be achievable for realistic models due to the computational effort needed. Nevertheless, a rough estimate of the optical dielectric constant, obtained for a charge separation reaction in a photosynthetic reaction center (*Rps. viridis*) in the latter way, yielded a value $\tilde{\varepsilon}_\infty = 1.9$,[141b] in fair agreement with our estimate of the average effective high-frequency dielectric constant $< \tilde{\varepsilon}_\infty >_{I,II} = 1.80\pm0.27$ for water.

Overall, the present findings on the solvent reorganization energy seem to corroborate the quality of the POL3 water model, which tends to underestimate the electronic polarization. The latter property has been related[213] to the neglect of mutual induction of atoms in 1-2 and 1-3 positions in the AMBER force field *ff02*.[191,219,237] In consequence, the resulting effective high-frequency dielectric constant may slightly underestimate the experimental optical dielectric constant.

Table 6.7. Solvent reorganization energies λ_s (eV) obtained for the model (POL3) as well as for the model (TIP3P) scaled with the factor $<\tilde{\varepsilon}_\infty>_{\mathrm{I,II}} = 1.80$. Results from both methods (I) and (II) are shown.

R_{DA}	(I)		(II)[a]	
	(POL3)	(TIP3P)$^{\mathrm{scaled}}$	(POL3)	(TIP3P)$^{\mathrm{scaled}}$
5	1.10±0.18	1.09±0.13	1.19±0.16	1.22±0.17
6	1.38±0.19	1.36±0.14	1.41±0.14	1.46±0.17
7	1.59±0.20	1.57±0.15	1.61±0.13	1.65±0.18
8	1.72±0.22	1.76±0.16	1.81±0.18	1.75±0.17
9	1.83±0.22	1.87±0.17	1.84±0.16	1.86±0.18
10	1.98±0.23	1.92±0.17	1.99±0.15	1.95±0.16

[a] The range $\Delta = |\lambda_s^{CS} - \lambda_s^{CR}|/2$ characterizes the difference of the λ_s values of charge separation and recombination processes that are averaged for obtaining the result of method (II).

The appreciable reduction of the solvent reorganization energy, by ~45 %, found when the polarization of the solvent is properly accounted for, nicely agrees with the dielectric continuum model of Marcus.[93] The present results are at variance with those of quite a few earlier simulations, which either resulted in smaller (~30%)[184] or almost negligible (6%)[88] changes from those of reference calculations with non-polarizable force fields. In the former case,[184] Monte-Carlo simulations, aiming at a generic solvent, modeled electronic polarization by Drude oscillators.[248] The latter studies[88] used the polarizable TIP4P-FQ water model,[247] which employs adjustable atomic charges, as mentioned above.[89]

King and Warshel were the first to demonstrate and analyze the effect of electronic polarization on values λ_s of the solvent reorganization energy that were obtained from MD simulations.[92] In contrast to the present work, the simpler model of that earlier study did not afford a quantitative reproduction of the dielectric continuum model which requires a reduction by ~45 %. King and Warshel simulated the polarizability of water via induced dipoles[249] and, probing the two-spheres donor-acceptor model at a single distance R_{DA}, found a reduction by ~35 %. This discrepancy may be related either to the choice of a solvent model[249] or the screening parameter introduced in order to reduce computational efforts.[92] Indeed, the computations with the earlier model[92] are substantially less demanding than the present iterative method (see above).

The response of the surrounding solvent to an instantaneous transfer of charge from the donor to the acceptor site comprises two contributions: fast electronic polarization on the timescale of femtoseconds and slow orientation polarization on the timescale of ten

picoseconds.[250] The latter contribution is reproduced in MD simulations with both polarizable and non-polarizable force fields. In polarizable force fields, electronic contributions are commonly simulated by assigning induced dipoles to atomic centers which effectively reduce fixed atomic charges of the force field. The parameters of either type of solvent model are adjusted to accurately reproduce static properties. In this way, a non-polarizable force field may implicitly account for some aspects of the electronic polarization. However, as demonstrated by the present systematic study, such simpler force fields result in a significant overestimation of solute-solvent potential energy gap between final and initial states of an ET process, as recorded along an MD trajectory.

It does not seem possible to rationalize here why earlier simulations[88,89] using the polarizable water TIPnP-FQ models lead to results for the effective optical dielectric constant substantially different from those of the present work. Both force fields describe the electronic polarization, albeit by different mechanisms, via the propagation of induced dipole moments, similar to the POL3 polarizable force field[209] used here. One possibility may be instabilities due to oscillations of the polarization contribution (Figure 6.4). After all, the FQ approach[247] is similar in spirit (Lagrangian constraints, fictitious masses) to the "Car-Parrinello" treatment of induced dipoles built into AMBER[242,243] which did not seem to afford the same stability for evaluating potential energy gaps (Figure 6.4) as the computationally more elaborate iterative method[242] ultimately chosen for the present work. The latter method ensures full, stable adjustment of the induced dipoles to the new electrostatic field.

6.7   Solvent reorganization energy in a Charge Shift (CSh) reaction

The present two-spheres model, embedded in an environment described by the water models TIP3P and POL3, can be adapted to afford a rough comparison with results of earlier computational efforts from our group on the reorganization energy of hole transfer in DNA.[112] To estimate the solvent reorganization energy in DNA, a charge shift reaction within the two-spheres model was employed. The earlier treatment relied on a dielectric continuum method.[112,167] The size of the spheres and range of distances R_{DA} used in the present work will furnish an estimate of λ_s for the shift of an electron hole along the π-stack of DNA. The currently employed radii of the spheres, 3.18±0.10 Å, are close to the estimate ~3Å for guanine bases as obtained from fitting the solvent reorganization energies in those earlier studies on DNA.[112] The range R_{DA} = 5–10 Å covers donor-acceptor distances between guanine units in DNA separated by one (6.8 Å) or two (10.1 Å) intervening base-pairs. Nevertheless, despite the general similarities between the descriptive geometric parameters of the system (which enter the expression for solvent reorganization energy in Marcus two-spheres model), one should note that the latter one could serve as a source of preliminary estimates, but require further justification.

Table 6.8. Solvent reorganization energy λ_s (eV) of a charge shift reaction for various donor-acceptor distances R_{DA} (Å) from a two-spheres model embedded in TIP3P or POL3 water models, determined with methods (I) and (II).

	R_{DA}	(TIP3P)		(POL3)	
		(I)	(II)	(I)	(II)
	5	1.52±0.28	1.54	0.81±0.21	0.85
	6	1.87±0.33	2.03	0.99±0.23	1.02
	7	2.23±0.36	2.50	1.23±0.25	1.21
	8	2.52±0.36	2.46	1.35±0.26	1.34
	9	2.85±0.40	3.07	1.48±0.28	1.54
	10	3.06±0.41	3.27	1.56±0.29	1.57
$\bar{\varepsilon}_\infty^a$		0.94±0.24	0.85±0.10	1.85±0.68	1.84±0.14
SD^b		0.270	0.166	0.139	0.048
R^c		0.990	0.973	0.995	0.989
$\tilde{\varepsilon}_\infty^d$		–	–	1.87±0.48	1.94±0.11

^{a} From fitting the distance dependence of λ_s to the Marcus model, Eq. (2.34).

^{b} Standard deviation of the linear fit of the solvent reorganization energy as function of the inverse R_{DA}^{-1} (Å^{-1}) of the donor-acceptor distance.

^{c} Correlation coefficient of the linear fit of the solvent reorganization energy as function of the inverse R_{DA}^{-1} (Å^{-1}) of the donor-acceptor distance.

^{d} From scaling the result for λ_s from model (TIP3P) (non-polarizable force field) to the result obtained with model (POL3) (polarizable force field).

Table 6.8 displays the resulting solvent reorganization energies λ_s. The values for model (TIP3P) lie in the range from 1.5 eV to 3.1 eV, depending on the separation R_{DA}. In contrast, the results of model (POL3) are just about half as large, ranging from 0.8 eV to 1.6 eV. These values are 0.3–0.5 eV smaller than the corresponding two-spheres results of the CS and CR reactions for the analogous water model (Table 6.1). Method (II) yields slightly higher values of λ_s (by ~ 0.2 eV) than method (I). The rather good agreement of the results of model (TIP3P) between the two methods in the case of the CS/CR reactions was due to some error compensation; the values λ_s^{CR} and λ_s^{CS} of the individual half reactions differ notably (Table 6.2). In case of a charge shift, the evaluation of the reorganization energy is based only on one trajectory and such error compensation will not occur. In contrast, the results of methods (I) and (II) for model (POL3) agree substantially better, within 0.06 eV for the whole range of distances studied (Table 6.8). This may be due to the specifics of the iterative adjustment of the

electrostatic field in the case of water model POL3, where the reduction of electrostatic energy fluctuations caused by thermal motions of nuclei is expected.

The results of both models, (POL3) and (TIP3P), show the anticipated linear behavior with R_{DA}^{-1}; for the quality of the least-squares fits see Table 6.8. From the slopes of these linear relationships one derives effective optical dielectric constants $\bar{\varepsilon}_\infty$, which agree with the appropriate theoretical results (1 and 1.79, respectively) within the standard deviations, just as for the CS/CR reactions (Table 6.5). If one relates λ_s values from the two water models in a point-by-point fashion, one obtains scaling factors κ, Eq. (6.6), which also give rise to the values of the effective optical dielectric constant, $\tilde{\varepsilon}_\infty \approx 1.9$ [methods (I), (II); Table 6.8] that are slightly larger than for the CS/CR reaction (Table 6.6).

Solvent reorganization energies of two particular points, namely for the R_{DA} distances of 7 Å (1.23±0.25 eV) and 10 Å (1.56±0.29 eV) [method (I), model (POL3), Table 6.8], may be helpful for further comparison with solvent reorganization energies of a charge shift reactions in DNA-related systems.[46,112,176,251] Before doing this, a caveat is in order. The present solute model does not undergo any geometrical changes during the MD runs. However, the internal reorganization energy of a DNA-derived solute (nucleotides, backbone vibrations) is known to contribute to the total reorganization energy several tenths of an electron volt.[46] From quantum chemical calculations,[112] this internal reorganization energy was estimated at ~0.7 eV for a charge shift between two GC base-pairs. On the other hand, the two-spheres model is notably more compact than donor and acceptor in a DNA-derived system. Therefore, in the present model, donor and acceptor are more exposed to interactions with the nearby solvent than, for instance, a cationic guanine unit between adjacent base-pairs in a π-stack. Thus, a larger polarization of the neighboring solvent, hence a higher solvent reorganization energy can be expected in the two-spheres model. These two effects, missing internal reorganization energy and overestimated solvent reorganization energy, partially compensate each other in the two-spheres model, as the following discussion suggests.

Experimental reorganization energies for hole transfer between guanines in DNA duplexes containing the sequences GA_nG or GT_nG (n = 1, 2) fall into the ranges 0.72–1.4 eV for n = 1 and 1.7–2.0 eV for n = 2;[251] for each n, the lower value corresponds to the sequence GA_nG. These values indeed are rather similar to the corresponding results of our two-spheres model (Table 6.8). For another approximate comparison with experimental data one may refer to the (non-symmetric) shift of an electron hole from 9-amino-6-chloro-2-methoxyacridine to a guanine unit in the DNA stack.[46] Those experimental values for the reorganization energy of hole transfer from the dye to a guanine, separated by one (AT) base-pair, fell into the range 0.85–1.20 eV,[46] which again is close to our estimate for $R_{DA} = 7$ Å.

Finally, we compare the present MD results obtained with a polarizable force field for a charge shift reaction to results of dielectric continuum models for hole transfer between guanine

units in the DNA stack employed.[112,168,176] As this latter type of modeling relies on a space partitioning associated with suitably assigned dielectric constants, results often depend notably on this parameterization. This is nicely illustrated in a study[112] where the dielectric constant ε_{bw} assigned to the "bound water" region around the DNA stack was varied from 2 to 32. The smallest results, 1.21±0.03 eV at $R_{DA} = 6.8$ Å and 1.46±0.04 eV at $R_{DA} = 10.1$ Å, obtained with $\varepsilon_{bw} = 2$, agree well with those of the present two-spheres model (Table 6.8), which in turn are expected to overestimate the solvent reorganization energies of DNA systems (see above). Thus, results of that dielectric continuum model[112] seem to overestimate somewhat solvent reorganization energies of hole transfer in DNA. Indeed, other studies using dielectric continuum models suggested slightly[176] or notably smaller values.[168] The latter low values show the desired agreement with some experiments[234] and results derived from a method that relies on approximate "polarization structure factors".[168]

6.8   Conclusion

In the present chapter a computational protocol for determining solvent reorganization energies for complex systems from atomistic simulations was established. The approach relies on the use of a force field, which adequately accounts for electronic polarization. While this issue has long been understood in principle,[92] the present results appear to be the first that agree quantitatively with the predictions of the two-spheres donor-acceptor model of Marcus.[93] According to the present study, it is of primary importance to choose a computational method that quantifies the potential energy gap, namely the dipole contribution to the solvent polarization at the atomistic level in a reliable fashion. For this purpose, a self-consistent iterative treatment of polarization[242] was successfully employed despite its relatively high computational cost.

Current results for charge separation and recombination reactions demonstrate a strictly linear dependence of the solvent reorganization energy λ_s on the inverse of the donor-acceptor distance R_{DA}. Unlike other earlier studies discussed in this chapter, the present results for λ_s agreed quantitatively with the predictions of the Marcus dielectric continuum model, yielding the theoretically expected reduction by ~45% due to electronic polarization effects. The distance dependence of λ_s from the present MD simulations with a polarizable water model suggests a scaling which is fully consistent with an experimental value of 1.79 for the effective optical dielectric constant of water. Thus, it was possible to clarify the situation of controversial choices between scaling factors that had been suggested in the literature to facilitate a consistency between the results of polarizable and non-polarizable simulations. Overall, a computational procedure was established that allows one to determine scaling factors for families of related molecular systems.

Preliminary results on a charge shift reaction for a two-spheres model yielded estimates of λ_s that suggest a substantial reduction of the values of published DNA-related systems. These results encourage further applications of the computational strategy elaborated here to estimate solvent reorganization energies in complex, heterogeneous systems that involve biomolecules, particularly DNA-based donor-acceptor complexes. A fully atomistic modeling avoids the ambiguities of continuum methods and the uncertainties when setting parameters for both the spatial partitioning and the corresponding dielectric constants. However, such studies put strict requirements on the quality of the polarizable force field used. The present model study probed (almost exclusively) the polarizable force field POL3 for water, which seems to serve well for that purpose.

7 Solvent Reorganization Energy in A-DNA and B-DNA Duplexes

7.1 State of the art

In recent years many efforts have been invested into studies of electron transfer (ET) in DNA because of its importance for oxidative damage and photorepair processes.[252,253] Expected benefits from possible applications of DNA in nanoelectronic devices are also of current interest.[254,255] As shown by experiments,[48] electron holes generated in DNA can propagate along the π-stack over long distances. The rates of such non-adiabatic hole transfer processes were found to depend on the structure of DNA, both on the base-pair sequence and the helical conformation.[31,34,35] Another important source controlling the rate constants is the structural relaxation of the solvent that surrounds the donor (D) and the acceptor (A) involved in the electron transfer.[94,126] This relaxation is taken into account through an exponential Franck-Condon factor (Eq. 3.1) via two key quantities, namely, the free energy difference $\Delta G°$ between D and A states and the reorganization energy λ.[94,256]

The contribution of the solvent to the reorganization energy is one order of magnitude larger than the contribution of the solute and is usually estimated by dielectric continuum models,[112,176,180] which exhibit serious drawbacks and limitations as discussed in Chapter 4. Despite well-known disadvantages, these models still represent the most popular simulation method, which, however, delivers contradicting results within a wide range: either a modest (less than 0.1 eV) distance dependence of the reorganization energy of ET in DNA,[180] or a prominent change of λ_s with the D-A distance.[112,168,176] Experimental results being contradictory themselves, e.g. yielding essentially distance-independent values[234,257] of λ_s or a notable distance dependence,[46,251] cannot be used to resolve the discrepancies between various predictions from dielectric continuum models.

In Chapter 6, it has been demonstrated[258] that electronic polarization is key for obtaining correct solvent reorganization energies and the procedure on the example of the two-spheres model of Marcus was elucidated. The current Chapter 7 describes the application of this protocol to evaluate λ_s of electron transfer in ideal A-DNA and B-DNA duplexes. The

following Chapter 8 illustrates MD results on solvent reorganization energies for ET processes in experimentally studied chromophore-DNA complexes and represents the first report of large-scale MD simulations on such systems where an atomistic treatment of water and a polarizable force field are applied.

7.2   Ideal A-DNA and B-DNA models

The MD simulations were carried out with two force field versions: polarizable *ff02*[219,237,259] and non-polarizable *ff99*[260] as implemented in the package AMBER 8.[220] The initial structures of the DNA duplexes were created with modules *nucgen* and *leap*. The appropriate number of Na$^+$ ions was added to neutralize the negative charges of the DNA phosphates; terminal ribose moieties were left without external phosphates and were capped by O5'H and O3'H groups. In all cases studied, the electrostatic interactions for fixed charges and induced dipoles were determined with the particle mesh Ewald (PME) method.[222,241,242] Four groups of DNA duplexes were treated in the MD simulations:

(i) The first group dealt with a symmetric ET reaction ($\Delta G° = 0$) between the 2nd and the 5th guanine (in italic font) of the 6-mer duplex 5'-GG^+GGGG-3', embedded in a periodic box of 3500 water molecules. For this system several model variants were explored: (a) force field (additive *ff99* vs. non-additive *ff02*), (b) water model (non-polarizable TIP3P[182] vs. polarizable POL3[209]), (c) ensemble (NVE vs. NPT), (d) absence or presence of electronic polarization simulated by induced dipoles for various molecular groups.

(ii) The second group included simulations of an ET reaction between guanines separated by AT-bridges of different length, which were modeled by a set of seven duplexes 5'-GG^+GT$_n$GGG-3' (n = 0–6), in A-DNA and B-DNA conformations (Figure 7.1a), each embedded in a periodic box filled with water molecules. For each of these systems two simulations were carried out: with polarizable (*ff02*, POL3) and non-polarizable force fields (*ff99*, TIP3P). For each AT base-pair, 250 water molecules were added to the amount used in model (i). Separate atomic charges were derived to describe the guanine radical-cation G^+ with *ff02* and *ff99*; details are provided in Appendix B (Table B1, Figures B1, B2).

(iii) The third group of simulations addressed four B-DNA duplexes of nucleotide sequence 5'-GAG^+X$^{(k)}G$AG-3' (X$^{(1)}$ = A, X$^{(2)}$ = AA, X$^{(3)}$ = T, X$^{(4)}$ = TT; k = 1–4; Figure 7.1b), with the polarizable force field *ff02*. In these calculations we used the same number of POL3 water molecules as in the analogous models of group (ii).

a 5'-GG$^+$G(T)$_n$GGG-3' n = 0–6

A-DNA B-DNA

b 5'-GAG$^+$X$^{(k)}$GAG-3'

X$^{(k)}$ = A, AA, T, TT
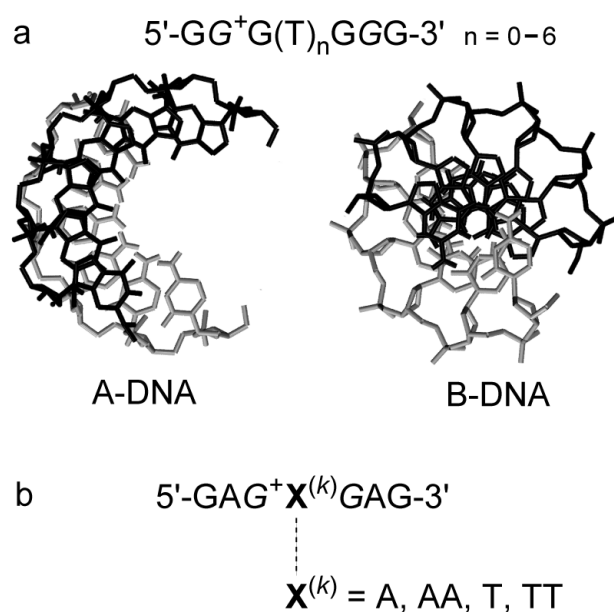
Figure 7.1. (a) Ideal structures of the hexamer duplex 5'-G*G*$^+$GG*G*G-3' as A-DNA (left panel) and B-DNA (right panel). (b) Schematic representation of model duplexes constructed in B-DNA form to simulate structures studied experimentally in Ref. 251.

7.3 MD simulations and evaluation of λ_s

The previously described equilibration procedure[261] was applied (Chapter 6), which employed an atom-based cutoff of 12 Å for the Lennard-Jones interactions and a heating stage of 50 ps where the temperature was increased from 0 K to 300 K. After heating the system to 300K, additional pre-production runs of 150 ps in an NPT ensemble for models (i) to (iii) were carried out. Throughout all stages of the simulation with a "rigid" solute geometry, the atoms of the solute were restricted to the coordinates of the ideal DNA structure by harmonic constraints with force constants of 500 kcal mol^{-1} Å^{-2}.

For the NVE simulations of model (i) we introduced an additional stage after the NPT pre-production run.[235] First, an NVT ensemble was invoked for 20 ps with an Andersen temperature coupling scheme (relaxation time of 0.4 ps).[239] After each of 15 cycles containing 2000 MD steps of 0.25 fs, the velocities were rescaled to the target temperature of 300 K. Finally, before beginning production runs in an NVE ensemble, an equilibration run of 20 ps at 300 K in a NVT ensemble was carried out, employing a Berendsen thermostat.[229]

Model (ii) aimed at a thorough evaluation of the D-A distance dependence of λ_s. Therefore, in an NPT ensemble with Berendsen thermostat at 300 K, a series of production runs of lengths

50 ps, 100 ps, or 150 ps for duplexes with 0, 1 to 3, and 4 to 6 intervening AT base-pairs, respectively, were conducted. The same atom-based cutoff of 12 Å for the Lennard-Jones interactions was applied. These simulations demonstrated that reorganization energies are rather stable and that an extension of a trajectory by 50 ps shifted the average λ_s value at most by 0.15 eV. Therefore, in all other cases, only trajectories of 50 ps were used.

All production runs were carried out with "frozen" hydrogen-containing bonds. For this purpose the SHAKE[238] algorithm with an integration time step of 0.5 fs was employed. The induced dipoles that simulated the electronic polarization were determined with an iterative procedure.[242,258] The convergence criterion for the minimization of the potential energy of the induced dipoles, which simulate the electronic polarization in the electrostatic field of the nuclei, was set to 10^{-7} Debye for the iterative procedure performed at each time step.

Snapshots from the trajectories were recorded every 2 fs during all production runs. For the analysis of the potential energy gap between the initial and final hole states of ET "single-point" energy calculations were performed. The analysis procedure was identical to the one described in Chapter 6: the nuclei were fixed at the positions of the snapshot, but the charge distribution was adjusted to represent the final state of the ET process during a single MD step of 0.005 fs, accompanied by the iterative procedure to determine the induced dipoles of the final state.[242] For ET between chemically different donor and acceptor moieties, the reorganization energy can be obtained by averaging the potential energy gaps ΔU of forward (i) and backward (f) processes [see method (I) in Chapter 6], $\lambda_s = (<\Delta U>_i - <\Delta U>_f)/2$. Here, ΔU is the difference between the two potential energies, calculated at the same solvent configuration, but with the hole located at the initial or final states of each of the two reactions. For such non-symmetric ET at the shortest distances, 3.4 Å and 6.8 Å, the standard deviations S_i and S_f of the corresponding potential energy gaps were averaged according to $S^2 = (S_i^2 + S_f^2)^{1/2}/2$. Further details of the procedure have been discussed in Chapter 6.[258]

7.4   Polarization effects of DNA molecular groups

7.4.1   *Computational strategy*

Despite the fact that the following discussion will deal with polarization in the framework of non-additive force fields, the polarization contributions will still be discussed in terms of additivity because this approach offers a convenient, albeit approximate way of interpreting the various energy contributions in such a complex system as DNA.

Table 7.1. Solvent reorganization energy λ_s (eV) of hole transfer between G_2 and G_5 in the rigid ideal B-DNA duplex 5'-GG^+GGGG-3' from calculations with polarizable (*ff02*) and non-polarizable (*ff99*) force fields (FF) of DNA and the corresponding water models POL3 and TIP3P, respectively. In the model (*ff02*, POL3), the electronic polarization was also partially switched off for various groups: guanosines G_2 and G_5, all backbone phosphates (PO$_4^-$), or the whole DNA duplex. Results from experiment and a dielectric continuum model (DCM) shown for comparison.

Setup	FF [a]	Pol. DNA[b]	Pol. $G_{2,5}$[c]	Solvent	Ensemble	λ_s^{np} [d]	λ_s^{pol} [e]
1	*ff99*	off	off	TIP3P	NVE	2.23±0.29	2.18±0.33
2		off	off		NPT	2.21±0.34	2.19±0.32
3	*ff02*	on	on			1.75±0.29	1.73±0.30
4		on	off			1.72±0.28	1.73±0.30
5	*ff99*	off	off	POL3		1.95±0.29	1.93±0.28
6	*ff02*	on	on			1.44±0.26	1.43±0.24
7		on	off			1.44±0.25	1.43±0.26
8		on, PO$_4^-$ off	on			−	1.54±0.24
9		off	off			−	1.77±0.27
DCM [f]	*ff99*	off	off	$\varepsilon_{bw} = 2$		1.46±0.03	−
				$\varepsilon_{bw} = 4$		1.64±0.02	−
				$\varepsilon_{bw} = 80$		2.04±0.07	−
Exp.[g]						1.60±0.10	

[a] Force field assigned to DNA, except for the charges of the guanine units G_2 and G_5.

[b] Polarizabilities assigned to DNA within corresponding force fields except for the units G_2 and G_5.

[c] Polarizabilities assigned to the units G_2 and G_5.

[d] Reorganization energy λ_s^{np} from a simulation with the charges of the units G_2 and G_5 derived for the non-polarizable force field *ff99*; see section 7.2.

[e] Reorganization energy λ_s^{pol} from simulations with the charges of the units G_2 and G_5 derived for the polarizable force field *ff02*; see section 7.2.

[f] Results for a dielectric continuum model (DCM); ε_{bw} is the dielectric constant of the region of bound water. See Ref. 112.

[g] Experimental total reorganization energy λ, Ref. 46.

The simplification of keeping the DNA rigid permitted to leave aside the internal reorganization energy. Furthermore, the partial polarization contributions of various atomic groups were probed by setting to zero their pertinent induced dipoles. Comparison of the

resulting reorganization energy to those of the completely polarized system provided indirect access to the polarization effects of specific groups of atoms.

Set (i) of the simulations aimed at a study of the overall influence of electronic polarization on the reorganization energy and at separating the effects of solute and solvent polarizations. In addition, an attempt was made to identify the effect of specific groups in the systems of interest. Two sets of simulations with charges assigned to guanines G_2 and G_5 that had been derived for non-polarizable *ff99* and polarizable *ff02* force fields for different setups of B-DNA were conducted; see Table 7.1 where the corresponding reorganization energies are denoted as λ_s^{np} and λ_s^{pol}. The absolute differences $|\lambda_s^{np} - \lambda_s^{pol}|$ between two corresponding values ranged up to 0.05 eV (Table 7.1, Setups 1–7), which is significantly lower than the typical standard deviation of the method (~0.3 eV). Therefore, we refrained from interpreting these differences. Thus, only the overall charge transferred between the two guanine sites, but not the individual atomic charge distribution, is essential for the reorganization energy. Later on, we will discuss only λ_s^{pol} values, unless stated otherwise (Table 7.1).

7.4.2   *Sensitivity of λ_s to force field parameters in TIP3P water*

In the following three subsections, the effects of polarizable force fields, for the example of a 6-mer B-DNA duplex with a donor-acceptor distance $R_{DA} = 10.1$ Å will be discussed in detail; see model (i) of section 7.2.

The calculations of reorganization energies of B-DNA were started from the completely non-polarizable setup (*ff99*, TIP3P) in NVE and NPT ensembles. These results, derived *with the same force field*, were the largest among all values of our study: (2.18±0.33) eV and (2.19±0.32) eV, respectively (Table 7.1). The results for the two ensembles for both sets of charges on G_2 and G_5 are identical to the accuracy of the method. In the following, only the results from NPT ensembles will be discussed, as they are the most straightforward to compare to experimental data.

As a next step the internal electronic polarization in the DNA solute by means of the polarizable force field *ff02* in the presence of a non-polarizable TIP3P solvent (Table 7.1, Setup 3) was introduced. The resulting reorganization energies, 1.73–1.75 eV, were 0.4–0.5 eV smaller than the values from completely non-polarizable setups (*ff99*, TIP3P). Setup 4 (*ff02*, TIP3P) allows one to examine the partial contributions due to the polarization of the guanines G_2 and G_5, where induced dipoles on the two bases were switched off. The results obtained with either set of atomic charges demonstrate that the induced dipoles on the guanine moieties contribute very little (0.01–0.02 eV) to the overall reorganization energies. Thus the reorganization energy of the ET process in the DNA related systems under study is overwhelmingly dominated by the cooperative effect of the induced dipoles of the whole DNA molecule (and the contribution due to the reorientation of the water molecules).

7.4.3   *Sensitivity of λ_s to force field parameters in POL3 water*

The simulations with the polarizable solvent model POL3 permit one to elucidate in more detail the effect of the atomic charges and the electronic polarization of the nucleobases (Table 7.1, Setups 5–9). The solvent reorganization energy is lowered by 0.5 eV, from 1.93±0.28 eV to 1.43±0.24 eV, when stepping from model (*ff99*, POL3) to the fully polarized model (*ff02*, POL3); cf. Setups 5 and 6. The latter model yields the lowest value among all setups studied. Interestingly, the reduction of the solvent reorganization energy due to electronic polarization of the entire DNA is independent of the choice of the solvent model: it is 0.5 eV in both POL3 (Table 7.1, Setups 5 and 6) and TIP3P solvents (Table 7.1, Setups 2 and 3). From this finding one concludes that the electrostatic field patterns generated by non-polarizable TIP3P water and polarizable POL3 water are similar; after all, the atomic descriptors of the *ff99* force field are intended to represent simultaneously atomic charges and electronic polarizations. As in the case of TIP3P water, the local polarization of G_2 and G_5 in POL3 water does not seem to exert a notable effect; cf. Setups 6 and 7.

Also, in the simulation with the force fields *ff02* and POL3, the polarizability of the PO_4^- groups of the entire DNA backbone was switched off (Table 7.1, Setup 8); these groups mainly carry the negative charge of the system. Apparently, the polarization of the phosphate groups reduces the reorganization energy by 0.11 eV; cf. Setups 6 and 8. This rather modest perturbation corroborates previous results.[262] Finally, the effect of the electronic polarization of the entire DNA duplex was examined; for this purpose, all induced dipoles of the solute (Setup 9) were switched off. The result, 1.77±0.27 eV, of this latter setup should be treated with caution because the DNA solute is artificially underpolarized. Therefore, this perturbation cannot be considered as small, as the energetics is notably affected. Comparison with the fully polarized model (*ff02*, POL3) (Setup 6) shows that the (intrinsic) electronic polarization of the duplex reduces λ_s by 0.34 eV; this reduction is twice as large as the effect of the charge set of the DNA, 0.16 eV; cf. Setups 5 and 9.

7.4.4   *Comparison to dielectric continuum models of the solvent*

Recently our group reported a computational study on solvent reorganization energies of charge shift reaction in rigid duplexes of B-DNA structure where a dielectric continuum model (DCM) had been used.[112] A notable ambiguity of that computational approach, in addition to the spatial partitioning itself, was the uncertainty in assigning dielectric properties to the various regions of the solvent. In particular, λ_s values of a hexamer duplex varied from 1.46±0.03 eV to 2.04±0.07 eV as the dielectric constant ε_{bw} of the bound water region changed from 2 to 80;[112]

see also Table 7.1, Setup DCM). Note that the charges of the force field *ff94*[191] used in that earlier work were the same as those of the force field *ff99*[260] used in the present study.

In the DCM calculations,[112] various regions of the DNA duplex (bases, sugar-phosphate backbone) were assigned different dielectric screening properties to mimic the electronic response of the solute. Therefore, those results of the reorganization energies are compared to those of the fully polarizable model (*ff02*, POL3), rather than to model (*ff99*, POL3). The bare correction due to the changes of charge sets is the difference of 0.16 eV between the λ_s values of models (*ff99*, POL3) (Setup 5) and (*ff02*(off), POL3) (Setup 9). With this correction added to the result of (*ff02*, POL3), the reorganization energy, 1.59 eV, falls between the two lowest λ_s values of the DCM model that correspond to $\varepsilon_{bw} = 2$ and $\varepsilon_{bw} = 4$ (Setup DCM). This remarkable consistency between results of the parameterized DCM model and the "parameter-free" explicit polarizable force field calculations of the present work does not guarantee adequate λ_s values because of the systematic, though small underestimation of the induced polarization that is intrinsic to the force field *ff02*.[213] The latter does not fully account for self-polarization because mutual induction arising from 1-2 and 1-3 atomic interactions is neglected.[213]

This underestimation of the polarization is expected to cause λ_s values to be too large. This tendency for DNA as solute will be estimated by comparison with similar effects in the water model POL3 where 1-2 and 1-3 interactions are missing as well. Water model POL3 yields a polarizability of water, 0.87 Å^3, that is only ~60% of the gas phase value, ~1.46 Å^3,[263] which is also obtained in the simulations when those interactions are included.[213] MD simulations with a reduced molecular polarizability of 1.0 Å^3 reproduced properties of bulk liquid water, including the static polarizability, in an excellent fashion.[250] Further support for a reduced value comes from *ab initio* calculations on small water clusters,[264,265] where the polarizability was determined 7–9% below the experimental value for a single molecule in the gas phase.[263] Modeling of λ_s for a Marcus two-spheres model (Chapter 6) suggested[258] that the POL3 force field satisfactorily reproduces the dielectric properties of water as solvent despite this slight underestimation of the polarizability, 0.87[213] vs. 1.0 Å^3.[250] The fact that the polarizability of bulk water is notably lower than that of a water molecule in the gas phase was attributed to Pauli repulsion between neighboring solvent molecules.[266] Therefore, assuming that Pauli repulsion plays a similar role when modeling DNA as solute (without 1-2 and 1-3 interactions), it seems appropriate to scale the resulting λ_s values by a factor $\kappa = 0.87/1.0$ before comparing with experiment (see below). Such scaling should be valid if the change of the polarization contribution induces a small perturbation of the total energy of the system. Therefore, the response is expected to be linear, even though the formal expressions of the polarizable force field are not.[213]

7.5   Comparison of λ_s with experimental studies on hole transfer in DNA

To facilitate a direct comparison of calculated reorganization energies with experimental data, a series of simulations with a polarizable force field was carried out for some recently studied DNA duplexes.[251] In these duplexes of 14 or 15 base-pairs (with tethered naphthalimide and phenotiazine), hole transfer occurs between two guanine bases separated by various bridges (Table 7.2). For the simulations, the experimentally studied systems were reduced to the models 5'-GA*G*X$^{(k)}$*G*AG-3' (X$^{(1)}$ = A, X$^{(2)}$ = AA, X$^{(3)}$ = T, X$^{(4)}$ = TT) by simplifying the terminal units to 5'-GA and AG-3' (Figure 7.1, Table 7.2). The two base-pairs GA and AG were left as termini of the strands to limit edge effects. Edge effects were found to be negligible. For instance, the reorganization energy λ_s = 1.23±0.24 eV was obtained for the sequence 5'-G*G*$^+$G*G*GG-3' (R_{DA} = 6.8 Å) and 1.43±0.24 eV for the sequence 5'-G*G*$^+$GG*G*G-3' (R_{DA} = 10.1 Å), both for B-DNA. The terminal sequences are different from the standard cases of the present work (Table 7.3), but the λ_s values are essentially the same within standard deviations: 1.17±0.22 eV (R_{DA} = 6.8 Å, X$^{(3)}$ = T) and 1.51±0.25 eV (R_{DA} = 6.8 Å, X$^{(4)}$ = TT).

Simulations of rigid as well as flexible duplexes showed a slight increase of the reorganization energies by 0.1 eV (A-bridges) and 0.2 eV (T-bridges) due to vibrations of the DNA backbone; one should recall that solvent reorganization energies are overestimated because 1-2 and 1-3 electrostatic interactions are missing in the force field.

For an adequate comparison with experimental results, (*i*) the calculated solvent reorganization energies λ_s were scaled by κ = 0.87 to account for the missing 1-2 and 1-3

Table 7.2. Reorganization energies (eV) of hole transfer in the rigid B-DNA duplexes 5'-GA*G*$^+$X$^{(k)}$*G*AG-3'.

G^+X$^{(k)}$G	λ_s	λ'_s ^{a}	(λ_s^κ) ^{b}	λ ^{c}	λ_{exp} ^{d}
G^+AG	1.32±0.24	1.41±0.25	1.15±0.21	1.49±0.21	0.72±0.14
G^+TG	1.17±0.22	1.40±0.30	1.02±0.19	1.36±0.19	1.40±0.28
G^+AAG	1.53±0.25	1.62±0.28	1.33±0.22	1.67±0.22	1.70±0.34
G^+TTG	1.51±0.25	1.73±0.26	1.31±0.22	1.67±0.22	2.00±0.40

^{a} Solvent reorganization energy calculated for a flexible duplex, reflecting the partial contribution from the internal reorganization energy due to DNA backbone vibrations.

^{b} Scaled solvent reorganization energy λ_s^κ = 0.87 λ_s to account for the reduced polarization in the force fields *ff02* and POL3 solvent due to lack of 1-2 and 1-3 interactions (see text).

^{c} Estimated total reorganization energy $\lambda = \lambda_s^\kappa + \lambda_i$ where λ_i = 0.34 eV is the internal reorganization energy of a GC pair of the hexamer duplex (GC)$_6$, calculated at the UB3P86/6-311+G* level, Ref. 116.

^{d} Experimental errors estimated according to the reported value of 20%; Ref. 251.

polarization, and (*ii*) the internal reorganization energy λ_i was added. There was no account for quantum effects,[267] because it was assumed that in the rigid model duplexes ET occurs only through one vibronic channel. For correction (*ii*) one should note that although the hole seems to be confined to a single base-pair due to solvation effects,[53,54,268] the estimate $\lambda_i = 0.72$ eV for the (GC) base-pair at the B3LYP/6-31G(d) level[112] is probably too high because it was determined for an isolated base-pair. Yet, the structure relaxation of a base-pair inside a DNA duplex should be sterically hindered from adjacent base-pairs and solvent, thereby leading to a lower value. A recent DFT study on λ_i in DNA duplexes supports this expectation: λ_i was shown to decrease with the length of the (GC)$_n$ duplexes from 0.72 eV (n = 1) to 0.34 eV (n = 6).[116] This model study did not account for solvent stabilization on the geometry relaxation. Therefore, one may consider the estimate of λ_i, 0.34 eV as an upper limit for hexamer DNA duplexes.

Scaling the four λ_s values of rigid DNA duplexes by κ and subsequent addition of $\lambda_i = 0.34$ eV resulted in total reorganization energies for the duplexes GA*G*X$^{(k)}$*G*AG-3' from 1.36±0.19 eV (X$^{(3)}$ = T) to 1.67±0.22 eV (X$^{(2,4)}$ = AA, TT) (Table 7.2). Two of these adjusted computational results agree remarkably well with the corresponding experimental values:[251] 1.40±0.28 eV (X$^{(3)}$ = T) and 1.70±0.34 eV (X$^{(2)}$ = AA). The computed result 1.67±0.22 eV for the duplex with X$^{(4)}$ = TT agrees with the corresponding experimental estimate, (2.00±0.40) eV, within standard deviations.[251] Only one MD result, 1.49±0.21 eV, for the oligomer 5'-GA*G*A*G*AG-3' (X$^{(1)}$ = A), is more than twice larger than the corresponding experimental value, 0.72 eV. On the one hand, the calculated result is fully consistent with the other calculated results of the series; on the other hand, the experimental result seems to be an outlier among the reported experimental data.[251]

From this success one can conclude that solvent reorganization energies λ_s, calculated for rigid duplexes with the polarizable force fields (*ff02*, POL3) and scaled by a factor $\kappa = 0.87$ for the missing 1-2 and 1-3 polarization effects in *ff02*,[213] ultimately yield sufficiently accurate estimates of total reorganization energies λ for ET in DNA-related systems when combined with recently reported values of λ_i for base-pairs in DNA duplexes.[116] In the following sections the main aim will be to relate solvent reorganization energies λ_s obtained by means of polarizable and non-polarizable force fields; therefore, the scaling factor $\kappa = 0.87$ will not be applied further on.

7.6   Distance dependence of λ_s in ideal A-DNA and B-DNA

Computer experiments[261,269] showed that A-DNA is able to change its conformation into B-form within several hundred picoseconds, given an appropriate nucleotide sequence and suitable simulation conditions. Before comparing calculated reorganization energies with

experimental results for systems where the macromolecule may undergo a conformational transformation, the influence of the DNA conformation on λ_s for hole transfer via a range of D-A distances R_{DA} was tested. For the two setups, (*ff02*, POL3) and (*ff99*, TIP3P), fully polarizable and fully non-polarizable, respectively, MD simulations on the ideal rigid duplexes 5'-GG^+GT$_n$GGG-3' (n = 0–6) were carried out, both in A- and B-DNA conformations (Figure 7.1a). Hole transfer was assumed to occur between the moieties G_2 and G_5, separated by (TA) bridges. In Table 7.3 the distance-dependent results are represented together with a formal R_{DA} parameter, defined as the distance between the molecular planes of the two pertinent (GC) base-pairs.

Inspection of Table 7.3 reveals that, within standard deviations, corresponding rigid models of duplexes in A- and B-forms exhibit essentially equal solvent reorganization energy at all D-A separations studied. Yet, λ_s values of the three shortest distances, R_{DA} = 3.4–10.1 Å, tend to be slightly lower for the B-form (by ~0.1–0.2 eV) for either setup, i.e. with non-polarizable and polarizable force fields. This observation is consistent with the 3D shape of A and B duplexes (Figure 7.1a) possessing different widths: the bases G_2 and G_5 are slightly farther apart in the A-

Table 7.3. Solvent reorganization energies λ_s^{np} and λ_s^{pol} (eV) from simulations with non-polarizable[a] and polarizable[b] force fields, respectively, for hole transfer between guanine units (G) in the rigid duplexes 5'-GG^+GT$_n$GGG-3' of A- and B-DNA. Donor-acceptor distances R_{DA} (Å) and available experimental reorganization energies are also shown.

| R_{DA} | n | A-DNA | | | B-DNA | | | |
		λ_s^{np}	λ_s^{pol}	$\tilde{\varepsilon}_\infty^{\,c}$	λ_s^{np}	λ_s^{pol}	$\tilde{\varepsilon}_\infty^{\,c}$	$\lambda_{exp}^{\,d}$
3.4 [e]	0	1.10±0.20	0.72±0.20	1.52±0.49	0.94±0.20	0.66±0.14	1.42±0.42	0.6±0.1
6.8 [f]	0	2.00±0.33	1.39±0.23	1.43±0.33	1.92±0.27	1.23±0.24	1.55±0.37	1.2±0.1
10.1	0	2.34±0.32	1.58±0.27	1.47±0.32	2.21±0.34	1.43±0.24	1.54±0.34	1.6±0.1
13.5	1	2.53±0.33	1.68±0.31	1.50±0.33	2.46±0.34	1.71±0.28	1.43±0.30	
16.9	2	2.63±0.34	1.84±0.30	1.42±0.29	2.78±0.34	1.82±0.28	1.52±0.29	
20.3	3	2.75±0.37	1.96±0.31	1.40±0.29	2.82±0.38	2.00±0.29	1.40±0.27	
23.7	4	2.85±0.35	2.02±0.30	1.40±0.27	2.94±0.38	2.05±0.28	1.43±0.26	
27.0	5	2.98±0.37	2.06±0.29	1.44±0.27	3.04±0.37	2.07±0.31	1.46±0.28	
30.4	6	3.00±0.37	2.08±0.30	1.43±0.25	3.14±0.34	2.12±0.30	1.47±0.26	

[a] Setup (*ff99*, TIP3P). [b] Setup (*ff02*, POL3).

[c] Effective optical dielectric constant, Eq. (4). Averages over the whole range of R_{DA} distances $\langle \tilde{\varepsilon}_\infty \rangle$ = 1.45±0.32 for A-DNA and $\langle \tilde{\varepsilon}_\infty \rangle$ = 1.47±0.31 for B-DNA.

[d] Experimental values of the total reorganization energy, Ref. 251.

[e] Hole transfer $G_3 \rightarrow G_4$. [f] Hole transfer $G_2 \rightarrow G_4$.

form, with its wider loop, than in the B-form. As these small differences between reorganization energies of A and B forms are of the same order as the standard deviations, they will be not treated as meaningful; rather, both sets of values will be considered as essentially identical.

The solvent reorganization energies from the simulations on the three flexible duplexes are similar to those of the analogous rigid duplexes of both forms of DNA also with respect to their distance dependence (Table 7.4). Comparison with the experimental data[46] listed in Table 7.3 for the three shortest distances R_{DA} = 3.4 Å–10.1 Å demonstrates that the theoretically obtained average values are slightly higher (~0.1–0.2 eV). Still, calculated and experimental results agree within the standard deviations.

It is also interesting to compare the present results from the polarizable force fields (*ff02*, POL3) to those obtained earlier by our group with a DCM approach (see above).[112] For large D-A separations, the λ_s values from both theoretical procedures are very similar (Figure 7.2a). A more detailed inspection shows that for R_{DA} > 13.5 Å λ_s values for both A- and B-DNA from the (*ff02*, POL3) setup agree best with the DCM results obtained with ε_{bw} = 4. Recall that the present MD approach on the basis of the polarizable force fields (*ff02*, POL3) avoids ambiguities of a DC model that are associated with the various parameters,[168] e.g., the spatial partitioning and the assignment of the corresponding dielectric constants.

Table 7.4. Variation of the solvent reorganization energy λ_s (eV) for hole transfer between guanines (*G*) in flexible duplexes 5'-G*G*$^+$GT$_n$G*G*G-3' of A- and B-DNA type with the donor-acceptor distance R_{DA} (Å). Comparison of results from MD simulations with the solute flexible or kept rigid.[a]

R_{DA}	n	A-DNA		B-DNA	
		$\lambda_s^{\,b}$	$\lambda_s^{\,c}$	$\lambda_s^{\,b}$	$\lambda_s^{\,c}$
3.4 ^{d}	0	0.72±0.20	0.95±0.20	0.66±0.14	0.84±0.20
6.8 ^{e}	0	1.39±0.23		1.23±0.24	
10.1	0	1.58±0.27	1.74±0.27	1.43±0.24	1.75±0.27
13.5	1	1.68±0.31		1.71±0.28	
16.9	2	1.84±0.30	1.94±0.31	1.82±0.28	1.95±0.30

[a] The simulations were carried out in an NPT ensemble with the AMBER force field *ff02* and the POL3 water model. n designates the number of A-T base pairs between donor and acceptor.

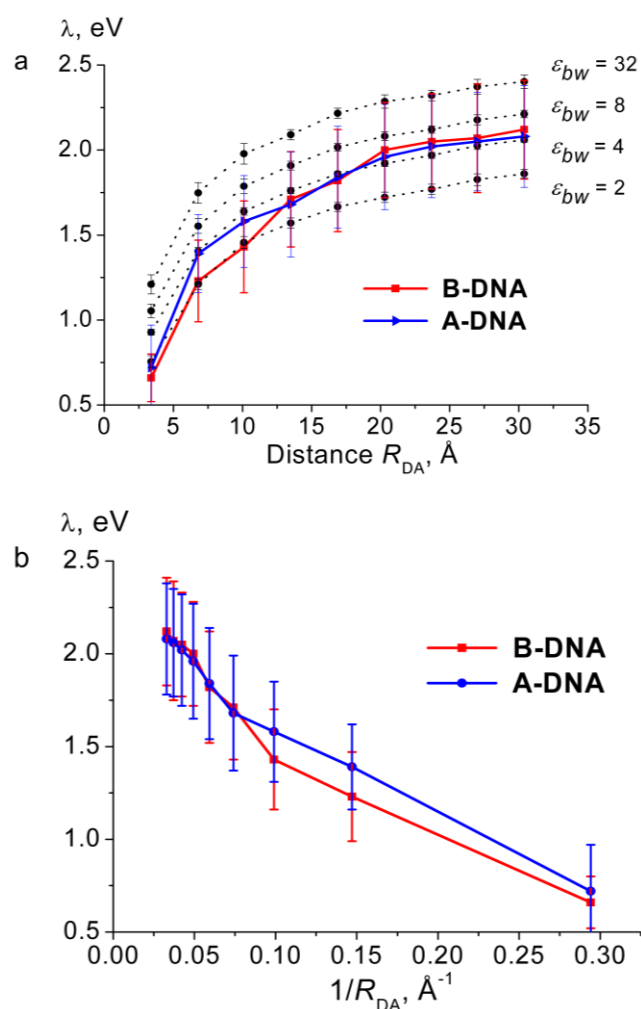[b] Solvent reorganization energy for rigid DNA duplexes.

[c] Solvent reorganization energy for flexible DNA duplexes.

[d] Hole transfer $G_3 \rightarrow G_4$.　　[e] Hole Transfer $G_2 \rightarrow G_4$.

Plots of the reorganization energies of A- and B-DNA forms from the polarizable force fields as a function of the reverse distance R_{DA}^{-1} clearly demonstrate two ranges of linear behavior, below and above $R_{DA} = 10.1$ Å (Figure 7.2b; for details of the linear fits, see Table 7.5).

The two-spheres model of Marcus[93] predicts a strictly linear dependence of λ_s as function of R_{DA}^{-1} and this behavior can be expected to hold even for systems which strongly depart from that idealized geometry.[167,270] A plausible rationalization attributes the unusual behavior of λ_s, determined in the present MD simulations, to artifacts due to an insufficient representation of the polarization (or electronic screening) if donor and acceptor moieties are located too closely. In this context, one has to recall the inadequate self-polarization due to missing 1-2 and 1-3 inductions of the induced dipoles.[213]

Experimental studies[47,176,251] of charge transport in DNA duplexes noted an exponential

Figure 7.2. (a) Solvent reorganization energies (eV) for A-DNA and B-DNA duplexes 5'-GG^+GT$_n$GGG-3' (n = 0–6) from the MD simulations of this work and, for B-DNA, from the dielectric continuum model (DCM) approach for different choices ε_{bw} of the optical dielectric constants assigned to the region of bound water; see Ref. 112. (b) For the same model systems, dependence of the reorganization energy (eV) on the inverse of the donor-acceptor distance R_{DA}.

decay of the rate of ET with the donor-acceptor separation R_{DA}:

$$k_{ET}(R_{DA}) = k_0 \exp(-\beta R_{DA}) \tag{7.1}$$

With the Marcus expression for non-adiabatic ET in mind,[94,256]

$$k_{ET}(R_{DA}) = \frac{2\pi}{\hbar}\left|\left\langle H_{DA}(R_{DA})\right\rangle\right|^2 \exp\left[-\frac{(\Delta G^\circ(R_{DA}) + \lambda(R_{DA}))^2}{4\lambda(R_{DA})k_B T}\right] \tag{7.2}$$

one distinguishes two contributions to the falloff parameter β: β_e originating from the decay of the electronic coupling $|H_{DA}|^2$ and β_s steming from the distance dependence of ΔG° together with that of the reorganization energy λ. In the present case of ET between equivalent sites, $\Delta G^\circ = 0$. If one neglects the distance dependence of the internal reorganization energy λ_i, then the expression for the falloff parameter β_s simplifies to

$$\beta_s = \frac{1}{4k_B T}\frac{\partial \lambda_s}{\partial R_{DA}} \tag{7.3}$$

Here, k_B is the Boltzmann constant and T is the temperature. The present results for A- and B-forms of DNA duplexes yield falloff parameters β_s (The derivative is approximated as finite

Table 7.5. Coefficients A and B of linear fits y = A + Bx of the solvent reorganization energy λ_s (eV) as a function of the inverse x = R_{DA}^{-1} (Å^{-1}) of the donor-acceptor distance R_{DA}.

Model	Setup	R_{DA} (Å)	A (eV)	B (eV·Å)	R[a]	SD[b]
A-DNA	(*ff99*,TIP3P)	≤ 10.1	2.95±0.41	-6.29±1.74	0.999	0.084
		>10.1	3.37±0.53	-11.89±10.0	0.980	0.122
		All	3.10±0.17	-6.91±1.00	0.995	0.261
	(*ff02*,POL3)	≤ 10.1	2.03±0.35	-4.45±1.77	0.999	0.070
		>10.1	2.43±0.45	-9.95±8.84	0.995	0.056
		All	2.18±0.15	-5.11±1.10	0.989	0.267
B-DNA	(*ff99*,TIP3P)	≤ 10.1	2.88±0.40	-6.57±1.73	0.999	0.061
		>10.1	3.62±0.52	-15.35±10.0	0.985	0.134
		All	3.20±0.17	-7.88±1.00	0.989	0.448
	(*ff02*,POL3)	≤ 10.1	1.81±0.33	-3.92±1.33	0.999	0.033
		>10.1	2.47±0.43	-10.33±8.39	0.986	0.105
		All	2.17±0.14	-5.26±0.74	0.983	0.506

[a] Correlation coefficient of the linear fit of the solvent reorganization energy as function of the inverse x = R_{DA}^{-1} (Å^{-1}) of the donor-acceptor distance.

[b] Standard deviation of the linear fit of the solvent reorganization energy as function of the inverse R_{DA}^{-1} (Å^{-1}) of the donor-acceptor distance.

difference, $\partial\lambda_s/\partial R_{DA} \approx (\lambda_{i+1}-\lambda_i)/\Delta R_{DA}$ with $\Delta R_{DA} = 3.4$ Å in all cases.) that change fast with donor-acceptor separation, from 1.6–1.9 Å^{-1} for $R_{DA} = 3.4$ Å via 0.6 Å^{-1} at $R_{DA} = 6.8$ Å to ~0.1 Å^{-1} at the largest separations $R_{DA} \sim 25$–30 Å. This distance dependence of β_s is slightly stronger than that determined at the DCM level.[112] Before comparing to experimental values of β, one has to add the electronic contribution β_e which can be obtained from quantum chemical calculations of the coupling $|H_{DA}|^2$, usually estimated in the range 0.7–1.7 Å^{-1}.[73,271] Thus, with $\beta_s \approx 0.5$ Å^{-1} for $R_{DA} \approx 6$–10 Å, one estimates $\beta \approx 1.2$–2.2 Å^{-1}, similar to other theoretical studies.[168] These values corroborate fairly well the experimental results, 0.6–1.8 Å^{-1}, of Takada et al.,[251] but are notably larger than those reported[272] by Lewis et al.,[75,234] 0.7–0.9 Å^{-1}.

7.7 Scaling factors for λ_s in DNA hole transfer

Simulations of the solvent reorganization energy with a polarizable force field, especially of extended DNA-derived systems, require a notably larger computational effort than those with a non-polarizable force field. Therefore, attempts have been reported[91,187] to capture the effect of electronic screening via *a posteriori* scaling of solvent reorganization energies λ_s^{np} determined with a non-polarizable force field. Such a scaling factor may be derived from the Marcus two-spheres model[93] by relating solvent reorganization energies for polarizable and non-polarizable solvents; see the corresponding discussion in Chapter 6. Thus, one has: [91,187,258]

$$\lambda_s^{pol} / \lambda_s^{np} = \left(\tilde{\varepsilon}_\infty^{-1} - \varepsilon_0^{-1} \right) / \left(1 - \varepsilon_0^{-1} \right) \tag{7.4}$$

Here $\varepsilon_0 = 78.4$ is the static dielectric constant of water at the temperature 298 K and $\tilde{\varepsilon}_\infty$ is an effective optical dielectric constant; results of a non-polarizable force field are associated with $\tilde{\varepsilon}_\infty = 1$. One of the scaling factors recently applied to scale down λ_s in ET for dye-DNA hairpin complexes relied on the optical dielectric constant $\tilde{\varepsilon}_\infty = 1.11$.[91] This value arises from a study on the Marcus two-spheres model[89] and is considerably lower compared to our estimate 1.80 for polarizable water solvent.[258] Given the dissimilarity of the two-spheres model and a DNA duplex, before transferring[91] the scaling factors derived for a two-spheres model to DNA a thorough justification is expected.

Therefore, it is more reliable to use directly the data for calculated solvent reorganization energies for rigid A- and B-DNA duplexes from simulations with non-polarizable (*ff99*, TIP3P) and polarizable setups (*ff02*, POL3) to estimate the values of such a scaling factor and to judge their uniformity for different DNA duplexes and donor-acceptor distances. In Table 7.3 the resulting effective optical dielectric constants $\tilde{\varepsilon}_\infty$ are listed. Averaging performed over the range of distances $R_{DA} = 3.4$–30.4 Å studied yields $\langle\tilde{\varepsilon}_\infty\rangle = 1.45\pm0.32$ for A-DNA and $\langle\tilde{\varepsilon}_\infty\rangle = 1.47\pm0.31$ for B-DNA. Detailed inspection of Table 7.3 shows that there is no other apparent trend: neither related to donor-acceptor distance, nor to the type of DNA (A or B). This allows

us to suggest an overall average value $\langle \tilde{\varepsilon}_\infty \rangle = 1.46 \pm 0.32$ for all data represented in Table 7.3. The latter result is significantly larger than the value mentioned above, $\tilde{\varepsilon}_\infty = 1.11,$[89] but it is also notably smaller than the estimate, 1.80 ± 0.27, derived via MD simulations on models that reproduced quantitatively the classical Marcus two-spheres model[258] and corresponded well to the experimentally established effective optical dielectric constant 1.78 of pure water.[104] From the present results (Table 7.3), one may suggest that the difference between the estimates of $\tilde{\varepsilon}_\infty$ for the Marcus two-spheres model[258] and DNA reflects mainly the reduced effective polarizability within DNA. The region of the DNA stack is usually characterized by an optical dielectric constant close to 2,[112,176] which, in combination with static dielectric constants that vary from 3.4 to 20 for different DNA regions,[172,176] results in scaling factors close to that of the solvent water. In the present study the decay in the dielectric response, observed in the MD calculations and reflected in a scaling factor of ~1.5, is attributed to the reduced screening effect of induced dipoles within the guanine units G involved in the ET, where the effect of missing 1-2 and 1-3 interaction has to be most prominent.

This finding demands a thourough evaluation of the strategy, which suggests to transfer the scaling of a simple two-spheres model in aqueous solvent to a biomolecule, a practice that seems to be very effective for reducing the computational effort when modeling DNA-derived systems.[91] Another argument is that ET donor and acceptor sites of biomolecules are hardly ever fully accessible to the aqueous solvent, but rather surrounded by organic matter. Nevertheless, the idea of scaling reorganization energies obtained with non-polarizable force field to account for electronic polarization effects remains attractive. The question then arises: how to determine suitable scaling factors and to what extent they are transferable? It is tempting to assume that such transferability exists at least within a "family" of structurally similar biomolecules. In the following chapter this idea is explored by extending the study to chromophore-DNA complexes where the chromophore is semi-capped on top of DNA.

7.8   Conclusion

The solvent reorganization energy λ_s for hole transfer in a variety of DNA duplexes was estimated from MD simulations which employed the polarizable force field *ff02* in combination with the explicit water model POL3. The distance dependence of λ_s for A- and B-DNA duplexes (donor-acceptor distances 3.4–30.4 Å), the choice of the solvent model and the force field (including the influence of charge sets), and various molecular groups affecting the results, were discussed in detail. Results from MD simulations with the standard non-polarizable force field *ff99* and the TIP3P water model were used as reference to account for electronic polarization effect. It was demonstrated that values of λ_s are reduced by about 30% compared to those derived with the non-polarizable setup when one includes the electronic polarization with

a polarizable force field. The results from these atomistic calculations with a polarizable force field, which do not demand any "re-parameterization", are consistent with the lowest values of λ_s from earlier elaborations that employed an implicit solvent model.[112]

The λ_s from MD simulations performed according to the procedure established[258] (see Chapter 6) for calculations with a polarizable force field, were compared with recently reported experimental values. Simulations of ET between guanines *G* in experimentally studied duplexes[251] $G^+X^{(k)}G$ ($X^{(1)}$ = A, $X^{(2)}$ = AA, $X^{(3)}$ = T, $X^{(4)}$ = TT) agreed satisfactorily within the standard deviations of the method. A slight overestimation of λ_s was attributed to an intrinsic property of the force field used, which tends to be underpolarized.[213]

8 Solvent Reorganization Energy in Chromophore-DNA Complexes

8.1 Experimental study on Rhodamine 6G-DNA complexes

DNA complexes with chromophores have been studied[47,71,234,273,274] very intensively due to their potential application in the context of nano-electronic devices.[24,275] A chromophore attached to a duplex can act either as electron acceptor or electron donor[276] enhancing ET along the DNA π-stack.[277] The chromophore is usually covalently bound to one of the DNA strands
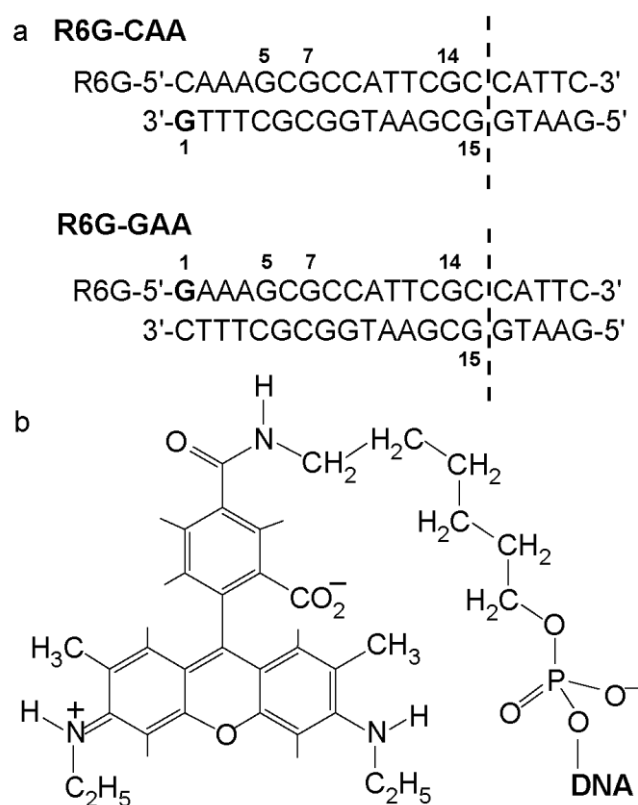
Figure 8.1. (a) Nucleotide sequence and designations of the R6G-DNA complexes studied. The NMR structure was resolved for the complex labeled R6G-CAA where Rhodamine 6G is tethered via a C_6 linker to the 5'-end cytosine (R6G-CAA, upper panel); Ref. 279b. Dashed lines indicate where the experimentally studied duplex was shortened to create models R6G-CAA and R6G-GAA for the MD simulations. (b) Schematic structure of Rhodamine 6G and its tether connection to the 5'-end of DNA.

through π-conjugated or aliphatic linker.[46,278] The rate of electron transfer strongly depends on the mutual alignment of the dye and DNA base-pair adjacent to it, influencing the degree of electronic overlap between them. The structure of dye-DNA hairpins with potential for effective hole transfer was studied by several groups.[58,70,71,279] Therefore, the structural characteristics of such complexes was also explored computationally.[280]

One of the chromophores studied both experimentally[279,281,282] and theoretically[280,283,284] was Rhodamine 6G (R6G) capping the DNA duplex (Figure 8.1a). The dye possesses zwitterionic properties due to a positively charged xanthene and negatively charged benzene rings lying in different planes; although bonded, these moieties are connected in a flexible fashion (Figure 8.1b). The xanthene ring acts as a source for electron holes in the DNA duplex. Recently two models of modified R6G-DNA duplexes (Figure 8.1a) were the subjects of MD studies in our group. For one of these complexes (Figure 8.1a, complex R6G-CAA), where the chromophore (Figure 8.1b) is attached to the 5' end of the DNA duplex, a fully resolved NMR structure[279a,282] suggested two distinct conformations of the dye. From experiments these two alignments of R6G with respect to the adjacent base-pair were estimated to occur with 20% and 80% population in R6G-CAA;[279] see Figure 8.2. The corresponding ratio was estimated to be 1:1 in R6G-GAA.[279a,282]

8.2   Model characterization of Rhodamine 6G-DNA complexes with MD refinement

To have more insight into the molecular structure and the dynamics of the R6G-DNA complexes, 10 ns molecular dynamics simulations were performed in our group[280] for two model R6G-DNA hairpin complexes that resembled those studied experimentally. The models were truncated along the dashed lines, shown in Figure 8.1a. With this MD study the presence
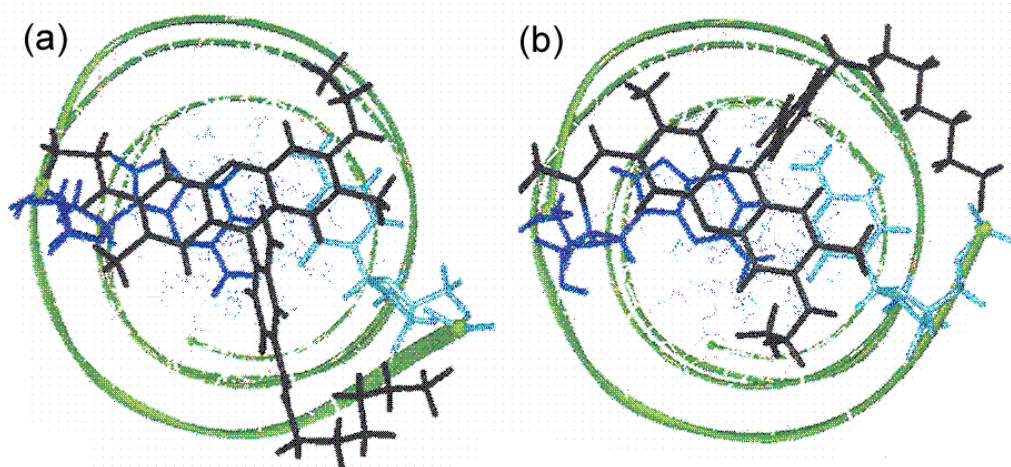
Figure 8.2. Top view of NMR resolved sub-structures of the R6G-CAA complex shown on Fig. 8.1a (upper panel). The relative population in the sample is: (a) 80 %; (b) 20 % (Adapted from Ref. 279a).
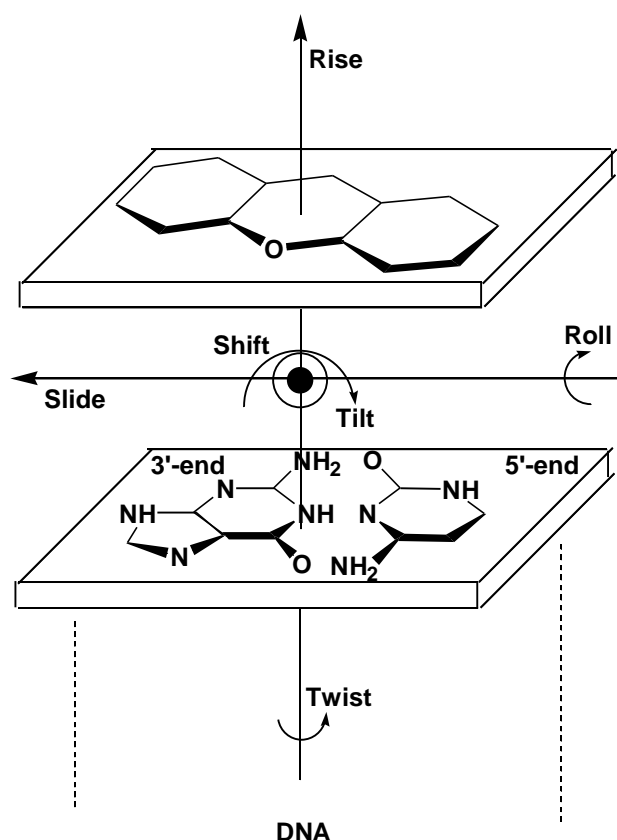
Figure 8.3. Coordinate system and designation of the six base-step parameters illustrated on the example of last GC pair of DNA capped with R6G; arrowheads indicate positive direction of translation (rotation); positive direction of Shift is away from the reader.

of two alignments and their transformation into each other on a timescale of several nanoseconds was confirmed.[280] Their geometry was quantified by standard base-pair step parameters[285] (three distances and three angles) redesigned for the system R6G base-pair.[280] This set of six parameters, three distances (Shift, Slide, Rise) and three angles (Tilt, Roll, Twist), delivers a detailed description of the mutual orientation of two stacked moieties (Figure 8.3).

In terms of these base-step parameters the realignment of R6G on top of DNA was analyzed during the course of MD simulations (Figure 8.4).[280]

From this MD trajectories[280] of length 10 ns four snapshots were selected (Figure 8.5) that reflect different alignments of the dye. These snapshots also differed from the experimentally studied structures by a short truncated segment at the end far from the dye (Figure 8.1a). Two snapshots (at 3.25 ns and 5.75 ns) were taken from the trajectory of R6G connected to the 5'-end of an adjacent cytosine (Figure 8.1a upper panel and Figure 8.5, upper panel) and two snapshots (at 4.25 ns and 8.50 ns) were taken from the trajectory for the complex with R6G connected to 5'-end of guanosine (Figure 8.1a, lower panel; Figure 8.5, lower panel). For the present work, these R6G-DNA complexes were embedded into POL3 water and equilibrated
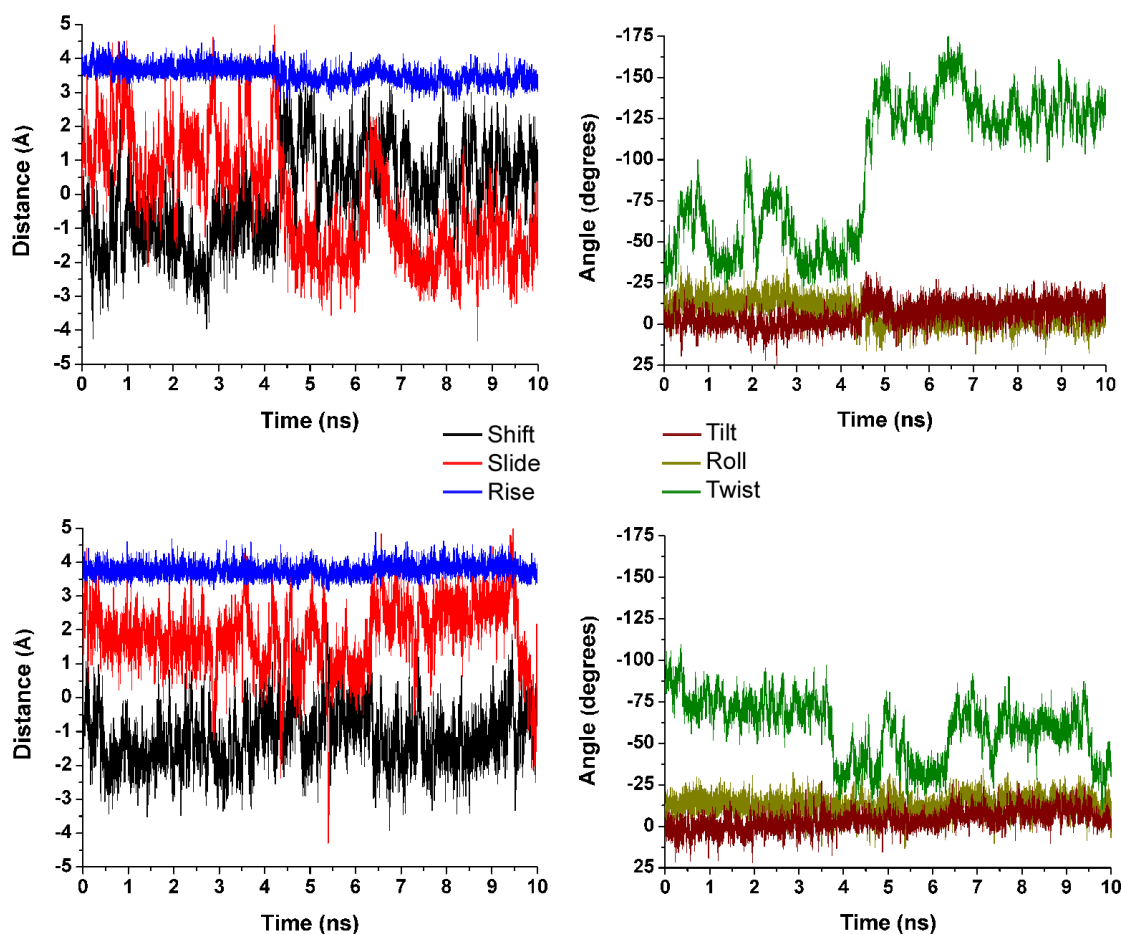
Figure 8.4. Evolution of the base-step parameters between Rhodamine 6G and adjacent GC base pair during 10 ns MD trajectory of **R6G-CAA** (top) and **R6G-GAA** (bottom).

with *ff02*, but subsequently kept rigid in their original geometries. The number of POL3 water molecules in the periodic box was set to 8000. To prevent any transformation of the dye alignment with respect to DNA during equilibration and production runs, the solute structures was kept fixed throughout the simulations. The atomic charges of the neutral and charged forms of R6G as well as those for the linker were derived separately for the force fields *ff02* and *ff99* (see Table B2, Figures B3a, b of Appendix B) to form the R6G-linker moiety (Figure 8.1b, Figure B3c of Appendix B).

8.3 Dependence of λ_s on Rhodamine 6G-DNA conformational alignment

First the influence of the dye alignment on the value of solvent reorganization energy was addressed. The most prominent effect of the R6G-DNA conformation on λ_s was expected for the shortest hole transfer distance, namely that to the first *G* unit; for the numbering see Figure 8.1a. There the strong local electrostatic interactions, reflecting the specificity of charge
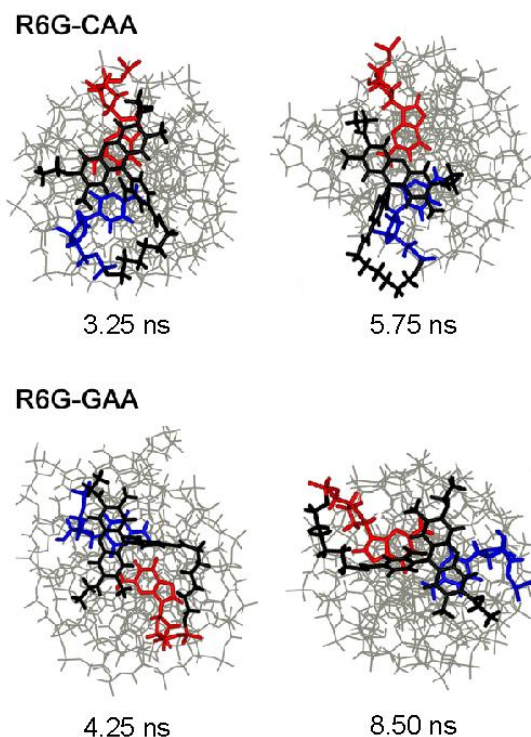
Figure 8.5. Upper panel: structure snapshots of the chromophore-DNA complex R6G-CAA, taken at $\tau = 3.25$ ns and $\tau = 5.75$ ns of a previously recorded MD trajectory (see text and Ref. 280); lower panel: similarly for the chromophore-DNA complex R6G-GAA, taken at $\tau = 4.25$ ns and $\tau = 8.50$ ns. The R6G-linker, cytosine (C), and guanosine (G) are marked in black, blue and red color, respectively.

distributions of the dye and the base-pair, should play the most prominent role. These effects will be discussed in terms of two parameters: the distance R_{DA} and the step parameter Twist (Tables 8.1 and 8.2), which were defined via a standard procedure.[280,285]

Estimates of λ_s for hole transfer along the shortest distance of 3.4 Å (Table 8.1) show that the most significant differences between the two configurations are observed for the R6G-CAA duplex (Figure 8.1a, upper panel), where the average values 0.61±0.16 eV (3.25 ns) and 0.79±0.19 eV (5.75 ns) differ by almost 0.2 eV. The latter difference, as anticipated, is mainly the result of a drastic change in the Twist angle (~75°, Table 8.1), whereas the R_{DA} parameters are rather similar, 4.20 Å and 3.97 Å, for the two selected configurations of R6G-CAA. The duplex R6G-GAA, which does not undergo such drastic conformational changes as the other one,[280] has identical values of λ_s for both snapshots: 1.04±0.19 eV (4.25 ns) and 0.97±0.23 eV (8.50 ns). The latter two snapshots are characterized by similar values of R_{DA} and Twist, respectively; the corresponding differences are 0.44 Å and 17°. The observed larger difference between the two configurations in R6G-CAA, as compared to R6G-GAA, can be rationalized in terms of the more significant change in the rotational parameters of R6G[280] (Table 8.2) rather than in the translational parameter R_{DA} (Table 8.1).

8.4   Scaling factors and effective optical dielectric constants

The values of the effective optical dielectric constants $\tilde{\varepsilon}_\infty$ derived from the scaling factors, Eq. (7.4), demonstrate a low sensitivity to the alignment of R6G on top of DNA (Table 8.1). The values vary from $\tilde{\varepsilon}_\infty = 1.41\pm0.25$ (R6G-GAA, snapshot 4.25 ns) to $\tilde{\varepsilon}_\infty = 1.63\pm0.37$ (R6G-CAA, snapshot 3.25 ns). Therefore, they may be considered as identical within the standard deviations of the method (~0.3); the resulting average value is $<\tilde{\varepsilon}_\infty> = 1.52\pm0.32$ for all four R6G-DNA conformations considered (see Footnote f of Table 8.1).

To confirm our assumption about the weak influence of the R6G-DNA conformation on the reorganization energy for the next-nearest G situated at the fifth base-pair (16.9 Å from R6G), an additional simulation was carried out for the conformation of the R6G-CAA duplex taken at 3.25 ns (Table 8.3, Footnote d). The reorganization energy values for hole transfer to G_5 obtained for the snapshots at 3.25 ns and 5.75 ns were found to be identical, 1.73±0.26 eV and 1.72±0.25 eV, respectively (see Footnote d in Table 8.3).

Table 8.1. Solvent reorganization energy λ_s (eV) of hole transfer to the adjacent guanine unit of a rigid complex R6G-DNA for different orientations of the chromophore R6G relative to the DNA duplex.[a] Also shown is the time τ (ns) of the simulation at which the snapshot was taken to generate the structure used.

Duplex	τ	R_{DA} [b]	Twist [c]	λ_s^{np} [d]	λ_s^{pol} [e]	$\tilde{\varepsilon}_\infty$ [f]
R6G-GAA	4.25	4.96	-43.9	1.47±0.18	1.04±0.14	1.41±0.25
	8.50	4.52	-61.0	1.45±0.17	0.97±0.16	1.51±0.31
R6G-CAA	3.25	4.20	-42.3	1.00±0.14	0.61±0.11	1.63±0.37
	5.75	3.97	-116.9	1.20±0.16	0.79±0.13	1.53±0.33

[a] For the structures of the chromophore-DNA complexes see text and Figs. 8.1, 8.5.

[b] Distance $R_{DA} = (\text{Shift}^2+\text{Slide}^2+\text{Rize}^2)^{1/2}$ (Å) defined here via standard DNA base-step parameters; for details see Table 8.2.

[c] Standard angular base step parameter (degree); see Table 8.2.

[d] Solvent reorganization energy calculated with the non-polarizable setup (*ff99*,TIP3P).

[e] Solvent reorganization energy calculated with the polarizable setup (*ff02*,POL3).

[f] Effective optical dielectric constant, Eq. (7.4); the average over R6G-DNA conformations is $\langle\tilde{\varepsilon}_\infty\rangle = 1.52\pm0.32$.

Table 8.2. Standard base step parameters[a] Roll, Tilt, Twist (degree) and Shift, Slide, Rise, R_{DA} (Å) of four different R6G-DNA configurations. Also shown is the time τ (ns) of the simulation at which the snapshot was taken to generate the structure used.

Duplex	τ	Roll	Tilt	Twist	Shift	Slide	Rize	R_{DA}[b]
R6G-GAA	4.25	-12.89	-9.88	-43.93	-1.87	2.45	3.88	4.96
	8.50	-10.04	-4.62	-60.98	-1.55	1.94	3.78	4.52
R6G-CAA	3.25	-20.22	0.48	-42.30	-1.67	0.59	3.80	4.20
	5.75	-2.80	-10.18	-116.86	-0.48	-2.00	3.40	3.97

[a] Base step parameters calculated according to Refs. 280, 285.

[b] Parameter R_{DA} defined here as $(Shift^2 + Slide^2 + Rize^2)^{1/2}$.

In view of the negligibly small differences between reorganization energies at separation distances larger than 3.4 Å, we investigated the distance dependence of λ_s only for the R6G-CAA duplex (snapshot at 5.75 ns). It has a similar trend (Table 8.3) as the one observed for the pure A- and B-DNA duplexes 5'-GG^+GT$_n$GGG-3' (Table 7.3) and asymptotically becomes independent of distance beyond 17 Å with the values of 2.0 eV [setup (*ff02*, POL3)] and 3.0 eV [setup (*ff99*, TIP3P)]. The calculated distance dependence of the hole transfer rate with the approximation that the driving force[279a] $\Delta G^\circ = 0$ for hole transfer to the first guanine results in

Table 8.3. Distance dependence of the solvent reorganization energy λ_s (eV) and the resulting effective optical dielectric constant $\tilde{\varepsilon}_\infty$, Eq. (7.4), for hole transfer from the chromophore R6G to various guanine units of the rigid complex R6G-CAA.[a]

R_{DA}(Å)	n[b]	λ_s^{np}[c]	λ_s^{pol}[d]	$\tilde{\varepsilon}_\infty$[e]
3.4	1	1.20±0.16	0.79±0.14	1.52±0.32
16.9	5	2.42±0.22	1.72±0.18	1.40±0.19
23.7	7	2.51±0.24	1.86±0.19	1.34±0.18
47.6	14	2.84±0.25	1.98±0.21	1.42±0.19
50.0	15	2.96±0.27	1.99±0.24	1.54±0.23

[a] Snapshot taken at $\tau = 5.75$ ns; for details see text and Figs. 8.1a and 8.5 (upper panels each).

[b] For the numbering of the *G* bases in the chromophore-DNA complex R6G-CAA see Fig. 8.1a, upper panel.

[c] Solvent reorganization energy from the non-polarizable setup (*ff99*,TIP3P).

[d] Solvent reorganization energy from the polarizable setup (*ff02*,POL3). A simulation for the conformation at $\tau = 3.25$ ns and the distance $R_{DA} = 16.9$ Å yielded $\lambda_s^{pol} = (1.73\pm0.26)$ eV.

[e] Effective optical dielectric constant, Eq. (7.4); average over all distances R_{DA} listed $\langle \tilde{\varepsilon}_\infty \rangle = 1.45\pm0.31$ eV.

Table 8.4. Coefficients A and B of linear fits y = A+Bx of the solvent reorganization energy λ_s (eV) as a function of the inverse x = R_{DA}^{-1} of the donor-acceptor distance R_{DA} in R6G-CAA complex.

Model	Setup	R_{DA} (Å)	A (eV)	B (eV·Å)	R[a]	SD[b]
R6G-CAA[a]	(*ff99*,TIP3P)	All	2.87±0.14	-5.72±0.78	0.989	0.639
	(*ff02*,POL3)	All	2.02±0.12	-4.18±0.65	0.998	0.247

[a] Distance dependence of R6G-CAA (5.75 ns) conformation is considered.

β_s = 0.7±0.1 Å^{-1} (n = 1–5) and to a substantially lower value β_s ~ 0.1 Å^{-1} (n = 5–7, 14, 15) for the setup (*ff02*, POL3). The linear fits of the λ_s dependence on R_{DA}^{-1} for both setups are provided in Table 8.4.

In the case of the non-polarizable setup (*ff99*, TIP3P), the parameter β_s varies in a similar range: 0.9±0.1 Å^{-1} (n = 1–5) to β_s ~ 0.1 Å^{-1} (n = 5–7, 14, 15). Optical dielectric constants derived from the scaling factors, Eq. (7.4), for different ET distances (Table 8.3) show almost no variation with the distance: from $\tilde{\varepsilon}_\infty$ = 1.34±0.18 (n = 7) to $\tilde{\varepsilon}_\infty$ = 1.54±0.23 (n = 15) with an average $<\tilde{\varepsilon}_\infty>$ = 1.45±0.31 (Table 8.3) over the range R_{DA} = 3.4–50.0 Å. The latter average of the optical dielectric constant is identical (within the standard deviation) to the values derived above for A-DNA, 1.45±0.32, and B-DNA, 1.47±0.31, as well as for the R6G-DNA conformers studied, 1.52±0.32, evaluated from the polarizable setup. This suggests that the value $<\tilde{\varepsilon}_\infty>$ = 1.5, which accounts for electronic polarization effects, can be used to scale solvent reorganization energy values that were obtained from non-polarizable force field simulations of similar DNA-related systems.

8.5   Conclusion

We applied the computational procedure developed within the present work to determine the distance dependence of λ_s upon charge transfer between Rhodamine 6G and guanine units in Rhodamine 6G-DNA complexes (donor-acceptor distances 3.4–51.0 Å). Comparison of simulations for four distinctly different R6G-DNA conformations and A- and B-DNA forms for the wide range of studied donor-acceptor distances suggested a uniform scaling factor of λ_s that relates results from MD simulations with non-polarizable and polarizable force fields, independent of conformation and donor-acceptor distances. With the corresponding average effective optical dielectric constant $<\tilde{\varepsilon}_\infty>$ = 1.5, one obtains a computationally economic scaling approach to solvent reorganization energies for DNA-related systems from MD simulations with a non-polarizable force field.

9 Summary

Electron transfer (ET) along the π-stack of DNA and practical benefits expected from its potential utilization in nano-wires for electronics or as a source of genetic information in medical diagnostics inspired research interest in many scientific groups all over the world. While the physical principles of ET have been understood quite some time ago, contradictive experimental data about the conductivity of DNA necessitated its quantitative examination. Numerous theoretical descriptions attempting to approach the complexity of real processes in DNA were trying to provide definite answers to the question about ET rates, which are the main observables. Theories predict the values of rates based on three parameters: the free energy difference $\Delta G°$ between final and initial ET states, the quantum electronic coupling H_{fi} between them, and the energy associated with the structural reorganization of the surrounding medium. The latter phenomenon takes place in DNA as a response of atoms to the change of electrostatic field which is almost instantaneous compared to the thermal motion of atoms. Bridging the gap between theory and experiment in solutions unavoidably has to deal with the solvent facilitating electron transport along the π-stack of DNA, where its role is described in terms of the solvent reorganization energy λ_s. Being a corner stone of classical Marcus theory dating back to some 50 years, this parameter also is incorporated in numerous modern theories and its evaluation represents a serious challenge that resulted in a broad range of values. The reorganization energy enters the formal expression for ET rates through a quadratic form in an exponential factor, thereby making the values of ET rates extremely sensitive to its variation. The latter fact leaves much room for the interpretation of experimental kinetic data. Theoretical methods commonly used to evaluate solvent reorganization energies as a rule overestimate its values. To corroborate experimental data, somewhat ad-hoc parametrizations have been introduced. This parametrization is related to partitioning of the system into regions possesing distinctively different spatial and dielectric properties. The questionable definition of the size of the solute cavity and the artificial partitioning of the surrounding solvent medium into arbitrarily chosen regions of different dielectric constants lead to a broad range of solvent reorganization energies covering the entire spectrum of experimental data. Such computational practices in combination

with contradicting experimental data help very little for a consistent picture of the actual values of solvent reorganization energies.

The present work based on an atomistic treatment of DNA in aqueous solution by means of molecular dynamics simulations advances to close the existing gap in the field of electron transfer and to establish a thorough account of the role of solvent without invoking any *ad hoc* parametrization. For the first time, molecular dynamics studies incorporating polarizable force field with an explicit treatment of the solvent are employed to evaluate the solvent reorganization energy of a large biomolecular system. The work establishes a straightforward path and discusses complications which for some time prevented the application of polarizable force fields for evaluating solvent reorganization energies. The method was successfully tested on the original classical two-spheres model of Marcus and is then transferred to large-scale simulations of experimentally studied DNA duplexes and their complexes with the dye Rhodamine 6G.

The work started with establishing the computational method by considering the classic two-spheres solute model of Marcus, where the surrounding solvent is treated as a dielectric continuum. Despite the fact that this model served experimentalists for decades as a main tool of interpretation, its validity had never been successfully proved in computational experiments, which consider the atomistic nature of the solvent. Few attempts have addressed the microscopic characteristics of the solvent by representing it with existing water models that reproduce its thermodynamic properties and seems to serve well for other molecular dynamics simulations. Yet these attempts were not successful thus far when targeting solvent reorganization energies. The main conclusion, arising from those simulations with respect to the Marcus model, was that the experimental dielectric constant of water assumed in the mathematical expression for solvent reorganization energy cannot be reproduced. That conclusion brought up a more general question about the extent to which the electronic polarization expressed through the static dielectric constant affects the solvent reorganization energy.

The present work revisited the role of electronic polarization predicted by Marcus theory. In the current study it was shown that molecular dynamics simulations incorporating a polarizable force field fully reproduce the experimental (high-frequency) dielectric constant of water and reveal excellent agreement with the outcome of the Marcus two-sphere model, which predicts that accounting for the electronic polarization leads to a strong reduction of the solvent reorganization energy. According to the present methodological findings, it is of primary importance to choose a computational method that quantifies correctly the donor-acceptor potential energy gaps that lead to the solvent reorganization energy. For this purpose, a self-consistent iterative treatment of electronic polarization was successfully employed despite its relatively high computational cost. Full agreement was achieved between the results from three

approaches, existing in the literature, to evaluate solvent reorganization energy via MD simulations.

The present results for charge separation and recombination reactions in the two-spheres model show a strictly linear dependence of the solvent reorganization energy λ_s on the inverse of the donor-acceptor distance R_{DA}, in accordance with the classical results of Marcus. Unlike other studies, the present results for λ_s agree quantitatively with the predictions of the Marcus dielectric continuum model, yielding the theoretically expected reduction by ~45% due to electronic polarization effects. The evaluation of the distance dependent character of λ_s from MD simulations with a polarizable water model suggests a scaling which is fully consistent with the experimental value of 1.79 for the effective optical dielectric constant of water. Thus, it was possible to clarify the situation of controversial choices between scaling factors that had been suggested in the literature to achieve agreement between the results of polarizable and non-polarizable simulations. Preliminary results on a charge shift reaction for a two-spheres model fully confirmed the same reduction as obtained for charge separation and recombination reactions.

The estimates based on results for the charge shift reaction suggested substantial reduction of the values of λ_s of DNA-related systems compared to existing ones in the literature; thus further applications of this computational strategy for complex biomolecular systems were elaborated. Particularly, DNA-based donor-acceptor complexes with experimentally known solvent reorganization energies were studied by molecular dynamics simulations. The solvent reorganization energy λ_s for hole transfer between guanine units was calculated in a variety of DNA duplexes with a polarizable force field. These results are among the lowest reported in the literature. The dependence of λ_s on the inverse donor-acceptor distance for a series of model A- and B-DNA duplexes (donor-acceptor distances 3.4–30.4 Å) shows a linear decay similar to the one expected from the Marcus two-spheres model. For the long range ET ($R_{DA} > 10$ Å) the solvent reorganization energies of these DNA related systems are independent of whether DNA is in A- or B-form. It was shown that vibrations of the DNA backbone have a rather small effect on λ_s values. Besides that, the choice of the solvent model and the force field (including the influence of charge sets) and various molecular groups affecting the results were investigated. Results from MD simulations with the standard non-polarizable force field were used as reference to account for electronic polarization effects. It was demonstrated that the values of λ_s were reduced by about 30% compared to those derived with the non-polarizable setup when one accounts for the electronic polarization with a polarizable force field. The results from these atomistic calculations with a polarizable force field, which do not demand any "re-parameterization", are consistent with the lowest values of λ_s from earlier elaborations that employed an implicit solvent model. The current reduction of about 30% of λ_s due to electronic polarization observed for DNA duplexes casts some doubt on the common practice to transfer

scaling factors from simplified solute models to biomolecular systems in order to achieve agreement with experimental data.

Besides a series of DNA model systems, MD simulations with a polarizable force field were conducted also on fragments of DNA duplexes where experimental values of λ_s recently had been obtained from kinetic studies.[251] Solvent reorganization energies of ET between guanines G from the present simulations for the fragments $G^+X^{(k)}G$ ($X^{(1)} = A$, $X^{(2)} = AA$, $X^{(3)} = T$, $X^{(4)} = TT$) agreed well within the standard deviations of the method.

As a next step, this procedure to determine solvent reorganization energies was applied to large-scale systems, namely to 15 base-pair DNA duplexes with the dye Rhodamine 6G attached; the structure of these sytems had previously been resolved by NMR. The geometries from MD refinement of these complexes with several distinctly different conformational alignments of the dye were used for evaluating λ_s. The distance dependence of λ_s obtained upon charge transfer between Rhodamine 6G and guanine units in Rhodamine 6G-DNA complexes was studied for donor-acceptor distances from 3.4 Å to ~50 Å. Comparison of the simulations for four considerably different R6G-DNA conformations and the wide range of studied donor-acceptor distances suggested a uniform scaling factor for λ_s that relates results from MD simulations with non-polarizable and polarizable force fields, independent of conformation and donor-acceptor distances. With the corresponding average effective optical dielectric constant $<\tilde{\varepsilon}_\infty>$ = 1.5, one obtains a computationally economic scaling approach to solvent reorganization energies for these DNA-related systems from MD simulations even with a non-polarizable force field.

As shown by the present results, improved polarizable force fields for water and biological molecules are highly desirable. However, even now, the procedure established in this thesis holds great promise for further applications to large-scale applications in the area of biophysical chemistry.

Appendix A − Cumulant Expansion for γ(*t*)

Denoting the second exponential term in Eq. (3.35) as

$$\gamma(t) = \exp\left[\frac{i}{\hbar}\int_0^t \delta\Delta U(t')\,dt'\right],$$ (A.1)

one can use the cumulant series expansion to represent it as

$$\gamma(t) = \sum_0^\infty \left(\frac{i}{\hbar}\right)^n \int_0^{t_0} dt_1 \int_0^{t_1} dt_2 \int_0^{t_2} dt_3 \dots \int_0^{t_{n-1}} dt_n \left\langle \delta\Delta U(t_1)\dots\delta\Delta U(t_n)\right\rangle_c,$$ (A.2)

where $\left\langle\dots\right\rangle_c$ is the cumulant average.

The second-order approximation for γ(*t*) gives

$$\gamma(t) \approx \left(\frac{i}{\hbar}\right)\int_0^t \left\langle\delta\Delta U(t_1)\right\rangle_c dt_1 - \frac{1}{\hbar^2}\int_0^t dt_1 \int_0^{t_1} dt_2 \left\langle\delta\Delta U(t_1)\delta\Delta U(t_2)\right\rangle_c,$$ (A.3)

where

$$\left\langle\delta\Delta U(t_1)\right\rangle_c = \left\langle\delta\Delta U(t_1)\right\rangle_0 = 0$$ (A.4)

$$\left\langle\delta\Delta U(t_1)\delta\Delta U(t_2)\right\rangle_c = \left\langle\delta\Delta U(t_1)\delta\Delta U(t_2)\right\rangle_0 - \left\langle\delta\Delta U(t_1)\right\rangle_0 \left\langle\delta\Delta U(t_2)\right\rangle_0.$$ (A.5)

Finally one obtains an equation for γ(*t*)

$$\gamma(t) \approx -\frac{1}{\hbar^2}\int_0^t dt_1 \int_0^{t_1} dt_2 \left\langle\delta\Delta U(t_1)\delta\Delta U(t_2)\right\rangle_0 = -\frac{1}{\hbar^2}\int_0^t dt'(t-t')\left\langle\delta\Delta U(0)\delta\Delta U(t')\right\rangle_0$$ (A.6)

Appendix B − Derivation of Charges for G, G$^+$

R6G and R6G$^-$

When deriving atomic charges for the singly positively charged guanosine (G^+) and Rhodamine 6G (R6G) in case of the polarizable force field *ff02*, a previously described procedure was applied.[219] Here, a more detailed overview of some specific parameters of this procedure shall be given. All quantum mechanical calculations were carried out with the program Gaussian 03.[286]

The geometry of charged guanosine was optimized at the UHF/6-31G* level. For this geometry an initial electrostatic potential (ESP) was generated at the UB3LYP/cc-pVTZ level and RESP atomic charges[211,212,287] were fitted to this initial ESP. They were then used to

Table B1. Permanent, μ_{perm}, induced, μ_{ind}, and total, μ_{tot}, dipole moments (Debye) calculated with the polarizable version of the AMBER force field *ff02* after one MD step for the optimized geometry of a singly charged guanosine radical G$^+$, the linker (Fig. B3a), negatively charged Rhodamine R6G$^-$, and neutral R6G.^{a}

N	G$^+$			Linker			R6G$^-$			R6G		
	μ_{perm}	μ_{ind}	μ_{tot}	μ_{perm}	μ_{ind}	μ_{tot}	μ_{perm}	μ_{ind}	μ_{tot}	μ_{perm}	μ_{ind}	μ_{tot}
0	6.744	1.305	5.757	12.235	1.374	11.374	13.791	1.056	12.833	14.359	1.551	12.947
1	7.213	1.379	6.140	12.610	1.534	11.642	14.222	1.130	13.206	15.032	1.586	13.593
2	7.257	1.385	6.179	12.633	1.541	11.664	14.242	1.134	13.221	15.090	1.591	13.646
3	7.260	1.385	6.181	12.638	1.542	11.668	14.241	1.134	13.221	15.093	1.592	13.649
4	7.260	1.385	6.181	12.637	1.542	11.668	–	–	–	15.093	1.592	13.648

^{a} Dipole moments from single step MD calculations with the polarizable *ff02* force field, where charges were derived from the electrostatic potential obtained at the B3LYP/cc-pVTZ level for subsequent iterations *N* of the procedure described in the text. For comparison note the initial values of the *total* dipole moment at the B3LYP/cc-pVTZ level after geometry optimization (in absence of any external point-charge field): G$^+$ – 6.849 Debye, linker – 12.606 Debye, R6G$^-$ – 14.094 Debye, and R6G – 14.029 Debye.

generate induced dipoles on the optimized geometry through one MD step of 0.05 fs in the module *sander* of AMBER 8, treating the induced dipoles iteratively[243] without periodic boundary conditions. As initial guess, atomic polarizabilities were automatically invoked in the module *leap* from the polarizable force field *ff02*. In response to the charges present on the atoms, these induced dipoles, reflecting the atomic polarizations, adjusted their positions during a single MD step with the module *sander*. As for normal production MD runs, we used the iterative procedure[242] built into AMBER 8.[220] After relaxation of the induced dipoles, their positions and magnitudes were recorded and introduced as a point-charge field surrounding the optimized structure in a B3LYP/cc-pVTZ single-point calculation where the ESP for the next iteration was generated. The obtained ESP corresponds to the potential field without self-polarization of the molecule. The newly obtained charge set was used for the subsequent step where the induced dipoles were adjusted. After three to four cycles, the induced dipole moments converged (Table B1). The corresponding *ff02* RESP charges for neutral and charged guanosine are given in Figures B1 and B2. The charge set for neutral guanosine, shown in Figure B2 for comparison, is the one built into the *ff02* force field; it was not obtained by the current iterative procedure.

   The charges for the force field *ff02* for neutral and negatively charged R6G were obtained in an analogous iterative procedure. The B3LYP/6-31G* geometry optimization with a PCM water model[288] and the subsequent iterative procedure for generating the ESP at the B3LYP/cc-pVTZ level were carried out separately for the two modified fragments of the dye (Figures B3a, b): the R6G unit and the linker with methylated phosphate. Then the fragments with their corresponding charges were merged (based on common atoms in both fragments, the final set of charges was derived automatically in *antechamber* package) to deliver the final charges listed for the neutral and the negatively charged systems R6G-linker (Table B2), along with the charges for the non-polarizable force field *ff99*. The optimization was carried out with the PCM approach because the structure corresponding to the zwitterionic form cannot be generated in vacuum where the structure always converges to the lactone isomer.[289]

Table B2. Charges (*e*) for the polarizable (*ff02*) and the non-polarizable (*ff99*) version of the AMBER force field for neutral (R6G) and negatively charged Rhodamine 6G (R6G⁻). See Fig. B3c for the atom labels.

Atoms	R6G		R6G⁻		Atoms	R6G		R6G⁻	
	ff99	*ff02*	*ff99*	*ff02*		*ff99*	*ff02*	*ff99*	*ff02*
C1	-0.455	-0.310	-0.324	-0.313	H22	0.189	0.159	0.183	0.173
H1	0.163	0.126	0.126	0.104	C18	-0.416	-0.261	-0.103	-0.020
C2	0.252	0.105	0.214	0.140	C19	0.721	0.521	0.238	0.059
N1	-0.435	-0.311	-0.676	-0.507	C20	-0.221	-0.004	-0.033	0.064
C3	0.043	0.101	0.233	0.240	C26	-0.185	-0.195	-0.209	-0.154
C4	-0.286	-0.278	-0.377	-0.337	C25	-0.190	-0.108	-0.145	-0.171
H2,H3,H4	0.089	0.083	0.093	0.078	H24	0.170	0.115	0.119	0.102
H5,H6	0.088	0.060	0.040	0.022	H25	0.116	0.089	0.100	0.077
H7	0.325	0.280	0.362	0.307	C21	0.196	-0.027	0.039	-0.040
C5	0.034	0.126	0.068	0.079	C22	0.607	0.586	0.757	0.677
C6	-0.271	-0.267	-0.164	-0.147	O2, O3	-0.684	-0.608	-0.767	-0.700
H8,H9,H10	0.086	0.084	0.044	0.041	C23	-0.209	-0.112	-0.187	-0.151
C7	-0.097	-0.192	-0.268	-0.307	H23	0.162	0.114	0.136	0.107
H11	0.189	0.159	0.183	0.173	C24	-0.041	-0.131	-0.176	-0.124
C8	-0.416	-0.261	-0.103	-0.020	C27	0.691	0.566	0.749	0.573
C9	0.508	0.361	0.293	0.247	O4	-0.559	-0.551	-0.559	-0.544
O1	-0.335	-0.266	-0.342	-0.262	N3	-0.692	-0.507	-0.692	-0.500
C10	0.508	0.361	0.293	0.247	H26	0.321	0.262	0.321	0.262
C11	-0.455	-0.310	-0.324	-0.310	C28	0.097	0.156	0.097	0.156
H12	0.163	0.126	0.126	0.104	H27, H28	0.078	0.016	0.078	0.016
C12	0.252	0.105	0.214	0.140	C29	-0.114	-0.038	-0.114	-0.038
N2	-0.435	-0.311	-0.676	-0.507	H29, H30	0.044	0.011	0.044	0.011
C13	0.043	0.101	0.233	0.240	C30	0.005	0.042	0.005	0.042
C14	-0.286	-0.278	-0.377	-0.337	H31, H32	0.053	0.021	0.053	0.021
H13,H14,H15	0.089	0.083	0.092	0.078	C31	-0.263	-0.132	-0.263	-0.131
H16,H17	0.088	0.060	0.040	0.022	H33, H34	0.096	0.034	0.096	0.034
H18	0.325	0.280	0.362	0.307	C32	-0.034	0.013	-0.034	0.013
C15	0.034	0.126	0.068	0.079	H35, H36	-0.023	-0.012	-0.023	-0.012
C16	-0.271	-0.267	-0.164	-0.147	C33	0.396	0.268	0.396	0.211
H19,H20,H21	0.086	0.084	0.044	0.041	H37, H38	-0.024	-0.013	-0.024	-0.013
C17	-0.097	-0.192	-0.268	-0.307	O5	-0.539	-0.382	-0.539	-0.367

Atomic Charges for the Non-Polarizable Force Field. In the case of the non-polarizable *ff99* the atomic charge set for positively charged guanosine was obtained for a geometry optimized at the B3LYP/6-31G* level with a subsequent generation of the ESP with the UHF/6-31G* method. The geometries of the modified linker and of R6G (both in neutral and negatively charged forms) were optimized separately at the B3LYP/6-31G* level (Figure B3a, b). Then these optimized structures of the linker and the R6G unit were merged (based on common atoms in both fragments the final set of charges was derived automatically in *antechamber* package) to generate the ESP either at the RHF/6-31G* level (neutral R6G) or the UHF/6-31G* level (negatively charged R6G). In all cases the generated ESP was submitted to further RESP calculations as suggested for acquiring appropriate atomic charges for non-polarizable AMBER force fields (Table B2). [211,212,287]
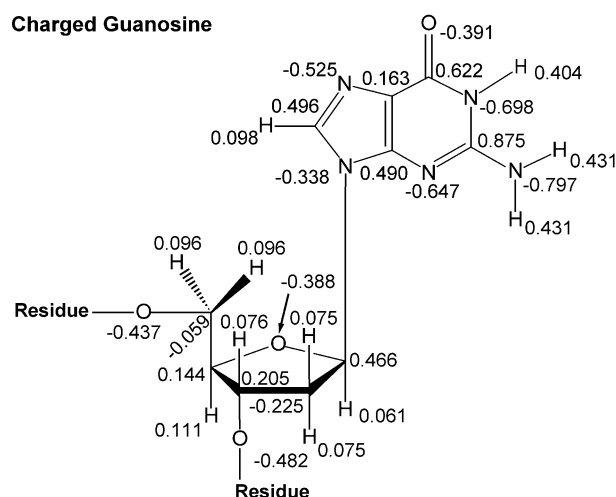
Figure B1. RESP atomic charges (*e*) of singly positively charged guanosine for use with the polarizable force field *ff02*.
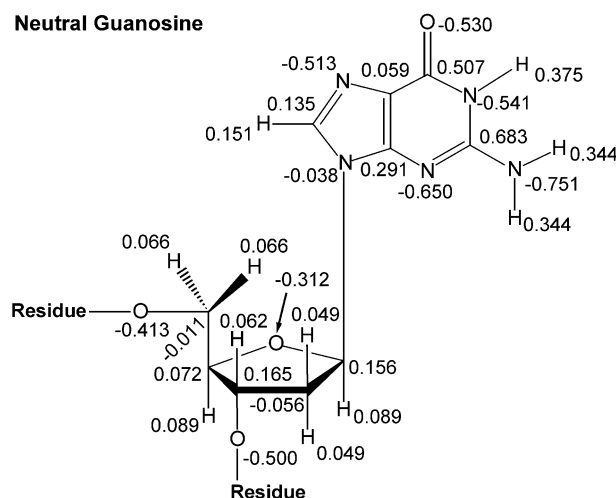
Figure B2. RESP atomic charges (*e*) of neutral guanosine used with the polarizable force field *ff02*. The numbers are taken directly from the *ff02* library implemented in AMBER 8.

Appendix C − How to Record Potential Energy Gaps

To estimate MD parameters needed for recording the potential energy gaps that are required one evaluates the solvent reorganization energy, consider a typical spectral density of an ET reaction coordinate coupled simultaneously to nuclear degrees of freedom of the solute and the solvent. The spectral density decays exponentially with the frequency ω:[5]

$$\frac{J(\omega)}{\omega} = \eta \exp\left(-\frac{\omega}{\Lambda}\right),$$ (C.1)

where Λ is some constant referred to as the highest frequency cutoff and η is a friction coefficient. From a typical spectral density calculated for DNA (Figure C.1) one notes that the estimated value for Λ is about 750–1000 cm^{-1}. Eq. (C.1) arises from an approximate solution of the equations of motion for a system of harmonic oscillators coupled to one reaction coordinate.[5]

Spectral Density, arb. units

5'-GG⁺GTTTGGG-3'
TCF, 250 ps
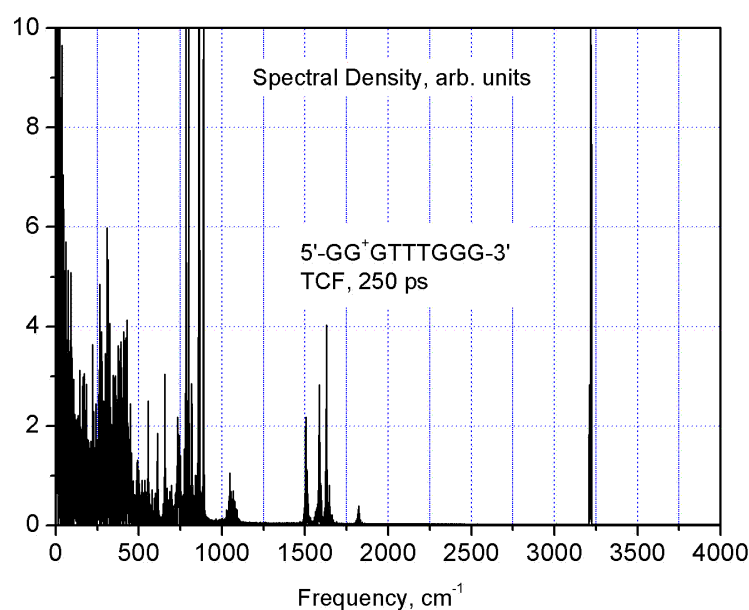
Figure C1. Typical falloff character of the spectral density function of the sovent calculated from a time correlation function of 250 ps for a rigid DNA duplex (MD simulations).

Despite an essentially non-harmonic character, in case of large systems one can regard such a spectrum (Figure C1) as being produced by an array of harmonic oscillators.[5,152,166] Their evolution in time can be approximated by a model function:

$$f(t) = \exp\left(-\frac{t}{\Gamma}\right) \cdot \sum_i g_i \cos(2\pi\nu_i t), \qquad (C.2)$$

where g_i [eV^2] is the relative contribution of the oscillator with frequency ν_i (cm^{-1}). From MD simulations it had been shown that for pure water,[187] DNA,[91] and other biomolecular systems,[5,97c,145] the decay in Eq. (C.2) has an approximately exponential character with Γ estimated at ~500 fs. The spectrum covers the range 0–4000 cm^{-1} where the highest frequency peaks around 3500 cm^{-1} correspond to vibrations involving H (Figure C1). In order to evaluate their contribution to the reorganization energy, it is important to record properly these high-frequency vibrations. Thus, using the upper limit of 4000 cm^{-1} one can estimate the lowest limiting frequency ν_{lim} for dumping the snapshots from MD simulations:

$$\nu_{\text{lim}} = 4000 \text{ cm}^{-1} = 120 \text{ ps}^{-1} = 120 \cdot 10^{12} \text{ Hz} \qquad (C.3)$$

The limiting frequency ν_{lim} corresponds to a vibration period $T_{\text{lim}} = 1/\nu_{\text{lim}} \approx 10$ fs, therefore MD sampling has to be performed with a time step substantially less than the latter value. The value usually chosen[235,244] is around 1 fs. To reduce the computational cost in the present work by a factor of two, the trajectory snapshots were dumped each 2 fs.

Appendix D − Calculation of the Time Correlation Function (TCF)

According to the mathematical formalism the time correlation function (Eq. 4.11) is defined for an infinitely long period of time T:

$$A(\tau) = \lim_{T \to \infty} \frac{1}{T} \int_0^T \delta U_{fi}(t+\tau)\delta U_{fi}(t)dt \,. \tag{D.1}$$

On the other hand, data from MD trajectories are recorded during a finite period of time $T_{finit} < \infty$; thus, the autocorrelation function $A(\tau)$ is accurate only for lags $\tau \ll T_{finit}$. As a rule of thumb, only the first 10–20% of the calculated TCF data can be subjected to further Fourier transform.[290,291]

From Figure D1 one can see that the TCFs calculated for the data sets of different lengths
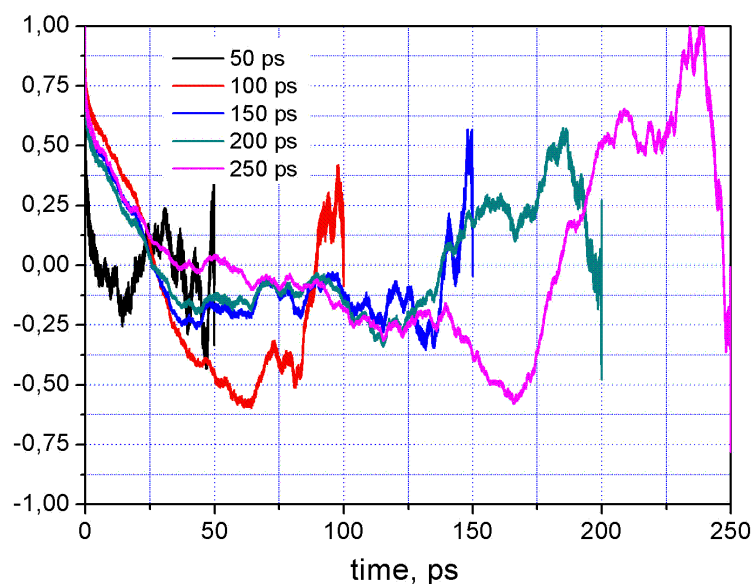
Figure D1. Convergence of TCF as a function of the trajectory length for ET between guanine units (in italics) in a model duplex 5'-G*G*⁺GTTTG*G*G-3'. The trajectory was recordered each 2 fs.
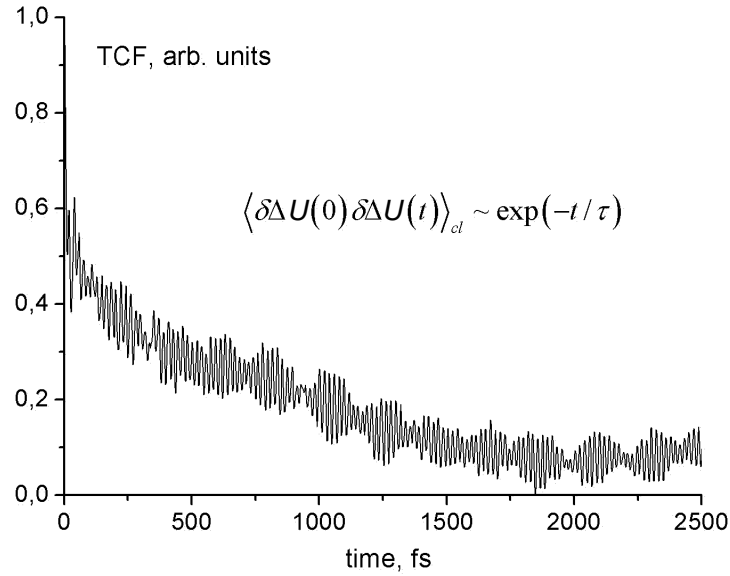
Figure D2. High resolution (first 2.5 ps) of the typical falloff character of a TCF calculated for the donor-acceptor energy gap.

converge for the lag $\tau \approx 25$–30 ps, where they remain positive. Only the latter part, which empirically corresponds to the first 10–20%, is useful for a subsequent FT. The the first 2.5 ps of one of the decaying TCFs is shown in Figure D2 at high resolution.

   Increase of the lag τ reduces the quality of the information recorded as can clearly be seen from the discrete representation of the TCF:

$$\frac{1}{T}\int_0^T \delta U_{fi}(t)\,\delta U_{fi}(t+\tau)\,dt = \frac{1}{N\Delta t - n\Delta t}\sum_{k=0}^{N-n}\delta U_{fi}(t_k)\,\delta U_{fi}(t_k + n\Delta t)\cdot\Delta t\,, \qquad (D.2)$$

where the lag $\tau = n\Delta t$ in the denominator decreases the useful length $N\Delta t - n\Delta t$ of the data set.

Appendix E – Fourier Transform (FT) of TCF

Continuous cosine FT. According to Eq. (6.4) (Chapter 6), the spectral density function and the autocorrelation function are related through a cosine Fourier transform. In order to find the spectral density function from the known time correlation correlation, one has to extend it artificially in a symmetric way into the area $t < 0$.

Consider an arbitrary function $f(t)$ defined on $t \in (-\infty; +\infty)$. Then one has:

$$f(t) = \int_0^\infty \left[a(\omega) \cdot \cos(\omega t) + b(\omega) \cdot \sin(\omega t) \right] d\omega, \tag{E.1}$$

where

$$a(\omega) = \frac{1}{\pi} \int_{-\infty}^{+\infty} f(t) \cdot \cos(\omega t)\, dt \tag{E.2}$$

$$b(\omega) = \frac{1}{\pi} \int_{-\infty}^{+\infty} f(t) \cdot \sin(\omega t)\, dt. \tag{E.3}$$

In order to represent it as an integral of cosines, one needs to have the second coefficient $b(\omega) = 0$, too. Assuming now that $f(t)$ corresponds to the time correlation function defined for $t \in (0; +\infty)$, the latter can be done if it would be *extended* into the negative region of *t in an even way*:

$$f(t) \to \hat{f}(t): \begin{cases} f(t), t > 0 \\ f(|t|), t < 0 \end{cases} \tag{E.4}$$

In this case the coefficients $b(\omega)$ become identical to zero and only $a(\omega)$ remains:

$$a(\omega) = \frac{1}{\pi} \int_{-\infty}^{+\infty} f(t) \cdot \cos(\omega t)\, dt = \frac{2}{\pi} \int_0^{+\infty} f(t) \cdot \cos(\omega t)\, dt. \tag{E.5}$$

Thus, if the correlation function is formally extended to negative values of *t*, even if originally defined only for positive $t \in [0; +\infty)$, then Eq. (E.1) with $b(\omega) = 0$ and $a(\omega)$ according to Eq. (E.5) are also valid *only* for positive $t \in [0; +\infty)$.

Assume a TCF similar to one shown in Figure D2 that contains only one of the harmonic contributions which comprise the spectral density function Eq. (C.2), namely the one with the highest frequency ν_{lim} at relative weight g_{lim}:

$$f(t) = \exp\left(-\frac{t}{\Gamma}\right) \cdot g_{\text{lim}} \cos\left(2\pi v_{\text{lim}} t\right) \tag{E.6}$$

The corresponding cosine FT according to Eq. (E.5) results in:

$$\frac{J(\omega_{\text{lim}})}{\omega_{\text{lim}}} = \frac{2}{\pi} \int_0^\infty f_{\text{lim}}(t) \cos(\omega t)\,dt = g_i \frac{1}{2\Gamma} \frac{1}{\left(\dfrac{1}{\Gamma}\right)^2 + \left(\omega - \omega_{\text{lim}}\right)^2} + g_i \frac{1}{2\Gamma} \frac{1}{\left(\dfrac{1}{\Gamma}\right)^2 + \left(\omega + \omega_{\text{lim}}\right)^2}, \tag{E.7}$$

where $\omega_{\text{lim}} = 2\pi v_{\text{lim}}$. The redundant part of Eq. (E.7), corresponding to the negative values of the frequency ω, should be omitted. From Eq. (E.6) one notices that the decay parameter Γ of the TCF defines the width of the FT peaks, which is independent of frequency ω_{lim}.

Discrete cosine FT. The discrete FT $g'(k)$ of the function $f(t_n)$ defined on a series of values $t_n \in (0;T)$ for the arbitrary k is given by:

$$g'(k) = \sum_{n=0}^{N-1} f(t_n) \cdot \exp\left(-i \frac{2\pi k}{T} t_n\right). \tag{E.8}$$

Here, k corresponds to the frequency according to $\omega_k = 2\pi k/T$. To relate continuous and discrete FT, the sum in Eq. (E.8) has to be rearranged multiplying and dividing the expression by $\Delta\tau$:

$$g'(k) = \frac{1}{\Delta\tau} \cdot \sum_{n=0}^{N-1} f(t_n) \cdot \Delta\tau \cdot \exp\left(-i \frac{2\pi k}{T} t_n\right) \tag{E.9}$$

Choosing $\Delta\tau$ to be rather small, one obtains the integral as limit of the sum $g'(k)$ at $\Delta\tau \to 0$:

$$g'(k) \approx \frac{1}{\Delta\tau} \cdot \int_0^T f(t) \cdot \exp\left(-i \frac{2\pi k}{T} t\right) dt \tag{E.10}$$

Recalling that the index k numerates frequencies ω_k, the integral can be expressed for a continous range of ω:

$$g'(\omega) \approx \frac{1}{\Delta\tau} \cdot \int_0^T f(t) \cdot \exp\left(-i\omega t\right) dt \tag{E.11}$$

Thus, discrete and continuous Fourier transforms are related through the constant multiplier $1/\Delta\tau$. The limit of the errors when stepping from a discrete summation to the integration can be estimated by the "trapezoid formula":

$$\left| I_k(\tau) - \int_0^T f(t) \cdot \exp\left(-i \frac{2\pi k t}{T}\right) dt \right| \leq \frac{T-0}{12} \cdot \Delta\tau^2 \cdot M, \tag{E.12}$$

where $M = \max\left\{\left| f'^{(2)} \right|; 0 \leq t \leq T\right\}$.

Appendix F – Estimate of Leakage Artifacts

When taking a FT in approximate, discretized form, often artifacts can be observed that are known as leakage errors. When data are not sampled long enough and a truncation occurs, the intensities (peaks) resulting from the numerical procedure differ from the exact analytical solutions. One of the reasons is that the quality of the TCF decreases at larger values of the righthand side of Figures D1 and D2; see also the discussion in Appendix D. Truncation of TCFs around the first 10–20% of the collected data series and application of different "window functions", which reduce the relative contribution of the values at the ends of data series, improves the quality of FT, but still disrete FT unavoidably introduces a representation through a finite set of frequencies instead of a continuum. The number of data points collected results in the same number of discrete frequencies Eq. (E.8). The deviation from the theoretical peak intensity can be obtained for a particular implementation of the FT and the length of the recorded TCF data set in a straightforward way:

$$Error = \frac{\left| FT\left(continuum\right) - FT\left(discrete\right) \right|}{FT\left(continuum\right)} \cdot 100\% \,, \tag{F.1}$$

where FT is the Fourier transform of an arbitrary analytical function.

In the present work the FTs were calculated using the program *xmgrace*.[292] Assume a data set of 25000 points, recorded with a time step $\Delta\tau = 4$ fs to represent the function given in Eq. (E.6) with parameters $\Gamma = 500$ fs and $v_{\lim} = 1000$ cm^{-1}, and invoke the definition of cosine FT similar to Eq. (E.5). Then integration of the function yields a peak height at $\omega > 0$:

$$FT_{\cos}\left[f\left(t\right) \right] = \int_0^\infty f\left(t\right) \cos\left(\omega t\right) dt \Bigg|_{\omega_{\lim}} = \frac{\Gamma}{2} \,, \tag{F.2}$$

where $\omega = 2\pi v$. Note that the height of the peak is independent of the frequency ω of the assumed TCF.

Data (with a precision of 10 digits after the comma) for the TCF function, Eq. (E.6), with the latter parameters, have been imported into the program *xmgrace*, where the cosine FT is implemented as follows

$$g'(k) = \sum_{n=0}^{N-1} f(t_n) \cdot \cos\left(\frac{2\pi k}{T} t_n\right). \tag{F.3}$$

This results in a peak height of 63.00158 (dimensionless units). To connect continuous and discrete transforms, one has to recall Eq. (E.11), which relates them through the parameter $\Delta\tau$. Finally, one estimates the relative leakage error according to Eq. (E.1):

$$Error = \frac{\left|1/250\,fs - 1/63.00158 \cdot 4\,fs\right|}{1/250\,fs} \cdot 100\% \approx 0.8\% \tag{F.4}$$

This is a rather small value compared to experimental standard deviations.

Appendix G – Integration of the Spectral Density Function

The accuracy when one calculates reorganization energies depends not only on leakage artifacts that arise from the discrete FT, but also on the subsequent numerical integration of the spectral density function obtained from a FT,

$$\lambda = \frac{4}{\pi} \sum_{0}^{\omega_{max}} \frac{J(\omega_i)}{\omega_i} \cdot \Delta\omega, \tag{G.1}$$

which is a discrete representation of Eq. (6.3). The integrand consists of sharp peaks (see Figure C1); therefore, the resolution of the frequency grid $\Delta\omega$ must be high enough, so that the area is estimated precisely. The required grid resolution can be estimated from the "width" of the peaks of the assumed TCF, see Eq. (E.6). As seen from the resulting FT in Eq. (E.7), the characteristic width of the peak is

$$\Delta\omega \approx \frac{1}{\Gamma}. \tag{G.2}$$

It is noteworthy, that the grid resolution $\Delta\omega$ depends only on the decay constant Γ of the TCF.

Assuming one needs at least 10 points to estimate the area under a single peak at a reasonable accuracy, one derives a grid resolution:

$$\Delta\omega = \frac{1}{\Gamma}\frac{1}{100} \approx 7 \ cm^{-1}. \tag{G.3}$$

Given the latter condition, the total data length of a TCF submitted to FT can be estimated as

$$T = \frac{1}{\Delta\omega} = 5 \ ps, \tag{G.4}$$

which directly follows from the definition of the discrete FT, Eq. (E.8). Recall that the useful length of a TCF comprises only 10–20% of the total sampling time (see Appendix D). Then one estimates that data have to be collected at least for about 25–50 ps.

Appendix H − *Bash* Scripts for MD Calculations

H.1 General operations of the *Bash* scripts for energy gap calculations

The currently developed system of the *bash* scripts assists with analyzing the trajectory simultaneously with its production. The resulting data is generated in standard AMBER 8^{220} energy output format as two files: *MD.out* and *AN.out* which correspond to the same series of snapshots with initial and final ET states, respectively.

The trajectory is produced with a parallel version of module *sander*[220] that invokes program *mpirun* and operationally is controlled by the script *cycles.sh.* Due to extremely voluminous data to be operated by analysis scripts the main trajectory is partitioined into 25 sections with a length of 2 ps each. The script *ghost.sh* ensures that the last snapshot of previous trajectory piece becomes the starting snapshot for the next subsequent section of the trajectory.

The analysis is done as recommended (Appendices C–G) each 2 fs at every fourth snapshot produced with a timestep 0.5 fs in accordance with the input parameters of *sander* (enlisted in the command files *AN.in* and *MD.in*). The analysis is carried out as a set of single step MD calculations (0.005 fs), also performed by *sander*. This analysis can be carried out in "parallel" by invoking simultaneously several independent single processes; the number of simultaneous runs on single processors depends on the current load of the available compute platform. Its maximum target number `NUM_PROC` is preset in the script *analysis.sh*, which controls the single-step calculations. The two data streams, production and analysis, can be balanced with the script *bg_sander.sh* which controls the load of the processors by adjusting the number of simultaneous analysis runs relative to a target number `NUM_PROC`. The best speed of calculations is achieved on machines that feature a shared memory, where the total number of *sander* executables (invoked in production and analysis runs together) does not exceed the number of physically available processors by a factor of 2.

H.2 Main controlling script *MD.sh*

The system of communicating scripts operates is described in the following. The main script *MD.sh* is supposed to be submitted to the machine queue of waiting tasks with the command:

> qsub ./MD.sh

It copies all start files (command files *.in*, topology files *.prmtop*, pre-equilibrated DNA structure in a form of restart file `6equil_md.restrt`) needed for standard *sander* runs from the (variable) directory `STARTDIR`. In *MD.sh* script represented below the latter variable has the value `/bigstuff/vladimirov/DNA/`.

The script creates two directories

/scratch/vladimirov/R6G-GNP6_to_GNP0_MD

/scratch/vladimirov/R6G-GNP6_to_GNP0_AN

in directory `/scratch`. The topology files (`R6Gminus1-GNP6_6CAA.prmtop`, with a negative charge located on R6G) and (`R6G-GNP0_6CAA.prmtop`, with a positive charge located on R6G) are assigned to environment variable names that correspond to the initial (`TOPOLOGY`) and final (`TOPOLOGYII`) ET states, respectively.

Then the script assigns environmental variables for parallelizing *sander* via *mpirun*, which depend on the available software version and the architecture of the machine (for more instructive commands, see the manual of AMBER). After the environmental variables are assigned, script *MD.sh* invokes all other scripts which control the execution of simulations.

The scripts are designed such that no other parameter except those represented in *MD.sh* have to be changed.

```tcsh
#!/bin/tcsh
#$ -cwd
#$ -pe * 4
#$ -q opt34,opt35,opt36,opt37,opt38,opt39,quad1,quad2
setenv dirI /scratch/vladimirov/R6G-GNP6_to_GNP0_MD
setenv dirII /scratch/vladimirov/R6G-GNP6_to_GNP0_AN
rm -rf $dirI
rm -rf $dirII
mkdir -p /scratch/vladimirov/
mkdir -p $dirI
mkdir -p $dirII
###########################################################
setenv TOPOLOGY R6Gminus1-GNP6_6CAA.prmtop
setenv TOPOLOGYII R6G-GNP0_6CAA.prmtop
setenv STARTDIR /bigstuff/vladimirov/DNA/
cd $STARTDIR
###########################################################
cp 6equil_md.restrt $dirI/8equil_md.restrt
###########################################################
```

```
cp *.in   *.prmtop ENERGY.dat  ghost.sh  egor.host  cycles.sh
analysis.sh bg_sander.sh  $dirI
cp ZERO_VEL.restrt $dirII
cd $dirI
source /home/vladimirov/.cshrc
################ mpirun  variables ######################
echo '++++++++++++ ENV ++++++++++++'
setenv
echo '++++++++ HOSTFILE ++++++++++++'
cat $PE_HOSTFILE
setenv TTFS_HOSTFILE $PE_HOSTFILE
/home/ttfs/bin/pvmconf.pl -g -m > egor.host
echo '++++++++ HOSTFILE:N ++++++++++'
cat egor.host
######### Don't use this command for analysis runs!!! ########
setenv  PARAL "mpirun -v  -np  4  -machinefile  egor.host
$AMBERHOME/exe/sander "
#############################################################
./ghost.sh &
./analysis.sh &
./cycles.sh
#############################################################
```

H.3 Trajectory production script *cycles.sh*

```
#!/bin/bash
#$ -cwd
cd $dirI
####### The number of trajectory pieces             #######
maxi=25
####### The number of steps in each trajectory piece  #######
####### should be always of format e00+1 and the same #######
####### as in "MD.in" file                         #######
nstlim=4001
######################### CYCLES #########################
ntwr=4
let prenstlim=$nstlim-1
let maxsnap=$prenstlim/$ntwr
#############################################################
cp 8equil_md.restrt MD_1.restrt
```

```
cp ENERGY.dat MD_ENERGY_0.dat
############################################################
for ((i=1;i<=maxi;i++))
do
############################################################
let k=$i+1
############################################################
$PARAL -O -i MD.in -o MD_$i.out -p $TOPOLOGY  -c MD_$i.restrt
-ref MD_$i.restrt -r MDf_$i.restrt -x MDf_$i.mdcrd
grep -v writing MD_$i.out | grep -v COM > temp_$i.out
let nlines=184+$nstlim*12
##### here
let plines=$prenstlim*12
##### here
mv temp_$i.out MD_$i.out
head -$nlines  MD_$i.out | tail -$plines > MD_ENERGY_$i.dat
cp ENERGY.dat MD_snapshot_0.dat
for ((j=1;j<=maxsnap;j++))
do
let snapshot=$j*$ntwr
let snapline=$snapshot*12
##### here
head   -$snapline   MD_ENERGY_$i.dat   |   tail   -12   >
MD_snapshot_$j.dat
#### here
let jp=$j-1
cat MD_snapshot_$jp.dat MD_snapshot_$j.dat > intermediate.dat
mv intermediate.dat MD_snapshot_$j.dat
done
mv MD_snapshot_$maxsnap.dat MD_ENERGY_$i.dat
rm -f MD_snapshot_*.dat
######## Prepare files for the next MD cycle in dirI ########
cp MDf_$i.restrt_$prenstlim MD_$k.restrt
rm -f MDf_$i.restrt_$nstlim
done
##########  archive and  copy to "home" directory  ##########
tar -cvf MD.restrt.tar MD_*.restrt
tar -cvf MD.mdcrd.tar MDf_*.mdcrd
gzip MD.*.tar
for ((i=1;i<=maxi;i++))
```

```
do
let ip=$i-1
cat MD_ENERGY_$ip.dat  MD_ENERGY_$i.dat > intermediate.dat
mv intermediate.dat MD_ENERGY_$i.dat
done
mv MD_ENERGY_$maxi.dat MD_ENERGY.dat
rm -f MD_ENERGY_*.dat
cp *.gz MD_ENERGY.dat $STARTDIR
################### kill background job ####################
cd $dirII
while [ ! -f AN_ENERGY.dat ] ; do
wait
done
kill -9 analysis.sh
##########################################################
```

H.4 Trajectory analysis script *analysis.sh*

```
#!/bin/bash
#$ -cwd
cd $dirI
#################### Parameter to change ###################
NUM_PROC=3
############ The number of trajectory pieces ##############
maxi=25
####### The number of the xyz lines in restart files  #######
####### to be analyzed                                #######
atomlines=12532
####### The number of snapshots analyzed in each      #######
####### trajectory piece                              #######
####### It should be always:  maxl=(nstlim-1)/ntwr    #######
####### where nstlim corresponds to nstlim            #######
####### in "MD.in" file                               #######
maxl=1000
###################### Cycles ##########################
ntwr=4
##########################################################
cp egor.host $dirII
mv AN.in $TOPOLOGYII bg_sander.sh $dirII
cp ENERGY.dat $dirII/AN_ENERGY_1.0.dat
```

```
cp ENERGY.dat $dirII/bgPID.dat
##############################################################
for ((i=1;i<=maxi;i++))
do
##############################################################
for ((l=1;l<=maxl;l++))
do
let p=$ntwr*$l-$ntwr
let m=$ntwr*$l
let o=$ntwr*$l+$ntwr
##############################################################
let maxm=$maxl*$ntwr
##############################################################
while [ ! -f MDf_$i.restrt_$o ] ;
do
wait
done
while [ ! -f rstdip_$o ] ;
do
wait
done
##############################################################
if [ -f MDf_$i.restrt_$m ]
then
cp MDf_$i.restrt_$m $dirII
fi
##############################################################
cd $dirII
############## Prepare zero velocities file ################
head -$atomlines MDf_$i.restrt_$m  > MDf_XYZ.restrt
tail -1    MDf_$i.restrt_$m  > MDf_BOX.restrt
cat   MDf_XYZ.restrt   ZERO_VEL.restrt   MDf_BOX.restrt   >
MDf_$i.restrt_$m
##############################################################
cd $dirI
if [ -f MDf_$i.restrt_$o ]
then
cd $dirII
##### The control of the number of background processes #####
num_proc=(`ls -l bgPID*.dat | wc -l `)
```

```
echo $num_proc >> num_procI.dat
while [ $num_proc -gt $NUM_PROC ]; do
sleep 5s
num_proc=(`ls -l bgPID*.dat | wc -l `)
echo $num_proc >> num_procF.dat
done
############################################################
echo $i  $p  $m  $maxm > ipm.dat
./bg_sander.sh $TOPOLOGYII  $dirI &
sleep 2s
cd $dirI
else
cd $dirII
sander    -O  -i  AN.in  -o  AN_$m.out  -p  $TOPOLOGYII  -c
MDf_$i.restrt_$m -ref MDf_$i.restrt_$m
head -186 AN_$m.out | tail -9 > AN_$m.mdinfo
cat AN_$m.mdinfo > AN_ENERGY_$i.$m.dat
rm -f AN_$m.mdinfo
rm -f MDf_$i.restrt_$m  MDf_$i.rstdip_$m
cd $dirI
############# Clean MD directory from used files ###########
if [ $m -lt $maxm ]
then
rm -f  MDf_$i.restrt_$m  MDf_$i.rstdip_$m
fi
############################################################
fi
done
######### Concatenate all the AN_ENERGY*.dat files #########
cd $dirII
##### Check that all analysis's sander RUNS are complete ####
complete=(`ls -l AN_ENERGY_$i.*.dat | wc -l`)
if [ $complete -eq $maxl ]
then
echo "complete" $i >> complete.dat
for ((l=1;l<maxl;l++))
do
let m=$ntwr*$l
rm -f $dirI/MDf_$i.restrt_$m
rm -f $dirII/MDf_$i.restrt_$m
```

```
done
fi
while [ $complete -lt $maxl ]; do
sleep 30s
complete=(`ls -l AN_ENERGY_$i.*.dat | wc -l`)
echo $complete >> complete.dat
for ((l=1;l<=maxl;l++))
do
let m=$ntwr*$l
let maxm=$ntwr*$maxl
if [ -f AN_ENERGY_$i.$m.dat ] && [ $m -lt $maxm ]
then
rm -f $dirI/MDf_$i.restrt_$m
rm -f $dirII/MDf_$i.restrt_$m
else
sander  -O  -i  AN.in  -o  AN_$m.out  -p  $TOPOLOGYII  -c
MDf_$i.restrt_$m -ref MDf_$i.restrt_$m
head -186 AN_$m.out | tail -9  > AN_$m.mdinfo
cat AN_$m.mdinfo > AN_ENERGY_$i.$m.dat
rm -f AN_$m.mdinfo
rm -f $dirI/MDf_$i.restrt_$m
rm -f $dirII/MDf_$i.restrt_$m
fi
done
let complete=$maxl
echo "complete checked" $i >> complete.dat
done
###### Concatenate the data of the current set of runs ######
for ((l=1;l<=maxl;l++))
do
let p=$ntwr*$l-$ntwr
let m=$ntwr*$l
cat AN_ENERGY_$i.$p.dat AN_ENERGY_$i.$m.dat > intermediate.dat
mv intermediate.dat AN_ENERGY_$i.$m.dat
done
let maxm=$maxl*$ntwr
echo $maxm > TEST.dat
mv AN_ENERGY_$i.$maxm.dat AN_ENERGY_$i.dat
rm -f AN_ENERGY_$i.*.dat
cp $dirI/ENERGY.dat AN_ENERGY_1.0.dat
```

```
cd $dirI
########## Copy result to "home" directory  ##############
done
############## Concatenate the data of all sets ###########
cd $dirII
cp $dirI/ENERGY.dat AN_ENERGY_0.dat
for ((i=1;i<=maxi;i++))
do
let ip=$i-1
cp AN_ENERGY_$i.dat AN_ENERGYT_$i.dat
cat AN_ENERGY_$ip.dat  AN_ENERGY_$i.dat > intermediate.dat
mv intermediate.dat AN_ENERGY_$i.dat
done
mv AN_ENERGY_$maxi.dat AN_ENERGY.dat
rm -f AN_ENERGY_0.dat AN_ENERGY_*.dat
###########################################################
cp AN_ENERGY.dat $STARTDIR
tar -cvf AN_ENERGY.tar AN_ENERGYT_*.dat
gzip AN_ENERGY.tar
cp AN_ENERGY.tar.gz $STARTDIR
###########################################################
```

H.5 Single step calculation script *bg_sander.sh*

```
#!/bin/bash
bgPID=$$
touch bgPID.$bgPID.dat
###########################################################
exec 3<> ipm.dat # Open file "ipm.dat" and assign fd 3 to it.
read i p m maxm <&3  # Read only var1 var2 var3
exec 3>&-
###########################################################
sander  -O  -i  AN.in  -o  ANbg_$m.out  -p  $TOPOLOGYII  -c
MDf_$i.restrt_$m -ref MDf_$i.restrt_$m
### calculate how many sanders from analysis.sh are run ####
rm -f bgPID.$bgPID.dat
###########################################################
head -186 ANbg_$m.out | tail -9  > ANbg_$m.mdinfo
cat ANbg_$m.mdinfo > AN_ENERGY_$i.$m.dat
rm -f ANbg_$m.mdinfo
```

```
###### rm -f MDf_$i.restrt_$m  MDf_$i.rstdip_$m ###########
cd $dirI
############ Clean MD directory from used files ###########
if [ $m -lt $maxm ]
then
rm -f  MDf_$i.restrt_$m  MDf_$i.rstdip_$m
fi
##########################################################
```

Trajectory concatenation script ghost.sh

```
#!/bin/bash
#$ -cwd
ghostPID=$$
maxi=25
for ((i=1;i<=maxi;i++))
do
while [ ! -f MDf_$i.restrt_3996 ] ;
do
wait
done
if [ -f MDf_$i.restrt_3996 ]
then
cp MDf_$i.restrt_3996 MDf_$i.restrt_4004
cp rstdip_4 rstdip_4004
fi
done
kill -9 $ghostPID
##########################################################
```

H.6 *Sander* command file *MD.in* for trajectory production

```
Production RUN 10ps, NVE,H-bons are free
&cntrl

ipol    = 0,
ntx     = 5,      irest = 1,     ntrx = 1,      ntxo = 1,
ntpr    = 1,      ntwx  = 400,   ntwv = 5,      ntwe = 5,
ntwr    = -4,
```

```
ntf      = 2,        ntb   = 2,      ntr  = 1,
cut      = 12.0,   nsnb  = 5,       nscm = 4, tol = 0.0000001,


nstlim  = 4001,
t        = 0.0,     dt    = 0.0005,


ig       = 71277,
ntt      = 1,        temp0 = 300.0, tautp = 5.0,
vlimit = 20.0,


ntp      = 1,        pres0 = 1.0,    comp  = 44.6,
taup     = 2.0,    npscal = 1,


ntc      = 2,


&end
&ewald
dsum_tol = 0.000001,
indmeth = 2, maxiter = 50,
irstdip = 1, diptol = 0.0000001,
&end
Constraints
500.0
RES 1   31
END
END
```

H.7 *Sander* **command file** *AN.in* **for trajectory analysis**

```
Input file for Analysis
&cntrl


ipol     = 0,
ntx      = 5,        irest = 1,      ntrx = 1,       ntxo = 1,
ntpr     = 1,        ntwx  = 1,      ntwv = 1,       ntwe = 1,
ntwr     = 1,


ntf      = 2,        ntb   = 1,      ntr = 1,
cut      = 12.0,   nsnb  = 4,       nscm = 4, tol = 0.0000001,
```

```
nstlim   = 1,
t        = 0.0,   dt    = 0.00005,


ig       = 71277,
ntt      = 0,
vlimit   = 20.0,
ntc      = 2,
&end
&ewald
dsum_tol = 0.000001,
indmeth = 2, maxiter = 50,
irstdip = 1, diptol = 0.0000001
&end
Constraints
500.0
RES 1  31
END
END
```

Bibliography

1   Watson, J. D.; Crick, F. H. C. *Nature* **1953**, *171*, 737.

2   Eley, D. D.; Spivey, D. I. *Trans. Faraday Soc.* **1962**, *58*, 411.

3   Roth, S. R.: *One-Dimensional Metals*; VCG Verlagsgesellschaft: Weinheim, **1995**.

4   (a) Straus, J. B.; Voth, G. A. *J. Phys. Chem.* **1993**, *97*, 7388. (b) Straus, J. B.; Calhoun, A.; Voth, G. A. *J. Chem. Phys.* **1995**, *102*, 529. (c) Calhoun, A.; Voth, G. A. *J. Phys. Chem. B* **1998**, *102*, 8563.

5   Warshel, A.; Hwang, J.-K. *J. Chem. Phys.* **1986**, *84*, 4938.

6   (a) Garg, A.; Onuchic, J. N.; Ambegaokar, B. *J. Chem. Phys.* **1985**, *83*, 4491. (b) Leggett, A. J.; Chakravarty, S.; Dorsey, A. T.; Fischer M. P. A.; Garg, A.; Zwerger, W. *Rev. Mod. Phys.* **1987**, *59*, 1. (c) Barbara, P. F.; Meyer, T. J.; Ratner M. A. *J. Phys. Chem.* **1996**, *100*, 13148. (d) Bader, J. S.; Kuharski, R. A.; Chandler, D. *J. Chem. Phys.* **1990**, *93*, 230.

7   Murphy, C. J.; Arkin, M. R.; Jenkins, Y.; Ghatlia, N. D.; Bossman, S. H.; Turro, N. J.; Barton, J. K. *Science* **1993**, *262*, 1025.

8   Hall, D. B.; Holmlin, R. E.; Barton J. K. *Nature* **1996**, *382*, 731.

9   Berti, L.; Alessandrini, A.; Facci, P. *J. Am. Chem. Soc.* **2005**, *127*, 11216.

10 Keren, K.; Berman, R. S.; Buchstab, E.; Sivan, U.; Braun, E. *Science* **2003**, *302*, 1380.

11 Mao, C.; Sun, W.; Shen, Z.; Seeman, N. C. *Nature* **1999**, *397*, 144.

12 Brucale, M.; Zuccheri, G. P.; Samorì, B. *Org. Biomol. Chem.* **2005**, *3*, 575.

13 Alberti, P.; Mergny, J. L. *Proc. Natl. Acad. Sci. USA* **2003**, *100*, 1569.

14 Benenson, Y.; Paz-Elizur, T.; Adar, R.; Keinan, E.; Livneh, Z.; Shapiro, E. *Nature* **2001**, *414*, 430.

15 Seeman, N. C. *Angew. Chem. Int. Ed.* **1998**, *37*, 3220.

16 Seeman, N. C. *Nature* **2003**, *421*, 427.

17 Hansma, H. G. *Annu. Rev. Phys. Chem.* **2001**, *52*, 71.

18 Muir, T.; Morales, E.; Root, J.; Kumar, I.; Garcia, B.; Vellandi, B.; Jenigian, D.; Marsh, T.; Vesenka, J. *J. Vac. Sci. Technol. A* **1998**, *16*, 1172.

19 Shapir, E.; Cohen, H.; Sapir, T.; Borovok, N.; Kotlyar, A. B.; Porath, D. *J. Phys. Chem. B* **2006**, *110*, 4430.

20 Ceres, D. M.; Barton, J. K. *J. Am. Chem. Soc.* **2003**, *125*, 14964.

21 Saenger, W.: *Principles of Nucleic Acid Structure*; Springer Verlag: New York, **1984**.

22 Müller D. J.; Engel, A. *Biophys. J.* **1997**, *73*, 1633.

23   Kasumov, A. Y.; Klinov, D. V.; Roche, P. E.; Guéron, S.; Bouchiat, H. *Appl. Phys. Lett.* **2004**, *84*, 1007.

24   Braun, E.; Eichen, Y.; Sivan, U.; Ben-Yoseph, G. *Nature* **1998**, *391*, 775.

25   Cohen, H.; Nogues, C.; Naaman, R.; Porath, D. *Proc. Natl. Acad. Sci. USA* **2005**, *102*, 11589.

26   Xu, B.; Zhang, P.; Li, X.; Tao, N. *Nano Lett.* **2004**, *4*, 1105.

27   Cui, X. D.; Primak, A.; Zarate, X.; Tomfohr, J.; Sankey, O. F.; Moore, A. L.; Moore, T. A.; Gust, D.; Harris, G.; Lindsay, S. M. *Science* **2001**, *294*, 571.

28   Van Zalinge, H.; Schiffrin, D. J.; Bates, A. D.; Haiss, W.; Ulstrup, J.; Nichols, R. *Chem. Phys. Chem.* **2006**, *7*, 94.

29   Di Felice, R.; Selloni, A. *J. Chem. Phys.* **2004**, *120*, 4906.

30   Nogues, C.; Cohen, S. R.; Daube, S. S.; Naaman, R. *Phys. Chem. Chem. Phys.* **2004**, *6*, 4459.

31   Endres R. G.; Cox D. E.; Singh R. R. P. *Rev. Mod. Phys.* **2004**, *76*, 195.

32   Wagenknecht H.-A. *Nat. Prod. Rep.* **2006**, *23*, 973.

33   Odom, D. T.; Barton, J. K. *Biochem.* **2001**, *40*, 8727.

34   Meggers, E.; Michel-Beyerle, M. E.; Giese, B. *J. Am. Chem. Soc.* **1998**, *120*, 12950.

35   Bixon, M.; Giese, B.; Wessely, S.; Langenbacher, T.; Michel-Beyerle, M. E.; Jortner, J. *Proc. Natl. Acad. Sci. USA* **1999**, *96*, 11713.

36   Meggers, E.; Kusch, D.; Spichty, M.; Wille, U.; Giese, B. *Angew. Chem. Int. Ed. Engl.* **1998**, *37*, 460.

37   Douki, T.; Ravanat, J.-L.; Angelov, D.; Wagner, J. R.; Cadet, J. *Top. Curr. Chem.* **2004**, *236*, 1.

38   Giese, B.; Wessely, S.; Spormann, M.; Lindemann, U.; Meggers, E.; Michel-Beyerle, M. E. *Angew. Chem. Int. Ed.* **1999**, *38*, 996.

39   Giese, B. *Top. Curr. Chem.* **2004**, *236*, 27.

40   Giese, B. *Acc. Chem. Res.* **2000**, *33*, 631.

41   Seidel, C. A. M.; Schultz, A.; Sauer, M. H. M. *J. Phys. Chem.* **1996**, *100*, 5541.

42   Voityuk, A. A.; Jortner, J.; Bixon, M.; Rösch, N. *Chem. Phys. Lett.* **2000**, *324*, 430.

43   Prat, F.; Houk, K. N.; Foote, C. S. *J. Am. Chem. Soc.* **1998**, *120*, 845.

44   Takada, T.; Kawai, K.; Cai, X.; Sugimoto, A.; Fujitsuka, M.; Majima, T. *J. Am. Chem. Soc.* **2004**, *126*, 1125.

45   Lewis, F. D.; Wu, T. F.; Zhang, Y. F.; Letsinger, R. L.; Greenfield, S. R.; Wasielewski, M. R. *Science* **1997**, *277*, 673.

46   Davis, W. B.; Hess, S.; Naydenova, I.; Haselsberger, R.; Ogrodnik, A.; Newton, M. D.; Michel-Beyerle, M. E. *J. Am. Chem. Soc.* **2002**, *124*, 2422.

47   Hess, S.; Götz, M.; Davis, W. B.; Michel-Beyerle, M. E. *J. Am. Chem. Soc.* **2001**, *123*, 10046.

48   Nunez, M. E.; Hall, D. B.; Barton, J. K. *Chem. & Biol.* **1999**, *6*, 85.

49   Rajski, S. R.; Jackson, B. A.; Barton, J. K. *Mutation Research-Fundamental and Molecular Mechanisms of Mutagenesis* **2000**, *49*, 447.

50 Steenken, S.; Jovanovic, S. V. *J. Am. Chem. Soc.* **1997**, *119*, 617.

51 (a) Behrens, C.; Ober, M.; Carell, T. *Eur. J. Org. Chem.* **2002**, *19*, 3281. (b) Behrens, C.; Burgdorf, L. T.; Schwögler, A.; Carell, T. *Angew. Chem. Int. Ed.* **2002**, *41*, 1763. (c) Behrens, C.; Carell, T. *Chem. Commun.* **2003**, *14*, 1632. (d) Breeger, S.; Hennecke, U.; Carell, T. *J. Am. Chem. Soc.* **2004**, *126*, 1302.

52 Wagenknecht, H. A. *Angew. Chem. Int. Ed.* **2003**, *42*, 2454.

53 Voityuk, A. *J. Chem. Phys.* **2005**, *122*, 204904.

54 Burin A. L.; Uskov D. B. *J. Chem. Phys.* **2008**, *129*, 025101.

55 Rösch, N.; Voityuk, A. A.: *Quantum Chemical Calculation of Donor-Acceptor Coupling for Charge Transfer in DNA*, in: *Long-Range Charge Transfer in DNA II*, Topics in Current Chemistry, *237*; Schuster, G. Ed.: Springer, Heidelberg, **2004**, p. 37.

56 Bixon, M.; Jortner, J. *Chem. Phys.* **2002**, *281*, 393.

57 Jortner, J.; Bixon, M.; Voityuk, A. A.; Rösch, N. *J. Phys. Chem. A* **2002**, *106*, 7599.

58 Lewis, F. D.; Liu, X. Y.; Liu, J. Q.; Hayes, R. T.; Wasielewski, M. R. *J. Am. Chem. Soc.* **2000**, *122*, 12037.

59 Giese, B.; Amaudrut, J.; Köhler, A. K.; Spormann, M.; Wessely, S. *Nature* **2001**, *412*, 318.

60 Berlin, Y. A.; Burin, A. L.; Ratner, M. A. *Chem. Phys.* **2002**, *275*, 61.

61 Shimazaki, T.; Asai, Y.; Yamashita, K. *J. Phys. Chem. B* **2005**, *109*, 1295.

62 Jortner, J.; Bixon, M.; Langenbacher, T.; Michel-Beyerle, M. E. *Proc. Natl. Acad. Sci. USA* **1998**, *95*, 12759.

63 Grozema, F. C.; Berlin, Y. A.; Siebbeles, L. D. A. *J. Am. Chem. Soc.* **2000**, *122*, 10903.

64 Berlin, Y. A.; Burin, A. L.; Ratner, M. A. *J. Phys. Chem. A* **2000**, *104*, 443

65 Berlin, Y. A.; Burin, A. L.; Ratner, M. A. *J. Am. Chem. Soc.* **2001**, *123*, 260.

66 Nakatani, K.; Dohno, C.; Saito, I. *J. Am. Chem. Soc.* **1999**, *121*, 10854.

67 Ly, D.; Sanii, L.; Schuster, G. B. *J. Am. Chem. Soc.* **1999**, *121*, 9400.

68 Takada, T.; Kawai, K.; Cai, X.; Sugimoto, A.; Fujitsuka, M.; Majima, T. *J. Am. Chem. Soc.* **2004**, *126*, 1125.

69 Takada, T.; Kawai, K.; Tojo, S.; Majima, T. *J. Phys. Chem. B* **2003**, *107*, 14052.

70 Lewis, F. D.; Zuo, X.; Liu, J.; Hayes, R. T.; Wasielewski, M. R. *J. Am. Chem. Soc.* **2002**, *124*, 4568.

71 Lewis, F. D.; Liu, J.; Zuo, X.; Hayes, R. T.; Wasielewski, M. R. *J. Am. Chem. Soc.* **2003**, *125*, 4850.

72 Voityuk, A. A.; Michel-Beyerle, M. E.; Rösch, N. *Chem. Phys. Lett.* **2001**, *342*, 231.

73 Voityuk, A. A.; Rösch, N. *J. Phys. Chem. B* **2002**, *106*, 3013.

74 Marcus, R. A. *J. Chem. Phys.* **1956**, *24*, 979.

75 Lewis, F. D.; Letsinger, R. L.; Wasielewski, M. R. *Acc. Chem. Res.* **2001**, *34*, 159.

76 Pal S. K.; Zhao L.; Zewail A. H. *Proc. Natl. Acad. Sci. USA* **2003**, *100*, 8113.

77 Feig M.; Pettitt B. M. *Biophys. J.* **1999**, *77*, 1769.

78 Barnett R. N.; Cleveland C. L.; Joy A.; Landman U.; Schuster G. B. *Science* **2001**, *294*, 567.

[79] Barnett R. N.; Cleveland C. L.; Landman U.; Boone E.; Kanvah S.; Schuster G. B. *J. Phys. Chem. A* **2003**, *107*, 3525.

[80] Cave, R. J.; Newton, M. D.; Kumar, K.; Zimmt, M. B. *J. Phys. Chem.* **1995**, *99*, 17501.

[81] Kumar, K.; Lin, Z.; Waldeck, D. H.; Zimmt, M. B. *J. Am. Chem. Soc.* **1996**, *118*, 243.

[82] Han, H.; Zimmt, M. B. *J. Am. Chem. Soc.* **1998**, *120*, 8001.

[83] Williams, T. T.; Odom, D. T.; Barton, J. K. *J. Am. Chem. Soc.* **2000**, *122*, 9048.

[84] Wan, C. Z.; Fiebig, T.; Kelley, S. O.; Treadway, C. R.; Barton, J. K.; Zewail, A. H. *Proc. Natl. Acad. Sci. USA* **1999**, *96*, 6014.

[85] Cheatham III, T. E.; Kollman, P. A. *J. Am. Chem. Soc.* **1997**, *119*, 4805.

[86] Duan, Y.; Wilkosz, P.; Crowley, M.; Rosenberg, J. M. *J. Mol. Biol.* **1997**, *272*, 553.

[87] Cheatham III, T. E.; Kollman, P. A. *Ann. Rev. Phys. Chem.* **2000**, *51*, 435.

[88] Bader, J. S.; Berne, B. J. *J. Chem. Phys.* **1996**, *104*, 1293.

[89] Bader, J. S.; Cortis, C. M.; Berne, B. J. *J. Chem. Phys.* **1997**, *106*, 2372.

[90] Ando, K. *J. Chem. Phys.* **2001**, *115*, 5228.

[91] Tanaka, S.; Sengoku, Y. *Phys. Rev. E* **2003**, *68*, 031905.

[92] King, G.; Warshel, A. *J. Chem. Phys.* **1990**, *93*, 8682.

[93] Marcus, R. A. *J. Chem. Phys.* **1956**, *24*, 966.

[94] Marcus, R. A.; Sutin, N. *Biochim. Biophys. Acta* **1985**, *811*, 265.

[95] Barbara, P. F.; Meyer, T. J.; Ratner, M. A. *J. Phys. Chem.* **1996**, *100*, 13148.

[96] Kubo, R.: *Statistical Mechanics*; North-Holland: Amsterdam, **1965**.

[97] (a) Warshel, A. *Acad. Sci. Script. Var.* **1984**, *55*, 59. (b) Warshel, A.; Russell, S. T.; Sussman, F. *Isr. J. Chem.* **1987**, *27*, 217. (c) Hwang, J.-K.; Warshel, A. *J. Am. Chem. Soc.* **1987**, *109*, 715. (d) Hwang, J.-K.; King, G.; Creighton, S.; Warshel, A. *J. Am. Chem. Soc.* **1988**, *110*, 5297. (e) Hwang, J.-K.; Creighton, S.; King, G.; Whitney, D.; Warshel, A. *J. Chem. Phys.* **1988**, *89*, 859.

[98] (a) Kuharski, R. A.; Bader, J. S.; Chandler, D.; Sprik, M.; Klein, M. L.; Impey, R. W. *J. Chem. Phys.* **1988**, *89*, 3248.(b) Chandler, D.; Kuharski, R. A. *Faraday Discuss. Chem. Soc.* **1988**, *85*, 329.

[99] Marcus, R. A. *J. Chem. Phys.* **1965**, *43*, 679.

[100] Marcus, R. A. *J. Phys. Chem.* **1989**, *93*, 3078.

[101] Zhou, H.-X.; Szabo, A. *J. Chem. Phys.* **1995**, *103*, 3481.

[102] Hush, N. S. *Prog. Inorg. Chem.* **1967**, *8*, 391.

[103] Marcus, R. A. *Annu. Rev. Phys. Chem.* **1966**, *15*, 155.

[104] Buckingham, A. D. *Proc. R. Soc. London Ser. A* **1956**, *238*, 235.

[105] Gutmann, V.: *The Donor-Acceptor Approach to Molecular Interactions*; Plenum Press: New York, **1978**.

[106] Tachiya, M. *J. Phys. Chem.* **1989**, *93*, 7050.

[107] Tachiya, M. *Chem. Phys. Lett.* **1989**, *159*, 505.

[108] Carter, E. A.; Hynes, J. T. *J. Phys. Chem.* **1989**, *93*, 2184.

[109] Kuznetsov, A. M. *J. Phys. Chem.* **1992**, *96*, 3337.

[110] Sutin, N. *Prog. Inorg. Chem.* **1983**, *30*, 441.

[111] Brunschwig, B. S.; Creutz, C.; McCartney, D. H.; Sham, T.-K.; Sutin N. *Faraday Discuss. Chem. Soc.* **1982**, *74*, 113.

[112] Siriwong, K.; Voityuk, A. A.; Newton, M. D.; Rösch, N. *J. Phys. Chem. B* **2003**, *107*, 2595.

[113] Frisch, M. J.; Trucks, G. W.; Schlegel, H. B.; Scuseria, G. E.; Robb, M. A.; Cheeseman, J. R.; Zakrzewski, V. G.; Montgomery, J. A., Jr.; Stratmann, R. E.; Burant, J. C.; Dapprich, S.; Millam, J. M.; Daniels, A. D.; Kudin, K. N.; Strain, M. C.; Farkas, O.; Tomasi, J.; Barone, V.; Cossi, M.; Cammi, R.; Mennucci, B.; Pomelli, C.; Adamo, C.; Clifford, S.; Ochterski, J.; Petersson, G. A.; Ayala, P. Y.; Cui, Q.; Morokuma, K.; Malick, D. K.; Rabuck, A. D.; Raghavachari, K.; Foresman, J. B.; Cioslowski, J.;Ortiz, J. V.; Stefanov, B. B.; Liu, G.; Liashenko, A.; Piskorz, P.; Komaromi, I.; Gomperts, R.; Martin, R. L.; Fox, D. J.; Keith, T.; Al-Laham, M. A.; Peng, C. Y.; Nanayakkara, A.; Gonzalez, C.; Challacombe, M.; Gill, P. M. W.; Johnson, B. G.; Chen, W.; Wong, M. W.; Andres, J. L.; Head-Gordon, M.; Replogle, E. S.; Pople, J. A. *Gaussian 98*, Revision A.11; Gaussian, Inc.: Pittsburgh, PA, **2001**.

[114] Nelsen, S. F.; Balckstock, S. C.; Kim, Y. *J. Am. Chem. Soc.* **1987**, *109*, 677.

[115] Rauhut, G.; Clark, T. *J. Am. Chem. Soc.* **1993**, *115*, 9127.

[116] Berashevich, J. A.; Chakraborty, T. *Chem. Phys. Lett.* **2007**, *446*, 159.

[117] Newton, M. D.; Sutin, N. *Annu. Rev. Phys. Chem.* **1984**, *35*, 437.

[118] Newton, M. D. *Chem. Rev.* **1991**, *91*, 767.

[119] Sutin, N.; Brunschwig, B. S. *Mechanistic Aspects of Inorganic Reactions*; Rorabacher, D. B.; Endicott, J. F., Eds.: ACS Symp. Ser. 198; American Chemical Society: Washington, D.C., **1982**, p. 105.

[120] Dogonadze, R. R. in *Reaction of Molecules at Electrodes*; Hush, N. S., Ed.; Wiley: New York; 1971, Chapter 3.

[121] Simon, J. D. *Acc. Chem. Res.* **1988,** *128*, 21.

[122] Fleming, G. R.; Cho, M. *Annu. Rev. Phys. Chem.* **1996**, *47*, 109.

[123] DeVault, D.: *Quantum Mechanical Tunneling in Biological Systems*; Cambridge University Press: Cambridge, **1984**.

[124] (a) Miller, J. R.; Calcaterra, L. T.; Closs, G. L. *J. Am. Chem. Soc.* **1984**, *106*, 3047. (b) Wasielewski, M. R.; Niemczyk, M. P.; Svec, W. A.; Pewitt, E. B. *J. Am. Chem. Soc.* **1985**, *107*, 1080. (c) Kakitani, T.; Mataga, N. *J. Phys. Chem.* **1985**, *89*, 8. (d) Asahi, T.; Ohkohchi, M.; Matsusaka, R.; Mataga, N.; Zhang, R. P.; Osuka, A.; Maruyama, K. *J. Am. Chem. Soc.* **1993**, *115*, 5665. (e) Kakitani, T.; Matsuda, N.; Yoshimori, A.; Mataga, N. *Prog. React. Kinet.* **1995**, *20*, 347. (f) Yoshimori, A.; Mataga, N. *J. Phys. Soc. Jpn.* **1992**, *61*, 2577. (g) Mataga, N.; Chosrowjan, H.; Taniguchi, S.; Shibata, Y.; Yoshida, N.; Osuka, A.; Kikuzawa, T.; Okada, T. *J. Phys. Chem. A* **2002**, *106*, 12191. (h) Cortés, J.; Heitele, H.; Jortner, J. *J. Phys. Chem.* **1994**, *98*, 2527. (i) Bixon, M.; Jortner, J.; Cortés, J.; Heitele, H.; Michel-Beyerle, M. E. *J. Phys. Chem.* **1994**, *98*, 7289. (j) Tetreault, N.; Muthyala, R. S.; Liu, R. S. H.; Steer, R. P. *J. Phys. Chem. A* **1999**, *103*, 2524.

[125] Chen, P.; Meyer, T. J. *Chem. Rev.* **1998**, *98*, 1439.

[126] Bixon, M.; Jortner, J. *Adv. Chem. Phys.* **1999**, *106*, 35.

[127] Levich, V. *Adv. Electrochem. Electrochem. Eng.* **1966**, *4*, 249.

[128] Ulsrup J.: *Charge-Transfer Processes in Condensed Media, Lecture Notes in Chemistry*; Springer-Verlag: New-York, Vol. 10, **1979**.

[129] Ballhausen C. J.: *Molecular Electronic Structures of Transition Metal Complexes;* McGraw-Hill: New-York, **1979**.

[130] Wilson E. B., Decius J. C., Cross P. C.: *Molecular vibrations*; Dover Publications, Inc.: New York, **1980**.

[131] Huang, K.; Rhys, A. *Proc. Royal. Soc. A* **1950**, *204*, 406.

[132] Islampour, R.; Alden, R. G.; Wu, G. Y. C.; Lin, S. H. *J. Phys. Chem.* **1993**, *97*, 6793.

[133] Marcus, R. A. *J. Chem. Phys.* **1984**, *81*, 4494.

[134] Burshtein, A. I.; Frantsuzov, P. A.; Zharikov, A. A. *J . Chem. Phys.* **1992**, *96*, 4261.

[135] Bixon, M.; Jortner, J. *Faraday Discuss. Chem. Soc.* **1982**, *74*, 17.

[136] Zharikov, A. A.; Sherer, P. O. J.; Fischer, S. F. *J. Phys. Chem.* **1994**, *98*, 3424.

[137] Marcus, R. A. *Discuss. Faraday Soc.* **1960**, *29*, 21.

[138] Marcus, R. A. *Rev. Mod. Phys.* **1993**, *65*, 599.

[139] Ichiye, T. *J. Chem. Phys.* **1996**, *104*, 7561.

[140] Yelle, R. B.; Ichiye, T. *J. Phys. Chem. B* **1997**, *101*, 4127.

[141] (a) Kumar, P. V.; Maroncelli, M. *J. Chem. Phys.* **1995**, *103*, 3038. (b) Marchi, M.; Gehlen, J. N.; Chandler, D.; Newton, M. *J. Am. Chem. Soc.* **1993**, *115*, 4178. (c) Geissler, P. L.; Chandler, D. *J. Chem. Phys.* **2000**, *113*, 9759. (d) Nishiyama, K.; Hirata, F.; Okada, T. *J. Mol. Struct.* **2001**, *31,* 565.

[142] (a) Tominaga, K.; Walker, G. C.; Jarzeba, W.; Barbara, P. F. *J. Phys. Chem.* **1991**, *95*, 10475. (b) Bingemann, D.; Ernsting, N. P. *J. Chem. Phys.* **1992**, *102*, 2691. (c) Gustavsson, T.; Baldacchino, G.; Mialocq, J.-C.; Pommeret, S., *Chem. Phys. Lett.* **1995**, *236*, 587. (d) van der Meulen, P.; Jonkman, A. M.; Glasbeek, M. *J. Phys. Chem. A* **1998**, *102*, 1906. (e) Nishiyama K.; Okada, T. *J. Phys. Chem. A* **1998**, *102*, 9729. (f) Richert R. *J. Chem. Phys.* **2001**, *114*, 7471. (g) Kovalenko, S. A.; Ruthmann, J.; Ernsting, N. P. *Chem. Phys. Lett.* **1997**, *271*, 40. (h) Kovalenko, S. A.; Eilers-König, N.; Senyushkina, T. A.; Ernsting, N. P. *J. Phys. Chem. A* **2001**, *105*, 4834. (i) Sluch, M. I.; Godt, A.; Bunz, U. H. F.; Berg, M. A. *J. Am. Chem. Soc*. **2001**, *123*, 6447.

[143] (a) Matyushov, D. V.; Voth, G. A. *J. Phys. Chem. A* **1999**, *103*, 10981. (b) Matyushov, D. V.; Voth, G. A. *J. Phys. Chem. A* **2000**, *104*, 6470. (c) Matyushov, D. V.; Voth, G. A. *J. Phys. Chem. A* **2000**, *104*, 6485. (d) Matyushov, D. V.; Newton, M. D. *J. Phys. Chem. A* **2001**, *105*, 8516.

[144] Ando, K. *J. Chem. Phys.* **1997**, *107*, 4585.

[145] Warshel, A.; Chu, Z. T.; Parson, W. W. *Science* **1989**, *246*, 112.

[146] Hwang, J.-K., Warshel, A. *Chem. Phys. Letters* **1997**, *271*, 223.

[147] Warshel, A.; Parson, W. W. *Q. Rev. Biophys.* **2001**, *34*, 563.

[148] Warshel, A.; Russell, S. T. *Q. Rev. Biophys.* **1984**, *17*, 283.

[149] Tulley, J. C.; Preston, R. M. *J. Chem. Phys.* **1971**, *55*, 562.

[150] Leon, W. Couch II.: *Digital and Analog Communication Systems*; Sixth Edition, Prentice Hall: New Jersey, **2001**.

[151] Lax, M. *J. Chem. Phys.* **1952**, *20*, 1752.

[152] Kubo, R.; Toyozawa, Y. *Progr. Theor. Phys.* **1955**, *13*, 160.

[153] Matyushov, D. V.; Voth, G. A. *J. Chem. Phys.* **2000**, *113*, 5413.

[154] Marcus, R. A. *J. Chem. Phys.* **1965**, *43*, 1261.

[155] Englman, R.; Jortner, J. *Mol. Phys.* **1970**, *18*, 145.

[156] Kestner, N. R.; Logan, J.; Jortner, J. *J. Phys. Chem.* **1974**, *21*, 2148.

[157] Reiseborough, P. S. *Ann. Phys.* **1984**, *153*, 1.

[158] Skinner, J. L.; Hsu, D. *J. Phys. Chem.* **1986**, *90*, 4931.

[159] Kakitani, T.; Mataga, N. *J. Phys. Chem.* **1985**, *89*, 4752.

[160] Warshel, A. *J. Phys. Chem.* **1982**, *86*, 2218.

[161] Raineri, F. O.; Friedman, H. L. *Adv. Chem. Phys.* **1999**, *107*, 81.

[162] Gradshteyn, I. S.; Ryzhik, I. M.: *Table of Integrals, Series, and Products*; Academic Press: San Diego, **1994**.

[163] Marcus, R. A. *J. Chem. Phys.* **1963**, *38*, 1858.

[164] Marcus, R. A. *Annu. Rev. Phys. Chem.* **1966**, *15*, 155.

[165] Tachiya, M. *J. Phys. Chem.* **1993**, *97*, 5911.

[166] Makri, N. *J. Phys. Chem. B* **1999**, *103*, 2823.

[167] (a) Liu, Y.-P.; Newton, M. D. *J. Phys. Chem.* **1994**, *98*, 7162. (b) Liu, Y.-P.; Newton, M. D. *J. Phys. Chem.* **1995**, *99*, 12382.

[168] LeBard, D. N.; Lilichenko, M.; Matyushov, D. V.; Berlin, Y. A.; Ratner, M. A. *J. Phys. Chem. B* **2003**, *107*, 14509.

[169] Rocchia, W.; Alexov, E.; Honig, B. *J. Phys. Chem. B* **2001**, *105*, 6507.

[170] Rocchia, W.; Sridharan, S.; Nicholls, A.; Alexov, E.; Chiabrera, A.; Honig, B. *J. Comput. Chem.* **2002**, *23*, 128.

[171] Bottcher, C. J. F.: *Theory of Electric Polarization*; Elsevier Press: Amsterdam, **1973**.

[172] Yang, L.; Weerasinghe S.; Smith P. E.; Pettitt B. M. *Biophys. J.* **1995**, *69*, 1519.

[173] Shui, X.; McFail-Isom, L.; Hu, G. G.; Williams, L. D. *Biochemistry* **1998**, *37*, 8341.

[174] Young, M. A.; Jayaram, B.; Beveridge, D. L. *J. Phys. Chem. B* **1998**, *102*, 7666.

[175] Young, M. A.; Ravishanker, G.; Beveridge, D. L. *Biophys. J.* **1997**, *73*, 2313.

[176] Tavernier, H. L.; Fayer, M. D. *J. Phys. Chem. B* **2000**, *104*, 11541.

[177] Tong, G. S. M.; Kurnikov, I. V.; Beratan, D. N. *J. Phys. Chem. B* **2002**, *106*, 2381.

[178] Makarov, V.; Pettitt, B. M.; Feig, M. *Acc. Chem. Res.* **2002**, *35*, 376.

[179] Lewis, F. D.; Letsinger, R. L.; Wasielewski, M. R. *Acc. Chem. Res.* **2001**, *34*, 159.

[180] Berashevich, J. A.; Chakraborty, T. *J. Chem. Phys.* **2007**, *126*, 035104.

[181] Berendsen, H. J. C.; Postma, J. P. M.; van Gunsteren, W. F.; Hermans, I.: *Intermolecular Forces*; Reidel: Dordrecht, **1981**, p. 331.

[182] Jorgensen, W. L.; Chandrasekhar, J.; Madura, J. D.; Impey, R. W.; Klein, M. L. *J. Chem. Phys.* **1983**, *79*, 926.

[183] Mahoney, M. W.; Jorgensen, W. L. *J. Chem. Phys.* **2000**, *112*, 8910.

[184] Gupta, S.; Matyushov, D. V. *J. Phys. Chem. A* **2004**, *108*, 2087.

[185] Kim, H. J.; Hynes, J. T. *J. Chem. Phys.* **1992**, *96*, 5088.

[186] Gehlen, J. N.; Chandler, D.; Kim, H. J.; Hynes, J. T. *J. Phys. Chem.* **1992**, *96*, 1748.

[187] Ando, K. *J. Chem. Phys.* **2001**, *114*, 9470.

[188] Cheatham III, T. E.; Young, M. *Biopolymers* **2000**, *56*, 232.

[189] Karplus, M.; McCammon J. A. *Nature Struct. Biol.* **2002**, *9*, 646.

[190] Leach, A. R.: *Molecular modelling: Principles and applications*; Longman: Harlow, **1996**.

[191] Cornell, W. D.; Cieplak, P.; Bayly, C. I.; Gould, I. R.; Merz, K. M.; Ferguson, D. M.; Spellmeyer, D. C.; Fox, T.; Caldwell, J. W.; Kollman, P. A. *J. Am. Chem. Soc.* **1995**, *117*, 5179.

[192] MacKerell, A. D.; Wiórkiewicz-Kuczera, J.; Karplus, M. *J. Am. Chem. Soc.* **1995**, *117*, 11946.

[193] Scott, W. R. P.; Hünenberger, P. H.; Tironi, I. G.; Mark, A. E.; Billeter, S. R.; Fennen, J.; Torda, A. E.; Huber, T.; Krüger, P.; van Gunsteren, W. F. *J. Phys. Chem. A* **1999**, *103*, 3596.

[194] Allinger, N. L. *J. Am. Chem. Soc.* **1977**, *99*, 8127.

[195] Verlet, L. *Phys. Rev.* **1967**, *159*, 98.

[196] Hockney, R. W. *Methods Comput. Phys.* **1970**, *9*, 136.

[197] Swope, W. C.; Anderson, H. C.; Berens, P. H.; Wilson, K. R. *J. Chem. Phys.* **1982**, *76*, 637.

[198] Williams, D. E. *J. Comput. Chem.* **1988**, *9*, 745.

[199] Dyke, T. R.; Muenter J. S. *J. Chem. Phys.* **1973**, *59*, 3125.

[200] Gregory, J. K.; Clary, D. C.; Liu, K.; Brown, M. G.; Saykally, R. J. *Science* **1997**, *275*, 814.

[201] Badyal, Y. S.; Saboungi, M.-L.; Price, D. L.; Shastri, S. D.; Haeffner, D. R.; Soper, A. K. *J. Chem. Phys.* **2000**, *112*, 9206.

[202] Sprik, M. *J. Chem. Phys.* **1991**, *95*, 6762.

[203] Soetens, J.-C.; Costa, M. T. C. M.; Millot, C. *Mol. Phys.* **1998**, *94*, 577.

[204] (a) Cieplak, P.; Kollman, P. A.; Lybrand, T. *J. Chem. Phys.* **1990**, *92*, 6755. (b) Caldwell, J.; Dang, L. X.; Kollman, P. A. *J. Am. Chem. Soc.* **1990**, *112*, 9144. (c) Dang, L. X. *J. Chem. Phys.* **1992**, *97*, 2659. (d) Wallqvist, A.; Berne, B. J. *J. Phys. Chem.* **1993**, *97*, 13841. (e) Chialvo, A. A.; Cummings, P. T. *J. Chem. Phys.* **1996**, *105*, 8274. (f) Svishchev, I. M.; Kusalik, P. G.; Wang, J.; Boyd, R. J. *J. Chem. Phys.* **1996**, *105*, 4742. (g) Dang, L. X.; Chang, T. M. *J. Chem. Phys.* **1997**, *106*, 8149. (h) Chen, B.; Xing, J. H.; Siepmann, J. I. *J. Phys. Chem. B* **2000**, *104*, 2391.

[205] Burnham, C. J.; Li, J.; Xantheas, S. S.; Leslie, M. *J. Chem. Phys.* **1999**, *110*, 4566.

[206] Sprik, M.; Klein, M. L.; Watanabe, K. *J. Phys. Chem.* **1990**, *94*, 6483.

[207] Dang L. X.; Smith, D. E. *J. Chem. Phys.* **1993**, *99*, 6950.

[208] Babin, V.; Baucom J.; Darden, T. A.; Sagui C. *J. Phys. Chem. B* **2006**, *110*, 11571.

[209] Caldwell, J. W.; Kollman, P. A. *J. Phys. Chem.* **1995**, *99*, 6208.

[210] Applequist, J.; Carl, J. R.; Fung, K.-K. *J. Am. Chem. Soc.* **1972**, *94*, 2952.

[211] Bayly, C.; Cieplak, P.; Cornell, W.; Kollman, P. *J. Phys. Chem.* **1993**, *97*, 10269.

[212] Cieplak, P.; Cornell, W.; Bayly, C.; Kollman, P. *J. Comput. Chem.* **1995**, *16*, 1357.

[213] Ponder, J. W.; Case, D. A. *Adv. Prot. Chem.* **2003**, *66*, 27.

[214] Petrov, A. S.; Pack, G. R.; Lamm, G. *J. Phys. Chem. B* **2004**, *108*, 6072.

215 Eksterowitz, J.; Miller, J.; Kollman, P. *J. Phys. Chem. B* **1997**, *101*, 10971.

216 Warshel, A.; Levitt, M. *J. Mol. Biol.* **1976**, *103*, 227.

217 Becke, A. *J. Chem. Phys.* **1993**, *98*, 5648.

218 Dunning, T. Jr. *J. Chem. Phys.* **1989**, *90*, 1007.

219 Cieplak P.; Caldwell J.; Kollman P. *J. Comp. Chem.* **2001**, *22*, 1048.

220 Case, D.; Darden, T.; Cheatham III, T.; Simmerling, C.; Wang, J.; Duke, R.; Luo, R.; Merz, K.; Wang, B.; Pearlman, D.; Crowley, M.; Brozell, S.; Tsui, V.; Gohlke, H.; Mongan, J.; Hornak, V.; Cui, G.; Beroza, P.; Schafmeister, C.; Caldwell, J.; Ross, W.; Kollman, P. AMBER 8; University of California: San Francisco, **2004**.

221 Allen, M. P.; Tildesley, D. J.: *Computer Simulation of Liquids*; Clarendon: Oxford, **1987**.

222 Darden, T.; York, D.; Pedersen, L. *J. Chem. Phys.* **1993**, *98*, 10089.

223 van Gunsteren, W. F.; Berendsen, H. J. C. *Angew. Chem. Int. Ed.* **1990**, *29*, 992.

224 Steinbach, P. J.; Brooks, B. R. *J. Comput. Chem.* **1994**, *15*, 667.

225 Brooks, B. R.; Bruccoleri, R. E.; Olafson, B. D.; States, D. J.; Swaminathan, S.; Karplus, M. *J. Comput. Chem.* **1983**, *4*, 187.

226 (a) Grubmüller, H.; Heller, H.; Windemuth, A.; Shulten, K. *Molec. Simulation* **1991**, *6*, 121. (b) Alejandre, J.; Tildesley, D. J. *J. Chem. Phys.* **1995**, *102*, 4574. (c) Feller, S. E.; Pastor R. W.; Rojnuckarin A.; Bogusz S.; Brooks B. R. *J. Phys. Chem.* **1996**, *100*, 17011.

227 Ewald, P. P. *Ann. Phys.* **1921**, *64*, 253.

228 Pérez, A.; Luque J. F.; Orozco, M. *J. Am. Chem. Soc.* **2007**, *129*, 14739.

229 Berendsen, H. J. C.; Postma, J. P. M.; van Gunsteren, W. F.; Di Nola, A.; Haak, J. R.; *J. Chem. Phys.* **1984**, *81*, 3684.

230 Parson, W. W.; Chu, Z. T.; Warshel, A. *Biophys. J.* **1998**, *74*, 182.

231 Böttcher, C. J. F.: *Theory of electric polarization*; Elsevier: Amsterdam, **1973**.

232 Song X.; Marcus, R. A. *J. Chem. Phys.* **1993**, *99*, 7768.

233 Milischuk, A. A.; Matyushov, D. V.; Newton, M. D. *Chem. Phys.* **2006**, *324*, 172.

234 Lewis F. D.; Kalgutkar, R. S.; Wu, Y.; Liu, X.; Liu, J.; Hayes, R. T.; Miller, S. E.; Wasielewski, M. R. *J. Am. Chem. Soc.* **2000**, *122*, 12346.

235 Ando, K. *J. Chem. Phys.* **1997**, *106*, 116.

236 Ando, K. *J. Chem. Phys.* **1994**, *101*, 2850.

237 Meng, E.; Cieplak, P.; Caldwell, J. W.; Kollman, P. A. *J. Am. Chem. Soc.* **1994**, *116*, 12061.

238 Ryckaert, J.-P.; Cicciotti, G.; Berendsen, H. J. C. *J. Comput. Phys.* **1977**, *23*, 327.

239 Andersen, H. C. *J. Chem. Phys.* **1980**, *72*, 2384.

240 Phillips, J. C.; Braun, R.; Wang, W.; Gumbart, J.; Tajkhorshid, E.; Villa, E.; Chipot, C.; Skeel, R. D.; Kale, L.; Schulten, K. *J. Comp. Chem.* **2005**, *26*, 1781.

241 Essmann, U.; Perera, L.; Berkowitz, M. L.; Darden, T.; Lee, H.; Pedersen, L. G. *J. Chem. Phys.* **1995**, *103*, 8577.

242 Toukmaji, A.; Sagui, C.; Board, J. A.; Darden, T. *J. Chem. Phys.* **2000**, *113*, 10913.

243 (a) Saboungi, M. L.; Rahman, A.; Halley, J. W.; Blander, M. *J. Chem. Phys.* **1988**, *88*, 5818. (b) Sprik, M.; Klein, M. A. *J. Chem. Phys.* **1988**, *89*, 7556; (c)Wilson, M.; Madden, P. A. *J. Phys. Cond. Matter* **1993**, *5*, 2687.

[244] Small, D. W.; Matyushov, D. V.; Voth, G. A. *J. Am. Chem. Soc.* **2003**, *125*, 7470.

[245] (a) Marcus, R. A.; Siders, P. *J. Phys. Chem.* **1982**, *86*, 622; (b) Kira, A. *J. Phys. Chem.* **1981**, *85*, 3047.

[246] Rehm, D.; Weller, A. *Israel. J. Chem.* **1970**, *8*, 259.

[247] (a) Rick, S. W.; Stuart, S. J.; Berne, B. J. *J. Chem. Phys.* **1994**, *101*, 6141. (b) Stuart S. J.; Berne B. J. *J. Phys. Chem.* **1996**, *100*, 11934. (c) Rick, S. W.; Berne, B. J. *J. Phys. Chem. B* **1997**, *101*, 10488. (d) Liu, Y.-P.; Kim, K.; Berne, B. J.; Friesner R. A.; Rick, S. W. *J. Chem. Phys.* **1998**, *108*, 4739.

[248] (a) Pratt, L. R. *Mol. Phys.* **1980**, *40*, 347. (b) Thompson, M. J.; Schweizer, K. S.; Chandler, D. *J. Chem. Phys.* **1982**, *76*, 1128. (c) Cao J.; Berne, B. J. *J. Chem. Phys.* **1993**, *99*, 2902.

[249] King, G.; Warshel, A. *J. Chem. Phys.* **1989**, *91*, 3647.

[250] Lamoureux, G.; MacKerell, A. D. Jr.; Roux, B. *J. Chem. Phys.* **2003**, *119*, 5185.

[251] Takada, T.; Kawai, K.; Fujitsuka, M.; Majima T. *Chem. Eur. J.* **2005**, *11*, 3835.

[252] Armitage, B. *Chem. Rev.* **1998**, *98*, 1171.

[253] Burrows, C. J.; Muller, J. G. *Chem. Rev.* **1998**, *98*, 1109.

[254] (a) Kelley, S. O.; Jackson, N. M.; Hill, M. G.; Barton, J. K. *Angew. Chem.* **1999**, *111*, 991. (b) Kelley, S. O.; Jackson, N. M.; Hill, M. G.; Barton, J. K. *Angew. Chem. Int. Ed.* **1999**, *38*, 941.

[255] Boon, E. M.; Salas, J. E.; Barton, J. K. *Nat. Biotechnol.* **2002**, *20*, 282.

[256] Mikkelsen, K. V.; Ratner, M. A. *Chem. Rev.* **1997**, *87*, 1113.

[257] Harriman, A. *Angew. Chem. Int. Ed.* **1999**, *38*, 945.

[258] Vladimirov, E.; Ivanova, A.; Rösch, N. *J. Chem. Phys.* **2008**, *129*, 194515.

[259] Dixon, R. W.; Kollman, P. A. *J. Comp. Chem.* **1997**, *18*, 1632.

[260] Wang, J.; Cieplak, P.; Kollman, P. A. *J. Comp. Chem.* **2000**, *21*, 1049.

[261] Cheatham, T. E. III; Kollman, P. A. *J. Mol. Biol.* **1996**, *259*, 434.

[262] Olofsson, J.; Larsson, S. *J. Phys. Chem. B* **2001**, *105*, 10398.

[263] (a) Lide, D. R., *Ed. Handbook of Chemistry and Physics*; CRC Press: Boca Raton, FL, **2000**, 81st Ed. (b) Oki, M. et al., *Ed. Kagaku Binran*; Maruzen: Tokyo, **1993**, 4th Ed.

[264] Tu, Y.; Laaksonen, A. *Chem. Phys. Lett.* **2000**, *329*, 283.

[265] Morita, A. *J. Comp. Chem.* **2002**, *23*, 1466.

[266] Morita, A.; Kato, S. *J. Chem. Phys.* **1999**, *110*, 11987.

[267] Jortner, J.; Bixon, M. *J. Chem. Phys.* **1988**, *88*, 167.

[268] Lewis, F. D.; Zhu, H.; Daublain, P.; Sigmund, K.; Fiebig, T.; Raytchev, M.; Wang, Q.; Shafirovich V. *Photochem. Photobiol. Sci.* **2008**, *7*, 534.

[269] Cheatham, T. E. III; Kollman, P. A. *Structure* **1997**, *5*, 1297.

[270] Newton, M. D.; Basilevsky, M. V.; Rostov I. V. *Chem. Phys.* **1998**, *232*, 201.

[271] Priyadarshy, S.; Risser, S. M.; Beratan, D. N. *J. Phys. Chem.* **1996**, *100*, 17678.

[272] The earlier results of Lewis F. D. are referred (see Ref.234) despite the fact that they were recently reconsidered: Senthilkumar K.; Grozema F. C.; Guerra C. F.; Bickelhaupt F. M.; Lewis F. D.; Berlin Y. A.; Ratner M. A.; Siebbeles L. D. A. *J. Am. Chem. Soc.* **2005**, *127*, 14894.

[273] (a) Gasper, S. M.; Armitage, B.; Shui, X.; Hu, G. G.; Yu, Ch.; Schuster, G. B.; Dean Williams, L. *J. Am. Chem. Soc.* **1998**, *120*, 12402. (b) Trieb, M.; Rauch, C.; Wibowo, F. R.; Wellenzohn, B.; Liedl, K. R. *Nuc. Acids Res.* **2004**, *32*, 4696. (c) Alexopoulos, E.; Jares-Erijman, E. A.; Jovin, T. M.; Klement, R.; Machinek, R.; Sheldrick, G. M.; Uson, I. *Acta Crystallogr. D – Biol. Crystalogr.* **2005**, *61*, 407.

[274] Wagner, Th.; Davis, W. B.; Lorenz, K. B.; Michel-Beyerle, M. E.; Diederichsen, U. *Eur. J. Org. Chem.* **2003**, *18*, 3673.

[275] (a) Fink, H.-W.; Schönenberger, C. *Nature* **1999**, *398*, 407; (b) Porath, D.; Bezryadin, A.; De Vries, S.; Dekker, C. *Nature* **2000**, *403*, 635.

[276] Adams, D. M.; Brus, L.; Chidsey, C. E. D.; Creager, S.; Creutz, C.; Kagan, C. R.; Kamat, P. V.; Lieberman, M.; Lindsay, S.; Marcus, R. A.; Metzger, R. M.; Michel-Beyerle, M. E.; Miller, J. R.; Newton, M. D.; Rolison, D. R.; Sankey, O.; Schanze, K. S.; Yardley, J.; Zhu, X. *J. Phys. Chem. B.* **2003**, *107*, 6668.

[277] (a) Porath, D.; Cuniberti, G.; Di Felice, R. *Top. Curr. Chem.* **2004**, *237*, 183; (b) Lewis, F. D. *Photochem. Photobiol.* **2005**, *81*, 65.

[278] Gallego, J.; Reid, B. R. *Biochemistry* **1999**, *38*, 15104.

[279] (a) von Feilitsch, T. *PhD Thesis*, Technical University: Munich, **2002**; (b) Gaiko, N.; Volkmer, A.; Berger, S.; Schaffer, J.; Eggeling, C.; Seidel, C.; Griesinger, C. *Biophys. J.* **2003**, *84*, 313A.

[280] Ivanova, A.; Jezierski, G.; Vladimirov, E.; Rösch, N. *Biomacromolecules* **2007**, *8*, 3429.

[281] Vamosi, G.; Gohlke, C.; Clegg, R. M. *Biophys. J.* **1996**, *71*, 972.

[282] Neubauer, H. *Doctoral Thesis*, Johann Wolfgang Goethe-Universität: Frankfurt, **2004**.

[283] Chuichay, P.; Vladimirov, E.; Siriwong, K.; Hannongbua, S.; Rösch, N. *J. Mol. Model.* **2006**, *12*, 885.

[284] Vladimirov, E.; Ivanova, A.; Rösch, N. *J. Phys. Chem. B* **2009**, *113*, 4425.

[285] Diekmann, S. *J. Mol. Biol.* **1989**, *205*, 787.

[286] Frisch, M. J.; Trucks, G. W.; Schlegel, H. B.; Scuseria, G. E.; Robb, M. A.; Cheeseman, J. R.; Montgomery Jr. J. A.; Vreven, T.; Kudin, K. N.; Burant, J. C.; Millam, J. M.; Iyengar, S. S.; Tomasi, J.; Barone, V.; Mennucci, B.; Cossi, M.; Scalmani, G.; Rega, N.; Petersson, G. A.; Nakatsuji, H.; Hada, M.; Ehara, M.; Toyota, K.; Fukuda, R.; Hasegawa, J.; Ishida, M.; Nakajima, T.; Honda, Y.; Kitao, O.; Nakai, H.; Klene, M.; Li, X.; Knox, J. E.; Hratchian, H. P.; Cross, J. B.; Adamo, C.; Jaramillo, J.; Gomperts, R.; Stratmann, R. E.; Yazyev, O.; Austin, A. J.; Cammi, R.; Pomelli, C.; Ochterski, J. W.; Ayala, P. Y.; Morokuma, K.; Voth, G. A.; Salvador, P.; Dannenberg, J. J.; Zakrzewski, V. G.; Dapprich, S.; Daniels, A. D.; Strain, M. C.; Farkas, O.; Malick, D. K.; Rabuck, A. D.; Raghavachari, K.; Foresman, J. B.; Ortiz, J. V.; Cui, Q.; Baboul, A. G.; Clifford, S.; Cioslowski, J.; Stefanov, B. B.; Liu, G.; Liashenko, A.; Piskorz, P.; Komaromi, I.; Martin, R. L.; Fox, D. J.; Keith, T.; Al-Laham, M. A.; Peng, C. Y.; Nanayakkara, A.; Challacombe, M.; Gill, P. M. W.; Johnson, B.; Chen, W.; Wong, M. W.; Gonzalez, C.; Pople, J. A. *Gaussian 03, Revision C.01*, Gaussian, Inc.: Wallingford CT, **2004**.

[287] Cornell, W. D.; Cieplak, P.; Bayly, C. I.; Kollman, P. A. *J. Am. Chem. Soc.* **1993**, *115*, 9620.

[288] (a) Miertus, S.; Scrocco, E.; Tomasi, J. *Chem. Phys.* **1981**, *55*, 117. (b) Miertus, S.; Tomasi, J. *Chem. Phys.* **1982**, *65*, 239. (c) Cossi, M.; Barone, V.; Cammi, R.; Tomasi, J. *Chem. Phys. Lett.* **1996**, *255*, 327.

[289] Cavallo, L.; Moore, M. H.; Corrie, J. E. T.; Fraternali, F. *J. Phys. Chem. A* **2004**, *108*, 7744.

[290] Mitra, S. K.; Kaiser, J. F.: *Handbook for Digital Signal Processing*; John Wiley & Sons: New York, **1993**.

[291] Kay, S. M.: *Modern Spectral Analysis: Theory and Applications*; Prentice-Hall, Englewood Cliffs: New Jersey, **1988**.

[292] http://plasma-gate.weizmann.ac.il/Grace/